EFFECTS OF THE POLING PROCESS ON DIELECTRIC, PIEZOELECTRIC, AND FERROELECTRIC PROPERTIES OF LEAD ZIRCONATE TITANATE

By

ANDERSON D. PREWITT

A DISSERTATION PRESENTED TO THE GRADUATE SCHOOL
OF THE UNIVERSITY OF FLORIDA IN PARTIAL FULFILLMENT
OF THE REQUIREMENTS FOR THE DEGREE OF
DOCTOR OF PHILOSOPHY

UNIVERSITY OF FLORIDA

2012

© 2012 Anderson D. Prewitt

To my family

ACKNOWLEDGMENTS

I would like to thank my advisor Dr. Jacob L. Jones. I would like to thank my group members. I would like to thank Dr. Dragan Damjanovic and Dr. Abhijit Pramanick for their discussions and collaboration. I would like to thank my committee members Dr. Simon Philpot, Dr. David Arnold, Dr. Toshi Nishida, Dr. Steven Pearton and Dr. Franky So.

I want to acknowledge my appreciation for the funding I received through the McKnight Fellowship, the Alfred P. Sloan Foundation, the GEM Fellowship, the South Eastern Alliance for Graduate Education and the Professoriate (SEAGEP) Program and the Robert C. Pittman Foundation. I would like to acknowledge the following additional funding sources: funding for travel to the Swiss Federal Institute of Technology (EPFL) through National Science Foundation award number OISE-0755170; funding to travel to Oak Ridge National Laboratories through the Oak Ridge Associated Universities (ORAU) Powe Junior Faculty Enhancement Award; funding for travel to China through NSF; funding for travel to Los Alamos.

I want to thank the staff members in the Graduate School particularly in the Office of Graduate Minority Programs for their assistance and support. I'd like to thank the SEAGEP Office staff. I would also like to acknowledge the other graduate students who supported me during my time at the University of Florida.

TABLE OF CONTENTS

page

LIST OF TABLES

LIST OF FIGURES

Abstract of Dissertation Presented to the Graduate School
of the University of Florida in Partial Fulfillment of the
Requirements for the Degree of Doctor of Philosophy

EFFECTS OF THE POLING PROCESS ON DIELECTRIC, PIEZOELECTRIC, AND FERROELECTRIC PROPERTIES OF LEAD ZIRCONATE TITANATE

By

Anderson D. Prewitt

May 2012

Chair: Jacob L. Jones
Major: Materials Science and Engineering

Smart materials are widely used in many of today's relevant technologies such as nano and micro electromechanical systems (NEMS and MEMS), sensors, actuators, nonvolatile memory, and solid state devices. Many of these systems rely heavily on the electromechanical properties of certain smart materials, such as piezoelectricity and ferroelectricity. By definition, piezoelectricity is a mechanical stress in a material that produces an electric displacement (known as the direct piezoelectric effect) or electrical charge in a material which produces a mechanical strain (known as the converse piezoelectric effect). Ferroelectricity is a sub-class of piezoelectricity in which the polarization occurs spontaneously and the dipoles can be reoriented. Domain walls are the nanoscale regions separating two finite distinctively polarized areas in a ferroelectric. The reorientation of polarization in a material is called the poling process and many factors can influence the effectiveness of this process.

A more fundamental understanding of how electrical and mechanical loading changes the domain structure of these materials could lead to enhanced properties such as increased energy transduction and decreased nonlinear behavior.

This research demonstrates the influence of mechanical pressure and electrical field during and after the poling process on domain walls. The effects of strong mechanical forces on large-scale domain switching and weak cyclic forces on small-scale domain wall motion are investigated to show how they affect the macroscopic behavior of these materials.

Commercial lead zirconate titanate ceramics were studied under various poling conditions and the effect of domain wall motion on the piezoelectric, dielectric, and ferroelectric properties was investigated. Polarization and strain measurements from samples poled at specific conditions and converse piezoelectric coefficient and dielectric permittivity data was extracted and interpreted in the context of Rayleigh Law. Direct d_{33} was also measured. Mechanical loading measurements on the samples were conducted in situ during neutron diffraction experiments to determine how the domain structure behaved for the various poling conditions. The behavior of unpoled and poled samples under load was investigated.

The goal of this research is to develop a better understanding of the ferroelectric poling process and its influence on domain wall behavior in order to better engineer material and device properties. Experimental results have shown that significant changes occur in the electromechanical behavior of the material depending on the poling conditions. These results provide insight on how to better design materials and devices with enhanced performance, improved capacity, and less degradation as a result of mechanical stress and electrical fields. Possible microstructural origins for this behavior are discussed.

CHAPTER 1
INTRODUCTION

This chapter briefly introduces the key concepts addressed in this dissertation. Additionally, it gives a basic guideline for the experiments conducted by explaining the main objectives and plans for the different parts of the dissertation.

1.1 Ferroelectricity

An understanding of piezoelectricity (which translates as “pressure electricity”) is paramount to developing an understanding of the concept of ferroelectricity. Piezoelectricity is simply the occurrence of a mechanical stress or strain generating electricity or vice versa. The electric orientation of molecules in a piezoelectric material is defined as polarization.

All ferroelectric materials are generally piezoelectric, but not all piezoelectric materials are ferroelectric. Ferroelectrics can be permanently aligned in an electric field, similar to how ferromagnetic materials can be aligned in a magnetic field. Also both types of materials exhibit a property known as hysteresis, or a remnant polarization or magnetization, respectively even after the driving force has been removed, Figure 1-1. In a ferroelectric, each unit cell is essentially an electrical dipole, and materials exhibit the property of spontaneous and reversible polarization.

Spontaneous and switchable polarization is a requirement for ferroelectricity and all ferroelectric materials will, by definition, contain spontaneous and switchable dipoles. A dipole moment “**μ**” is generally defined as the product of the vector “***r***” which separates two charges multiplied by the magnitude of those charges “*q,*” or

$$\boldsymbol{\mu} = q^{*}\boldsymbol{r} \tag{1-1}$$

Ferroelectric materials have net permanent dipoles as a result of the vector sum of all of the individual dipole moments in each unit cell. In the presence of an electric field the polarization of dipoles in a ferroelectric material is non-linear and causes a phenomenon known as electrical hysteresis Figure 1-1.

The crystal structure is very important to the existence of piezoelectricity and ferroelectricity. A necessary condition for piezoelectricity (and subsequently ferroelectricity) to exist is the lack of a center of symmetry in the crystal structure's unit cell. This condition allows for a net movement of ions and the production of electric dipoles [1–3]. An example of this phenomenon is seen in Figure 1-2, which is an example of a perovskite crystal system for lead zirconate titanate (PZT). Perovskite systems generally have the form of ABO_3 where the valence of A atoms (e.g., Pb) ranges from +1 to +3 and that of the B atoms (e.g., Ti) ranges from +3 to +6. The structure shown in Figure 1-2 basically consists of a central TiO_6 octahedron surrounded by Pb atoms at the corners of a unit cell [4]. Generally, centrosymmetric cells can not be ferroelectric since equally spaced charges would cancel each other out. In most cases, this also means that the central atom must be in a non-equilibrium position. The polarization P_s of the cubic system is zero since all ions cancel due to the unit cell symmetry. The polarization of the tetragonal is non-zero due to unsymmetrical distortions of the unit cell.

It is worth noting that there are several important differences between bulk and thin-film ferroelectrics including the magnitude of the coercive field, E_c, which can be as much as an order of magnitude greater in a thin film than in a bulk sample of the same

material. Additionally, the intrinsic behavior of many ferroelectrics is a result of effects operating within the crystal [4–6].

1.1.1 Ferroelectricity Uses and Applications

There are a wide range of uses for ferroelectrics materials. The inherent electrical bistability of ferroelectrics makes them excellent materials for usage in Nonvolatile Memory. Some examples including ferroelectric random access memory (FeRAM) and ferroelectric field effect transistors are receiving considerable attention for research related to practical applications of the technology [7], [8]. When the ferroelectric properties of materials or systems are coupled with ferromagnetic or ferroelastic properties, the systems are considered to be multiferroic, and there is currently a significant amount of research interest in this field [7], [8]. Ferroelectrics are also used in some microelectromechanical systems (MEMS) architectures and other solid state devices such as ferroelectric capacitors for integrated circuits.

In most ferroelectrics, a structural phase transition from a high-temperature non-ferroelectric (or paraelectric) phase to a low-temperature ferroelectric phase occurs. The non-ferroelectric phase may or may not be piezoelectric and it may or may not be polar [1]. The Curie point, T_c, is the temperature where the phase transition takes place. The Curie–Weiss law describes how above the Curie point the dielectric permittivity (ε) falls off with temperature (T) according to the equation

$$\varepsilon = \varepsilon_o + C/(T-T_o) \approx C/(T-T_o) \qquad (1\text{-}2)$$

where ε_o and C are the dielectric permittivity of free space and the Curie-Weiss constant, respectively. T_o is some temperature less than T_c [4].

Spontaneous polarization at T_c can lead to the formation of surface charges which, in turn, can produce an electric field called a depolarizing field E_d. The depolarizing field

is orientated in the opposite direction of the polarization direction P_s [4]. In order to minimize the electrostatic energy of depolarizing fields and the elastic energy associated with mechanical constraints to which the ferroelectric material is subjected as it is cooled from the non-ferroelectric phase to ferroelectric phase, ferroelectric domains form [1], [4]. Domains are defined as small regions within the material which have the same direction of polarization [3]. Ferroelectric crystals often exhibit reduced pyroelectric and piezoelectric effects due to the presence of these domains if there is no compensation for depolarizing fields. The motion of the walls of these ferroelectric domains can provide valuable insight on the intrinsic and extrinsic properties of ferroelectric materials.

1.1.2 Representative Ferroelectric Materials

Lead zirconate titanate (PZT) is a representative material system that is a widely used electroceramic material and is both piezoelectric and ferroelectric. PZT has a perovskite crystal structure and a Curie temperature of generally above 390^{o}C, after which it transforms from a non-ferroelectric cubic phase to a ferroelectric tetragonal phase. Most of the ferroelectric materials that are of practical interest have perovskite structure and many form a solid solution with $Pb(Zr,Ti)O_3$. The spontaneous polarization in $Pb(Zr,Ti)O_3$ lies along the c -axis of the tetragonal unit cell and the distortion of the crystal is most often described as a function of shifts in O and (Zr,Ti) atoms relative to Pb atoms [4].

1.2 Ferroelectric Domains

1.2.1 Domain Effects in Ferroelectrics

In ferroelectric materials, domains of continuous crystallographic orientation and polarization form spontaneously upon cooling from above the Curie temperature. When

cooling a ferroelectric ceramic in the absence of an electric or mechanical field, these domains form in a manner that is elastically and electrically self-compensated. Because there is no net polarization in such a state, no piezoelectric effect is observed at the macroscopic scale. A net polarization and hence piezoelectricity is developed in the piezoelectric ceramic through a process known as poling. This process relies on the local spontaneous polarization of the unit cells which can be reoriented in the presence of a sufficiently strong electric field, i.e. the ferroelectric effect. Microstructurally, the process of spontaneous polarization reorientation occurs through the motion of domain walls, or the boundaries that separate different domains.

Numerous factors affect the degree of poling and thus the resultant piezoelectric properties that can be achieved in a material. For example, it is well known that the coercive field of a ferroelectric is influenced by chemical modification of the structure, or doping, since doping affects the point defect structure in a material [6]. Mechanical stress has also been shown to influence the degree of domain wall motion that occurs during the poling process [9], [10]. Moreover, one of the most influential parameters in the poling process is the temperature at which poling is performed. Because domain wall motion is thermally activated, the poling process is often performed at an elevated temperature to promote a higher degree of domain reorientation, a larger developed polarization in the ceramic, and higher piezoelectric coefficients. However, the influence of poling temperature on resultant piezoelectric coefficients has not often been investigated, though there has been some recent interest, e.g. [11].

Pinning sites (e.g. defects or trapped charges) are additionally known to influence the motion of domain walls [12]. It is important to distinguish between domain wall

motion and other types of domain behavior in ferroelectric materials, such as domain wall vibrations (vibrations of a domain wall between pinning sites) which are generally reversible, and domain switching (complete reorientation of a crystallographic domain) which may be reversible or irreversible.

1.2.2 Field Amplitude Dependence of Ferroelectric Behavior

A linear relationship generally exists for the piezoelectric coefficient as it relates strain(X) to an electric field amplitude (E) and the relationship between the dielectric displacement (D) and electric field is linearly related to the relative permittivity (ε_r) in many cases. Equation 1-3 shows these relationships.

$$X = dE \quad \text{and} \quad D = \varepsilon_0 \varepsilon_r E \tag{1-3}$$

Piezoelectric nonlinearity and dielectric nonlinearity occur more often at higher field and stress levels when ε_r and d depend more on the driving field. In fact there have been shown to be 3 distinct regions of material response. A low field region where the above equations apply and response is independent of field amplitude, a high field regions where the onset of switching, domain wall motion and other effects lead to significant nonlinear behavior, and a third region of behavior between the first two regions where the behavior is increases approximately linearly. This intermediate field region of linear response is know as the Rayleigh region and is useful to investigate in order to better understand material behavior. For materials that exhibit a field-amplitude dependence of d_{33} or ε_{33}, the Rayleigh relations can be used to interpret this behavior. Additionally, the Rayleigh behavior can be utilized to relate the macroscopic behavior (e.g. linear field dependence) to microscopic phenomena (e.g. random distribution of pinning centers) [4],[13],[14].

Plotting the sub-coercive field dependence of a material property within the Rayleigh region often yields a characteristic minor hysteresis loop. Low to intermediate (weak) field property measurements taken under these conditions can provide information on the material behavior without significantly changing the energetic landscape of the material sample. This contrasts with the high field strain or polarization hysteresis loops where the onset of domain switching will cause significant energetic landscape changes in the material.

An accepted methodology for extracting the total complex d_{33} or ε_r from sub-coercive field hysteresis loops is by applying Equation 1-4. The value of p' (d_{33} or ε_r) for a representative response versus electric field hysteresis loop (e.g. P-E loop or S-E loop) can be calculated by applying the equation

$$p' = \frac{R_{pp}}{2 * F_o} \tag{1-4}$$

where R_{pp} is the peak to peak value of the response (strain or polarization) and F_o is the applied cycling force (electric field E or applied pressure). The Rayleigh equations that describe the dielectric or piezoelectric response of a material are given by the following:

$$R'(F) = (p_{init} + \alpha_p F_o) F \pm \alpha_p (F_o^2 - F^2)/2, \tag{1-5}$$

$$R'(F_o) = (p_{init} + \alpha_p F_o) F_o,$$

$$p(F_o) = p_{init} + \alpha_p F_o, \tag{1-6}$$

where the general material response R = D or X, the material coefficient p = ε or d, and the general driving field F = applied pressure or electric field. The Rayleigh coefficient for the dielectric polarization or piezoelectric effect is α_p, and p_{init} is the zero-field value of the permittivity or piezoelectric coefficient. F_0 and R_0 are corresponding amplitudes. The positive sign and negative sign in Equation (1-5) describe the hysteresis

corresponding to the descending (‘+’), and to the ascending (‘−’) applied fields, respectively. Subsequently, a polarization or strain hysteresis loop taken at sub-switching conditions where Rayleigh law is applicable could be modeled with the two distinctive slopes representing the positive and negative applied field directions.

Although the poling process is used as a means to increase the value of the piezoelectric coefficient and relative dielectric permittivity, the nature of the piezoelectric and dielectric behavior obtained at different poling states is not well understood. In particular, commercial poling processes are generally selected based only on the resultant Berlincourt d_{33} values. A systematic evaluation on the influence of poling conditions on the d_{33} and ε_r values could lead to more precise control of properties that are influenced by the poling process.

1.3 Dissertation Organization

The organization of this dissertation is as follows:

Introduction of key concepts and description of materials (Chapter 1 and 2)

Key concepts discussed in this dissertation will be introduced in order to give context to the discussion and experiments in the remainder of the document. Fundamental theoretical framework and various approaches used to study material behavior in these results will be explained as well as the general objectives for this work. Additionally, a detailed description of the materials selected will be given.

Effects of the ferroelectric poling process (Chapter 3)

The effect of ferroelectric poling on the material response is first investigated by specifically examining the resultant direct (Berlincourt) d_{33} response of soft lead zirconate titanate (PZT) as a function of the initial poling conditions by varying the temperature and electric field of poling. The converse piezoelectric response was

further investigated in context of the Rayleigh Law to determine the extrinsic and intrinsic contributions to the piezoelectric material response.

Effects of an electric field on the motion of domain walls (Chapter 4 and 5)

The effect of ferroelectric poling on the extrinsic and intrinsic contributions are further investigated by further examining the converse piezoelectric as well as the dielectric response of differently poled PZT samples. The material response was investigated in terms of frequency as well as the field amplitude dependence of differently poled ferroelectric samples.

Effects of mechanical stress on domain wall motion (Chapter 6 and 7)

The effect of stress on the response of ferroelectrics poled in different ways is investigated to understand the intrinsic and extrinsic contributions to response as a result of the ferroelectric poling process. Large scale mechanical stress is applied in order to investigate how ferroelectric domains in differently poled materials behave. The direct d_{33} response was investigated as well to examine how small cyclic stresses affect the motion of domain walls in differently poled materials.

Summary and future work (Chapters 8 and 9)

Finally the summary and conclusions of this research are reported. Suggestions for future work in this area are discussed as well as possible applications of these results to other systems.

The goal of this research is to better understand what happens to ferroelectric materials during the ferroelectric poling process. Although the poling process is fairly important, the nature of the piezoelectric behavior obtained at different poling states is not well understood. In particular, commercial poling processes are generally selected

based only on the resultant Berlincourt d_{33} values. An evaluation on the influence of poling conditions on piezoelectric properties could lead to more precise control of properties that are influenced by the poling process. Therefore, the objective of this dissertation is to investigate the influence of poling conditions on the piezoelectric, ferroelectric, ferroelastic, and dielectric behavior of commercial lead zirconate titanate (PZT) ceramics. The materials selected for this study have commercial designations of K350 and EC65. These types of materials were chosen as a representative quantity of commercially available soft PZT that is used widely for various applications.

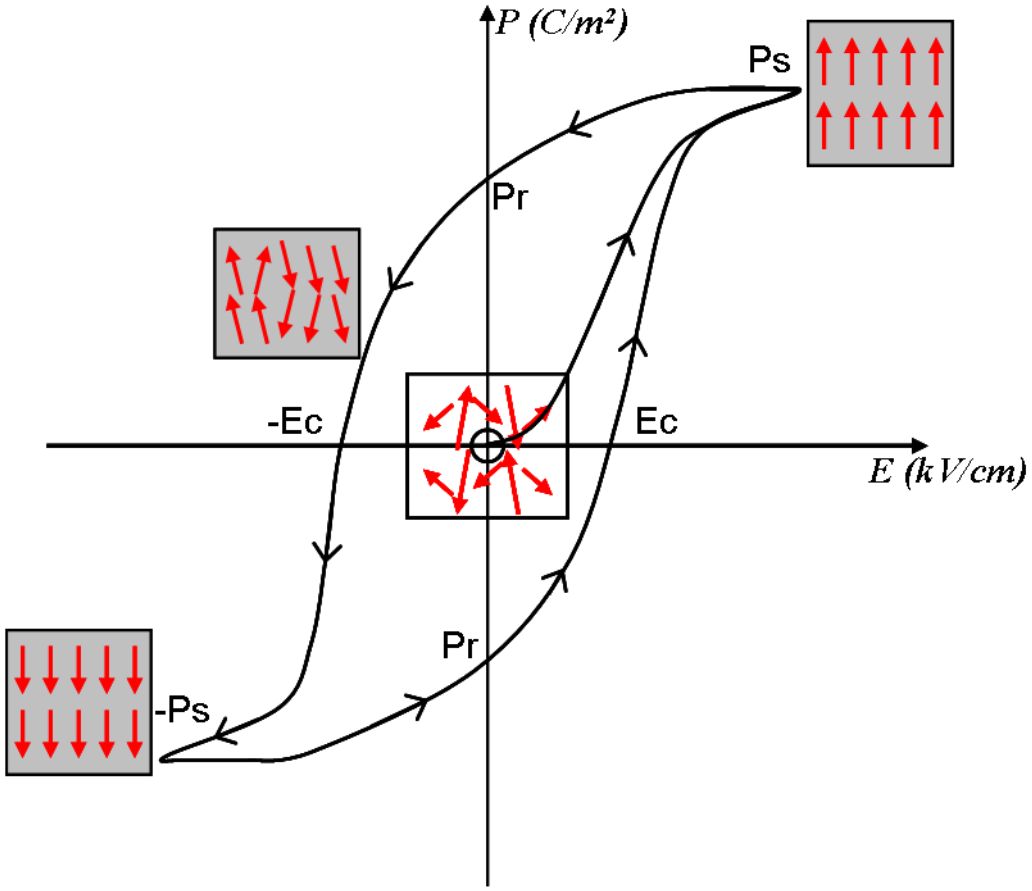

Figure 1-1. Schematic diagram of ferroelectric hysteresis graph. Here the definitions are as follows; E_c: coercive field; P_s: saturation polarization; P_r: remnant polarization. The arrows indicate direction of polarization for dipoles in a domain.

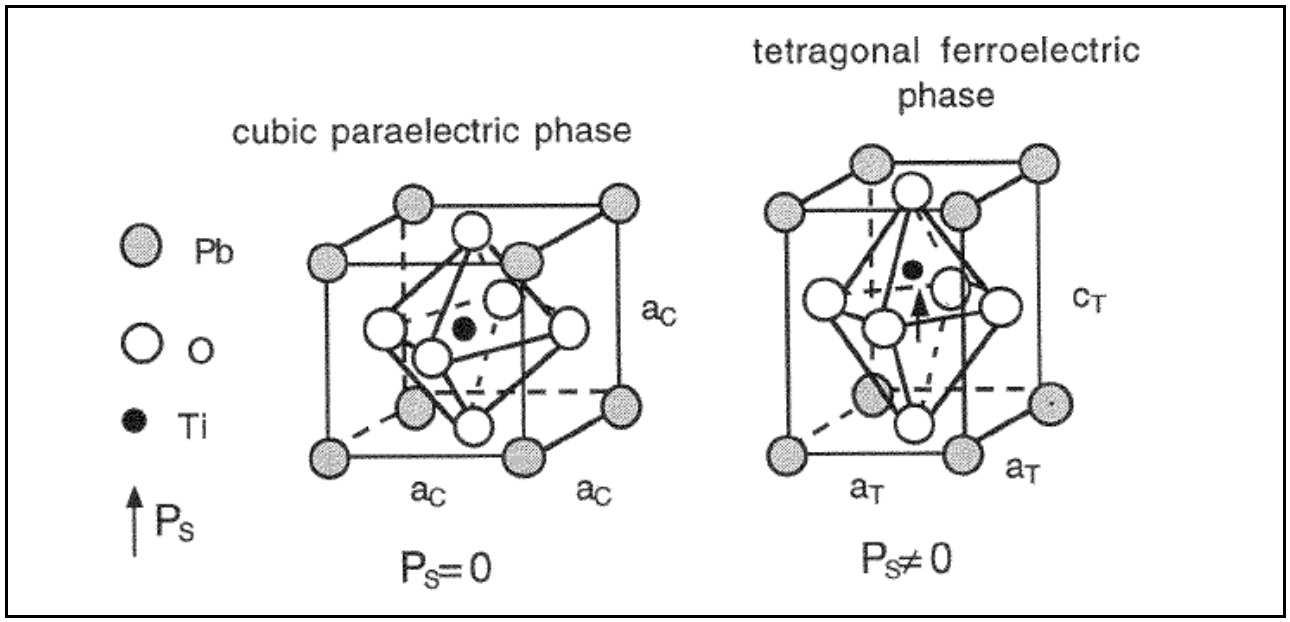

Figure 1-2. $PbTiO_3$ structures representing the non-ferroelectric cubic phase and the ferroelectric tetragonal phase for the system. From Damjanovic, D. "Ferroelectric, dielectric and piezoelectric properties of ferroelectric thin films and ceramics." *Rep. Prog. Phys* **61**, 97-98(1998) [4]

CHAPTER 2
MATERIALS

This section provides a brief overview of the materials used for the experiments performed in this work. All samples used in this work were purchased commercially from manufacturers in the United States.

2.1 "Soft" and "Hard" Ferroelectric Materials

2.1.1 General Material Properties

Chemical modification of ferroelectric ceramics can greatly enhance the properties of the materials being modified. Many commercial designations of lead zirconate titanate ceramics are based on solid solution compositions of $PbTiO_3$ $PbZrO_3$. Doping is the process of modifying the properties of piezoceramics by the addition of small amounts of impurities. In lead zirconate titanate (PZT) ceramics, the substitution of Pb^{2+} with dopants like Bi^{3+} or La^{3+} and Ti^{4+}/Zr^{4+} with dopants like Nb^{5+} or Ta^{5+} leads to reduced ageing effects, increased dielectric constants, high piezoelectric coupling factor, lower coercive fields, and greater dielectric losses. These compositions created by adding dopants with a higher valance are generally referred to as "soft" ferroelectrics.

In contrast, "hard" ferroelectrics have dopants with a lower valence. Materials classified as "hard" would exhibit lowered electrical resistivity and lower dielectric losses as well as higher coercive fields, lower dielectric constants, and poling would generally be more difficult. An example of "hard" PZT would be a system where Pb^{2+} is substituted with K^{+} or Na^{+} and Ti^{4+}/Zr^{4+} is substituted with Mg^{2+} or Fe^{3+} [6], [15], [16],[17].

2.1.2 Typical Navy Designations

There are several classical “navy” designations for PZT material behavior. Navy Type I PZT is suitable for repetitive and constant conditions in ultrasonic cleaning, sonar, and other high power applications. It is designed to serve as a driver in applications where design dictates high power and low losses for a particular application. This material maintains low mechanical and dielectric losses while producing large mechanical drive amplitudes. It is suitable for medical applications. Navy Type II PZT is designed for applications that require high electromechanical activity and high dielectric constant. Navy Type II materials have high permittivity and are very sensitive. They generally have decent time stability in applications when used as the receiver or generator element in various devices. Example applications include accelerometers, vibration pickups, hydrophones and medical transducers. Navy Type III PZT exhibits low losses when used in high power applications and has an extremely high mechanical quality. With the ability to withstand high levels of mechanical stress and electrical excitation, these materials have superb power handling capabilities. Applications include ultrasonic cleaners, high power ultrasonics and various medical applications. Navy Type V PZT ceramics are used in sensors that require a high sensitivity and dielectric constant, but need to have very low impedance. Navy Type VI is used in sensors that require high dielectric and piezoelectric constants as well as high coupling. There is very high permittivity but low time stability in this material system. This type of material is useful in very sensitive receivers.

2.2 Examples of Commercially Available “Soft” PZT

EC65 (ITT Corporation, formerly known as EDO, Salt Lake City, Utah) and K350 (Piezo Technologies, Indianapolis, IN) are both considered to be classical “soft” lead

zirconate titanate solid solution materials with compositions around the MPB and they would be most comparable to the Navy Type II PZT designation. Both EC65 and K350 are commercially available from US manufacturers. Some key properties of these materials are listed in Table 2-1. It is evident that both of these materials have very similar behavior. The properties of an additional Type II PZT, PIC 151 (Physik Instrumente (PI) Ceramic, Karlsruhe, Germany), are listed in the table as well for reference.

Figure 2-1 and Figure 2-2 show SEM images of the EC65 material and the K350 material, respectively. Tan and others have reported that the average grain size for EC65 is approximately 8 μm and it has a mixed micron-sized and nanodomain domain structure [18]. K350 is known to be chemically modified with niobium [19], [20]. EC65 has been similarly modified by proprietary dopants according to the manufacturer. More detailed structural refinement information about K350 is readily available in the literature [21].

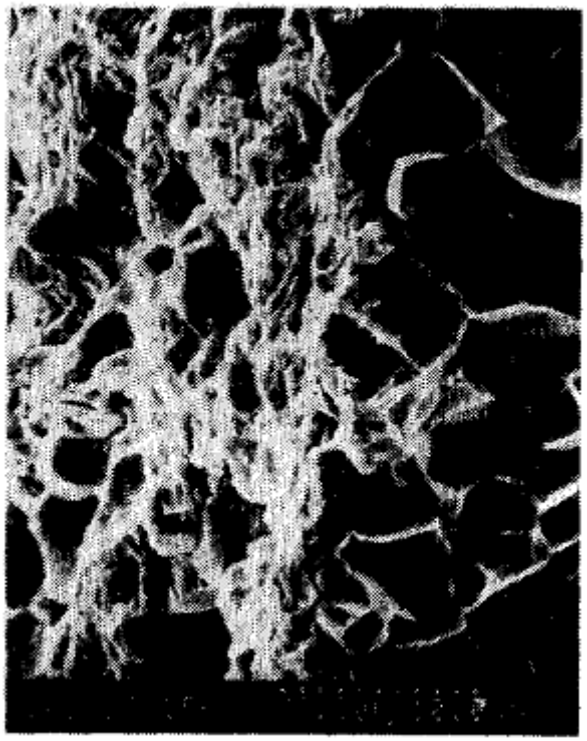

Figure 2-1. Scanning electron micrograph of EC65 ceramic. Reprinted from F. S. Foster et al., UFFC IEEE, 38, 5, 1991.

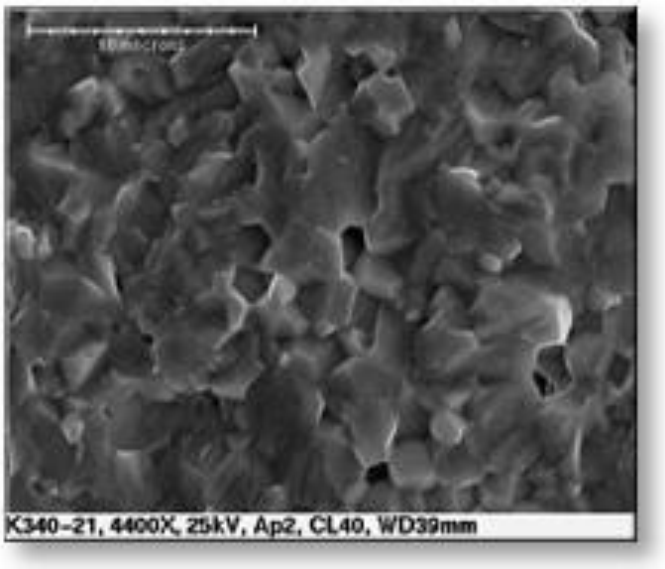

Figure 2-2. Scanning electron micrograph of K350 ceramic. Reprinted from Piezo Technologies, Inc.

Table 2-1. Typical properties of EC65 and K350. PIC 151 properties listed as well.

Property Coefficient	EC65 Ref. [22]	K350 Ref. [23]	PIC 151 Ref. [24]	Units
d_{33}	380	390	500	pm/V
ε_r	1725	1750	2400	unitless
d_{31}	-173	-175	-210	pm/V
k_p	0.62	0.61	.62	unitless
k_{33}	0.72	0.72	.69	unitless
T_c	350	360	250	°Celsius

CHAPTER 3
INFLUENCE OF FIELD AND TEMPERATURE ON PIEZOELECTRIC AND DIELECTRIC PROPERTIES

The present chapter investigates the influence of poling temperature and electric field amplitude on the piezoelectric behavior of a commercial lead zirconate titanate (PZT) ceramic. After electrical poling at various conditions, the direct and converse longitudinal piezoelectric coefficients are measured in samples that exhibit different degrees of poling.

3.1 Experimental Procedure

Gold electrodes were sputter coated on the 4 mm × 3.5 mm sample faces of commercial PZT ceramics of designation K350 (Piezo Technologies, Indianapolis, IN) and thickness ~1 mm. Different samples were poled at different electric field amplitudes and temperatures in a silicone oil bath. Initial experiments of poling times between 1 minute and 30 minutes did not reveal a significant dependence of this variable on the resulting Berlincourt d_{33} values and therefore a constant poling time of 5 minutes was used in all experiments reported in the present work. Electric field amplitudes ranged between 0 kV/mm and 2 kV/mm and temperatures ranged between 25°C and 175°C. The samples were poled using a high voltage source (Matsusada, AU-30P1). The samples were first connected to electrodes with the power supply turned off and heated to the given temperature. Next the specified electric field was applied at constant temperature. The electric field was then set to zero and the connection was shorted to ground. The samples were subsequently removed from the oil bath and cooled to room temperature under open circuit conditions. After poling, the longitudinal direct piezoelectric coefficient d_{33} was measured using a Berlincourt d_{33} meter (APC, YE2730A) and the strain was also measured as a function of electric field amplitude at

subcoercive (weak) fields using a linear variable displacement transducer (LVDT). The polarization was measured using a modified Sawyer-Tower circuit. Both sets of measurements were taken at least 24 hours after poling.

3.2 Results

The measured Berlincourt d_{33} values are shown in Figure 3-1 as a function of the temperature and electric field amplitude used during poling. The results in Figure 3-1 demonstrate d_{33} values ranging from 0 to 413 pC/N, indicating a strong dependence of d_{33} on poling conditions. For samples poled at 25°C, increasing the electric field amplitude from 0.5 kV/mm to 2 kV/mm increases the resultant d_{33} from 11 pC/N to 385 pC/N. The most dramatic changes in the piezoelectric coefficient were observed at electric field amplitudes of approximately 1 kV/mm. This value of electric field is equal to the coercive field extracted from polarization and strain measurements at room temperature on the same material composition[25]. For samples poled at 150°C and using different electric field amplitudes, the most dramatic changes in the piezoelectric coefficient were observed at electric field amplitudes of approximately 0.6 kV/mm. This is consistent with the expected temperature dependence of the coercive field in ferroelectric ceramics[4], [13]. For samples poled at a constant electric field amplitude of 0.5 kV/mm, increasing the temperature of poling from 25°C to 125°C increases the d_{33} from 11 pC/N to 155 pC/N. At room temperature, increasing the poling field from 0.5 kV/mm to 2 kV/mm increased the d_{33} from 11 pC/N to 385 pC/N, respectively. Thus, for the conditions explored in the current work and for this PZT composition, the direct longitudinal piezoelectric coefficient d_{33} is monotonic with respect to temperature and electric field amplitude during poling. It is also noted that, within the explored range of

electric field amplitude and temperature, the electric field amplitude more strongly influences the measured direct piezoelectric coefficient than the poling temperatures.

3.3 Discussion

The apparent piezoelectric coefficient measured in poled ferroelectric ceramics is comprised of both intrinsic and extrinsic contributions. The intrinsic piezoelectric effect results from the interaction of the remnant polarization with the applied electric field amplitude or mechanical stress. Examples of extrinsic contributions include 180° and non-180° domain wall motion and these mechanisms have been shown to also contribute to the apparent piezoelectric coefficient. For example, the motion of non-180° domain walls during measurement of the converse piezoelectric coefficient can result in an additional contribution to the electric-field-induced strain because the crystallographic *c* and *a* lattice parameters are interchanged for a given volume fraction of the material[26].

To more quantitatively analyze the structural origin of the apparent piezoelectric behavior measured at different poling states, the real component of the converse d_{33} coefficient, d'_{33}, is calculated from the strain measured in response to varying electric field amplitudes. A bipolar sinusoidal electric field below the amplitude required for large-scale domain switching (< 1 kV/mm) was applied to selected poled samples. The strain was measured as a function of driving electric field amplitude and an example of these measurements for one particular sample are shown in Figure 3-2. In order to calculate d'_{33} during the application of electric fields, the macroscopic peak-to-peak strain (X_{pp}) is divided by twice the applied sinusoidal electric field amplitude (E_o), i.e.

$$d'_{33} = X_{pp}/(2 \cdot E_o). \quad (3\text{-}1)$$

It can be observed that the electric-field-induced macroscopic peak-to-peak strain (X_{pp}) increases with increasing electric field amplitude. A constant (field-independent) piezoelectric coefficient would indicate that X_{pp} depends linearly on E_o, leading to a d'_{33} value that is independent of electric field amplitude. Nonlinearity in the electric-field-induced strain would be indicated by a d_{33}' value that changes with respect to E_o.

The calculated values of d'_{33} are shown in Figure 3-3 for samples obtained at selected poling conditions. In Figure 3-3(a), three different samples were poled at different conditions: one that is poled at 25°C and 1 kV/mm (i.e., minimally poled), one that is poled at 50°C and 1 kV/mm (moderately poled), and one that is poled at 100°C and 1 kV/mm (highly poled). In Figure 3-3(b), the poling electric field was varied and the poling temperature was held constant at 50°C: the poling field amplitudes applied for these samples were 0.75 kV/mm (minimally poled), 1 kV/mm (moderately poled), and 2 kV/mm (highly poled). For the results shown in Figures 3-3(a) and 3-3(b), the materials poled at different poling conditions exhibit different dependencies of d'_{33} on E_o. The materials that are minimally poled exhibit a near field-independence while the materials that are moderately and highly poled demonstrate an increasing dependence of d'_{33} on E_o.

Figure 3-4 shows the results of the polarization versus electric field measurement for the samples poled at different temperatures. Using a variant of Equation (1) to calculate the permittivity yields $\varepsilon_{33} = P_{pp}/(2 \cdot E_o)$ where ε_{33} is approximately equal to the relative permittivity and P_{pp} is the peak to peak polarization. The results show that the ε_{33} values increase relative to the increasing poling temperature.

The linear dependence of d'_{33} on E_o in the moderately and highly poled samples is further analyzed using the Rayleigh law[5]. The Rayleigh law, originally applied to ferromagnetic materials, has been useful in determining the relative extrinsic and intrinsic contributions to the piezoelectric effect in ferroelectric ceramics[4], [13], [27]. The Rayleigh law for the converse piezoelectric effect is expressed as

$$d'(E_o) = d'_{init} + \alpha_d \cdot E_o, \quad (3\text{-}2)$$

where the real value of the piezoelectric coefficient, d', can be expressed as a function of the applied electric field E_o. The Rayleigh coefficient (α_d) in Eq. 2 is a quantitative measure of the irreversibility of non-180° domain wall displacement and describes the field dependence of the piezoelectric coefficient. Moreover, the quantity $\alpha_d \cdot E_o$ describes the absolute extrinsic contribution due to the irreversible displacement of domain walls in the unit pm/V. The total piezoelectric coefficient, d', is the sum of this irreversible extrinsic contribution, $\alpha_d \cdot E_o$, and the reversible plus intrinsic contribution, d'_{init}. If $d'(E_o)$, d'_{init}, and α_d in Equation 2 are replaced by $\varepsilon_{33}(E_o)$, ε_{init}, and α, respectively, Equation 2 then represents the Rayleigh law for permittivity. In this case, the slope α represents the irreversible 180° domain wall displacement and describes the field dependence of the permittivity, and ε_{init} describes the intrinsic and reversible contribution of permittivity.

A linear fit for the values of d_{33}' was obtained for samples of different poling conditions. The slope of each line yields α_d for that particular poling condition and the y-axis intercept yields d'_{init}. The extracted α_d and d'_{init} values are reported in the inset of Figures 3-3(a) and 3-3(b) for the samples poled to different poling strengths. Table 3-1 also reports these values and the resulting values of $\alpha_d \cdot E_o$ for two different driving electric field strengths, E_o=500 V/mm and 900 V/mm. For the samples in Figure 3-3(a)

which were all poled at the same electric field amplitude (1 kV/mm) but different temperatures, the samples that were originally poled at a higher temperature had a larger absolute extrinsic contribution due to the irreversible displacement of domain walls ($\alpha_d \cdot E_o$) than the samples originally poled at lower temperatures. The trend in d_{init}', which includes contributions from the reversible displacement of domain walls and the intrinsic piezoelectric coefficient, correlates with the trend in $\alpha_d \cdot E_o$. For example, the sample initially poled at 25°C at 1 kV/mm exhibits a d'_{init} value of 96 pm/V and $\alpha_d \cdot E_o$ values between 10 and 18 pm/V while the sample poled at a higher temperature exhibits higher d'_{init} and $\alpha_d \cdot E_o$ values . The results in Figure 3-3(b) show a corresponding trend: the samples that are poled at higher electric fields exhibit values of d'_{init} and $\alpha_d \cdot E_o$ that are both greater than those obtained from samples poled at lower electric fields. Because the absolute extrinsic contribution due to the irreversible displacement of domain walls increases in samples poled at both higher temperatures and higher electric field amplitudes, the observed trends in nonlinearity are a demonstrated function of the poling state in the given material, not solely a function of one independent poling variable (e.g., temperature or electric field amplitude). The d_{33} results indicate that irreversible domain wall displacements increase when the materials are more highly poled.

For the permittivity measurements at constant field, α and ε_{init} values were calculated by fitting the datasets in Figure 3-4 to lines and calculating the slope and intercept, respectively. Both α and ε_{init} increase with poling temperature. The increase in both Rayleigh parameters suggests an increase in both the irreversible 180° domain wall motion and an increase in the intrinsic and reversible contribution to permittivity

from the motion of 180° domain walls. These results suggest that at the conditions tested, the irreversible and intrinsic reversible contribution to permittivity increases as poling temperature increases.

Possible mechanisms for this increase in degree of irreversible domain wall displacement and its contribution to the piezoelectric coefficient are now discussed. Because pinning centers are the primary impediment to irreversible domain wall motion, a change in the type or distribution of pinning centers is likely associated with such behavior. Since an increase in the contribution of irreversible domain wall motion is observed in materials that are highly poled, the energy required for a domain wall to irreversibly traverse a pinning center is likely reduced. This would enable a domain wall to displace a greater distance under the same driving electric field amplitude in a highly poled sample than in a minimally or moderately poled sample. Possible microstructural origins of such behavior in materials that are more highly poled may include dissociation or de-clustering of defect dipoles or complexes, a redistribution of trapped charge, or a reduction in domain wall density associated with poling that would reduce domain wall to domain wall interactions [28–30]. The increase in 180° domain wall motion with increased poling temperature could also be contributing to the piezoelectric effect by further changing the energy landscape of the materials during poling (e.g. possibly affecting defect dipoles or trapped charges). Additionally, Trolier-McKinstry et al. have proposed a model for how the electric field-induced movement of 180° domain walls contributes to the total strain through a dynamic poling process [27].

3.4 Conclusions

Because all piezoelectric ceramic materials require poling to exhibit a macroscopic piezoelectric effect, the present work has implications to a significant number of different

material systems. Measurements such as those presented in the present work will be useful to examine in other material systems to determine in which material systems the trends observed in the present work are demonstrated. Such investigations may provide more evidence regarding the microstructural origin of the observed trends and the universality of the behavior.

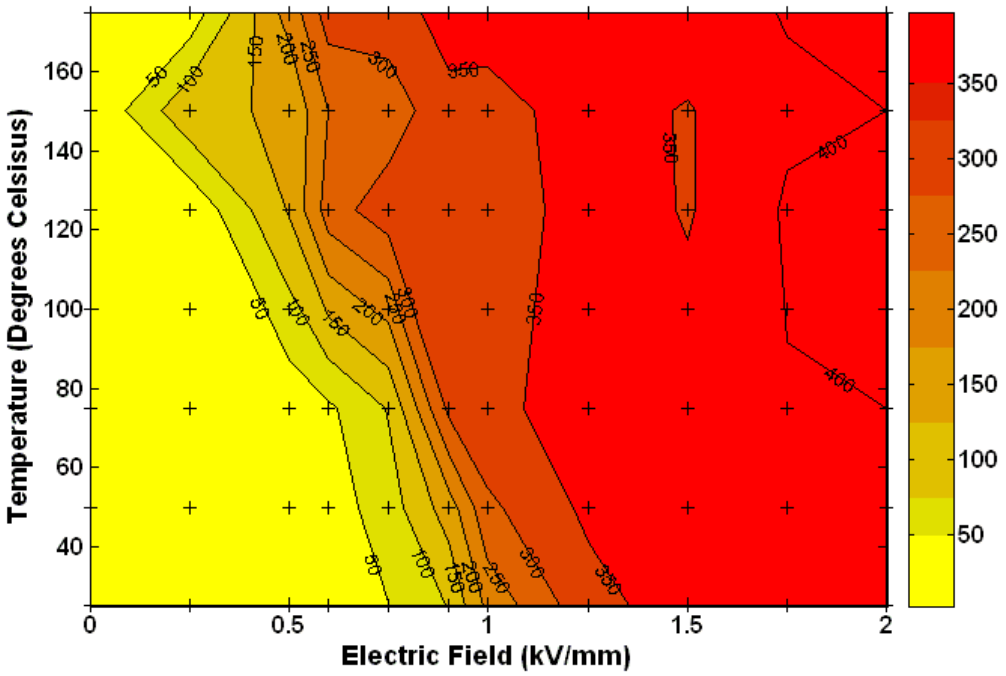

Figure 3-1. Measured direct piezoelectric coefficient, d_{33}, as a function of the electric field amplitude and temperature during poling. The "+" symbols indicate the temperature and electric field amplitude at which the samples were poled.

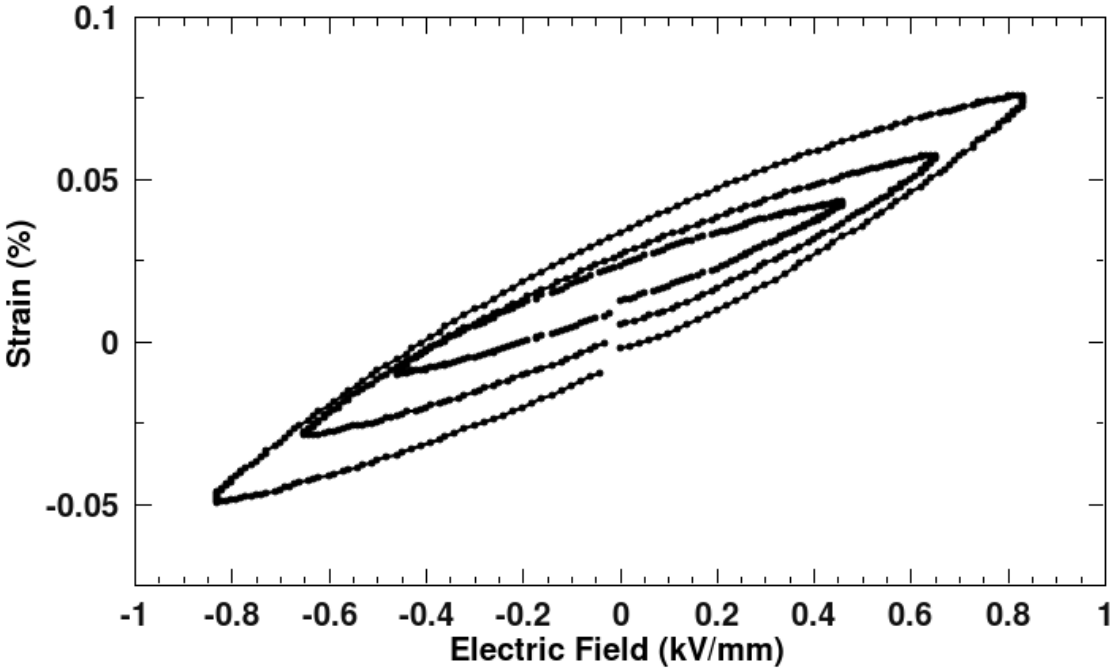

Figure 3-2. Representative electric -field-induced strain of a sample poled at 175°C and 1 kV/mm for three different electric field amplitudes, E_o.

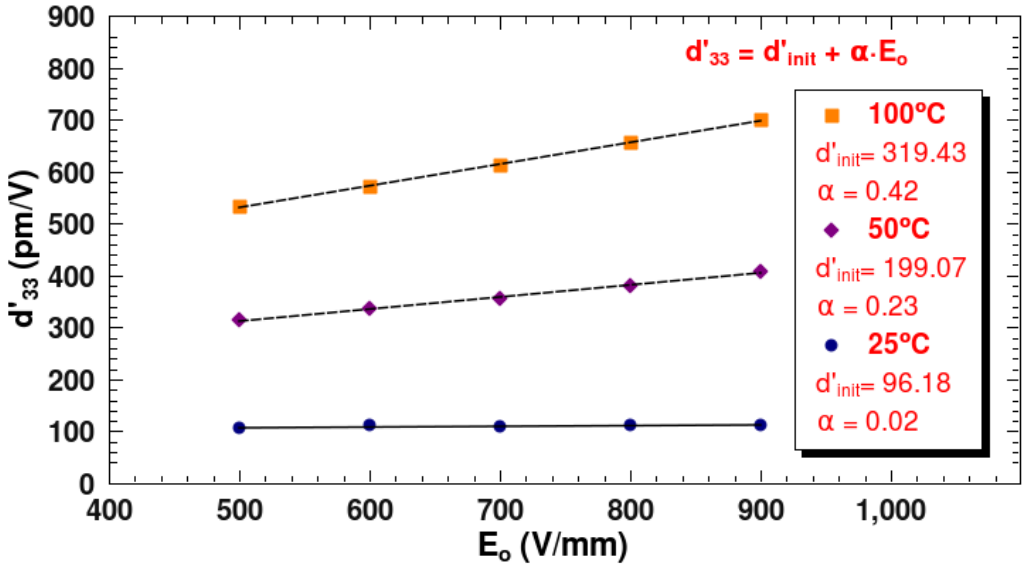

A

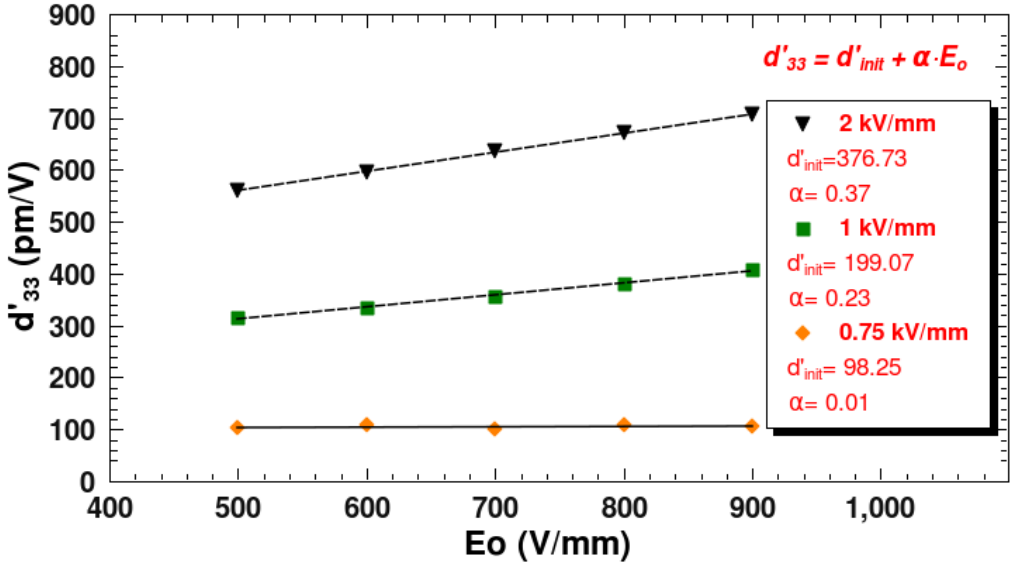

B

Figure 3-3. The influence of E_o on d'_{33} for samples poled at various conditions. A) Three samples poled at the same electric field amplitude (1 kV/mm) but differing temperatures (25°C, 50°C, and 100°C). B) Three samples poled at the same poling temperature (50°C) but differing electric field amplitudes (0.75, 1.0, and 2.0 kV/mm). The lines represent a linear fit to the data for each respective sample.

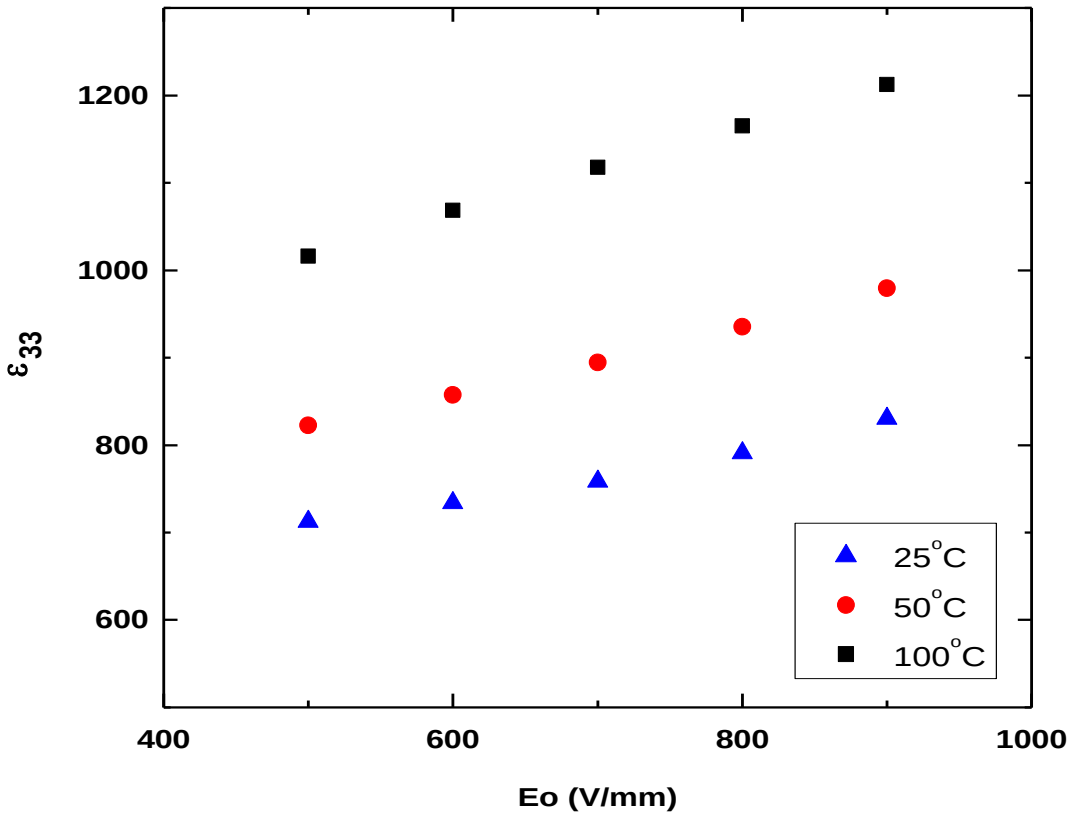

Figure 3-4. The influence of E_o on ε_{33} for three samples poled at the same electric field amplitude (1 kV/mm) but differing temperatures (25°C, 50°C, and 100°C).

Table 3-1.Values of α_{cp}, d'_{init}, and $\alpha_{cp} \cdot E_o$ for samples poled at different poling conditions.

Poling Temperature [°C]	Poling Field [kV/mm]	d'_{init} [pm/V]	α_{cp} [(pm/V)(V/mm)]	$\alpha_d \cdot E_o$ [pm/V] E_o=500 V/mm	E_o=900 V/mm
25	1.0	96.18	0.02	10	18
50	1.0	199.07	0.23	115	207
100	1.0	319.43	0.42	210	378
50	0.75	98.25	0.01	5	9
50	1.0	199.07	0.23	115	207
50	2.0	376.73	0.37	185	333

Table 3-2.Values of α, ε_{init}, and $\alpha / \varepsilon_{init}$ for samples poled at different poling conditions.

Poling Temperature [°C]	Poling Field [kV/mm]	α_ε [mm/V]	ε_{init}	$\alpha/\varepsilon_{init}$ [mm/V]
25	1.0	0.293	560	5.23E-4
50	1.0	0.391	624	6.27E-4
100	1.0	0.489	773	6.33E-4

CHAPTER 4
FIELD AND FREQUENCY DEPENDENCE OF CONVERSE d_{33}

In this chapter the extrinsic contribution to piezoelectric properties of a material is studied by taking strain versus electric field hysteresis measurements and calculating the converse piezoelectric response. The results are examined in the context of how the materials were poled. Some of the extrinsic contributions to piezoelectricity are calculated and discussed as well as the intrinsic and reversible contributions.

4.1 Experimental Procedure

4.1.1 Electrical Poling and Converse d_{33} Measurements

The samples were prepared by sputter coating gold electrodes on the parallel faces of the commercial PZT ceramics of designation K350 (Piezo Technologies, Indianapolis, IN, USA) with sample dimensions of 4 mm x 3.5 mm x 1 mm (±0.01 mm. Electrodes were placed on parallel sides of the longest dimension. The various samples were poled at a constant poling time of 5 minutes and electric field amplitudes from 0.75-2 kV/mm and constant temperatures from 25-100°C in a silicone oil bath. The poling conditions are listed in table 4-1. The samples were poled using a high voltage source (Matsusada, AU-30P1). The samples were first connected to electrodes with the power supply turned off then the specified electric field was applied at constant temperature. The electric field was then set to zero and the connection was shorted to ground. The samples were then subsequently removed from the oil bath. All subsequent measurements were taken at least 24 hours after poling.

4.1.2 Strain Hysteresis Measurement

To determine how the degree of poling affects the extrinsic contribution to piezoelectric properties of a material, strain versus electric field hysteresis measurements were taken and the converse d_{33} response was calculated. Electric field [E=V/l] Sin waves [V = Vo sin(ωt)]of differing amplitudes 500 to 900V were used and the response of the applied electric field (Eo) vs. the measured strain (X) using a measurement system for acquisition of X-E hysteresis curves. The system was a Trek 609C-6 high-voltage amplifier driven by a Stanford Research System DS360 function generator and that could supply a maximum of 5 kV and a variable frequency. The measured signals were acquired using a Tektronix TDS410 oscilloscope connected to a computer and a National Instruments Labview program. The frequencies selected were 0.06 Hz, 0.6 Hz, and 3 Hz. A schematic of the experimental set-up can be seen in Figure 4-1 A.

4.1.3 Calculation of Rayleigh Behavior

The Rayleigh law can be used to describe the dependence of piezoelectric coefficient d' on the electric field for differently poled ferroelectric materials[5]. Originally, the Rayleigh law was applied to ferromagnetic materials, but it has been very useful in describing the relative extrinsic and intrinsic contributions to the piezoelectric behavior in ferroelectric ceramics[4][13] [14]. The Rayleigh law for the piezoelectric coefficient is expressed as

$$d'(E_o) = d'_{init} + \alpha \cdot E_o, \qquad (4\text{-}1)$$

where the real value of the piezoelectric coefficient, d', can be expressed as a function of the applied electric field E_o. The Rayleigh coefficient (α) in equation

4-1 represents a quantitative measure of the irreversibility of domain wall displacement and describes the field dependence of the piezoelectric coefficient. The absolute extrinsic contribution due to the irreversible displacement of domain walls is described by the quantity $\alpha \cdot E_o$. Examples of extrinsic contributions could include 180° and non-180° domain wall motion. The total piezoelectric coefficient, d', is the sum of an irreversible extrinsic contribution, $\alpha \cdot E_o$, and the reversible plus intrinsic component d'_{init}. By calculating the α coefficient values, quantitative information about the extrinsic response of a particular material can be calculated. The value of the converse d_{33} for each S-E loop can be calculated by applying the equation

$$d' = \frac{X_{pp}}{2 * E_o} \tag{4-2}$$

where X_{pp} is the peak to peak value of the Strain and E_o is the applied cycling field. Figure 4-1 B illustrates the relationship between strain and electric field.

4.2 Results

4.2.1 Effect of Electrical Poling on Piezoelectric Response

4.2.1.1 Poling field amplitude dependence of converse d_{33}

The converse piezoelectric strain response was measured as a function of electric field amplitude and is shown in Figure 4-2 A, Figure 4-2 B, and Figure 4-2 C for the samples poled at 0.75 kV/mm, 1 kV/mm and 2 kV/mm, respectively. At the conditions measured, for lower poling fields (e.g. Figure 4-2 A) the X-E loops have a much smaller slope than those measured on samples poled with higher poling fields (e.g. Figure 4-2 C). The coercive field of K350 extracted from polarization and strain measurements at room temperature is ~1 kV/mm[25].

Using equation 4-2, the d_{33} value calculated from the slope of the loops yields the points in Figure 4-3. By fitting the results to a line, the Rayleigh parameters can be calculated and are displayed in the accompanying graphs on Figure 4-4, A, and B, for the samples poled at 0.75 kV/mm, 1 kV/mm and 2 kV/mm. The values of both α and d_{init} appear to increase as higher initial poling fields are applied.

4.2.1.2 Poling temperature dependence of converse d_{33}

Figure 4-5 A, Figure 4-5 B, and Figure 4-5 C show the strain versus electric field amplitude plots for the samples poled at 1 kV/mm and temperatures of 25°C, 50°C, and 100°C, respectively. At the conditions measured, there appears to be much less variation at different temperatures compared to the amount of variation that occurred at different poling fields. Figure 4-6 shows the d_{33} values for the differently poled samples. The Rayleigh parameters for the temperature dependent measurements are shown in Figure 4-7, A, and B. The value of α at the two higher poling temperatures is lower than the initial value of α while the values of d_{init} at the higher poling temperatures is greater than the value of d_{init} at the initial temperature tested.

4.2.1.3 Converse d_{33} as a function of frequency

The converse piezoelectric coefficient measured at different frequencies is plotted as a function of electric field in Figure 4-8. An increase in the frequency dispersion of the calculated d_{33} appears to occur at higher measurement field amplitudes. Table 4-2 and Table 4-3 show additional frequency data for samples poled at different temperatures and fields, respectively.

4.3 Discussion

Figure 4-3 shows a general increase of d_{33} with poling field for all measurement conditions E_o. The Rayleigh parameters shown in Figure 4-4 demonstrate the increase of both α and d_{init} as a result of electrical poling. The value of d_{init} increases significantly, from 28 pm/V for the sample poled at 0.75 kV/mm to 230 pm/V for the sample poled at 2 kV/mm, an increase of ~85%. The increase in the value of d_{init} likely represents an increase in the amount of the intrinsic linear contribution to the material response. Additionally, for the samples poled at 0.75 kV/mm and 2 kV/mm the value α increases from 0.014 (pm/V)(V/mm) to 0.133 (pm/V)(V/mm), respectively. This represents an approximately 89% increase in the value of α. Higher degrees of electrical poling create structures that respond differently during subcoercive field application. For example, with higher poling fields a large amount of nonlinear and irreversible domain wall motion is taking place in this material. It is appears that the value of α increases slightly more with poling than the value of d_{init}. The ratio of α to d_{init} is a way of semi-quantitatively assessing nonlinear (e.g. irreversible domain wall motion) to linear (e.g. reversible domain wall motion or intrinsic piezoelectric response) response and can be seen in Figure 4-4. The values of α/d_{init} do not seem to vary greatly as a function of initial electrical poling condition.

The effect of initial poling temperature on the piezoelectric coefficient is shown in Figure 4-6 as a function of electric measurement field. The samples poled at 25°C and 50°C had very similar d_{33} values within the measurement range explored varying by less than ~5% at each electric field amplitude step. The sample poled at 100°C actually had lower d_{33} values than the other samples.

This seems inconsistent since a higher poling temperature was used and the sample would be expected to be more well poled than the samples poled at the same field and lower temperatures. A number of factors can affect how well a material is actually poled and the piezoelectric properties achieved as a result of poling. Some of these factors include chemical modification, mechanical stress, and pinning centers such as trapped charges or defects [6], [9], [10], [12]. However, temperature is a very influential parameter in the poling process since domain wall motion is thermally activated and a higher poling temperature should promote more domain reorientation and domain wall mobility, as well as higher d_{33} values [11], [31].

The α and d_{init} values for the sample poled at a constant field and different temperatures is shown in Figure 4-7. For these samples the value of d_{init} increases while the value of α decreases. This suggests that less non-linear domain wall motion is taking place in the samples poled at higher temperatures and that the degree of irreversible domain wall motion has the greatest influence on the overall d_{33} response. These result corresponds well with the work of Damjanovic and others who have suggested that the majority of the piezoelectric response in materials may come from irreversible domain wall motion [5]. Additionally, the parameter α/d_{init} seems to vary more with initial poling temperature than it did in response to poling field amplitude. Some of the possible sources of error in these results could be due to a number of factors such as the location of electrical poling or equipment resolution. All measurements were taken at sub-coercive electric fields, though the Rayleigh

region for this material may be at values less than 1/3 to 1/2 of the coercive field [32], [33].

4.4 Conclusions

In conclusion, it appears that the electric field at which materials are poled has a more significant effect on increasing the converse piezoelectric coefficient than poling temperature does. Additionally, through calculation of Rayleigh parameters it has been demonstrated that the irreversible non-linear response of materials has the greatest impact on the resulting d_{33}.

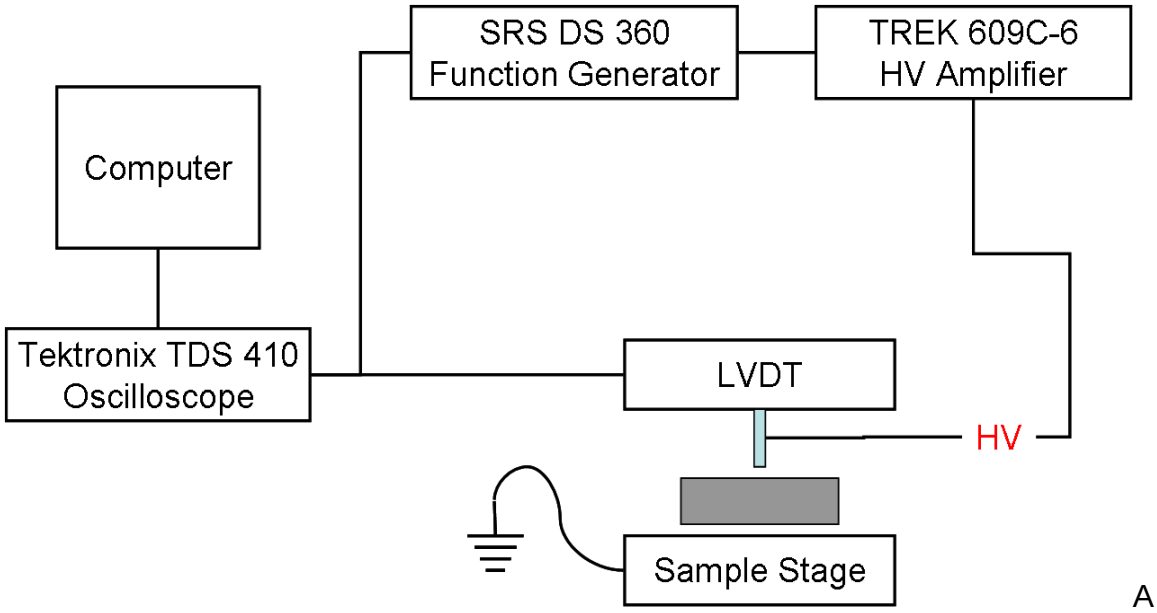

A

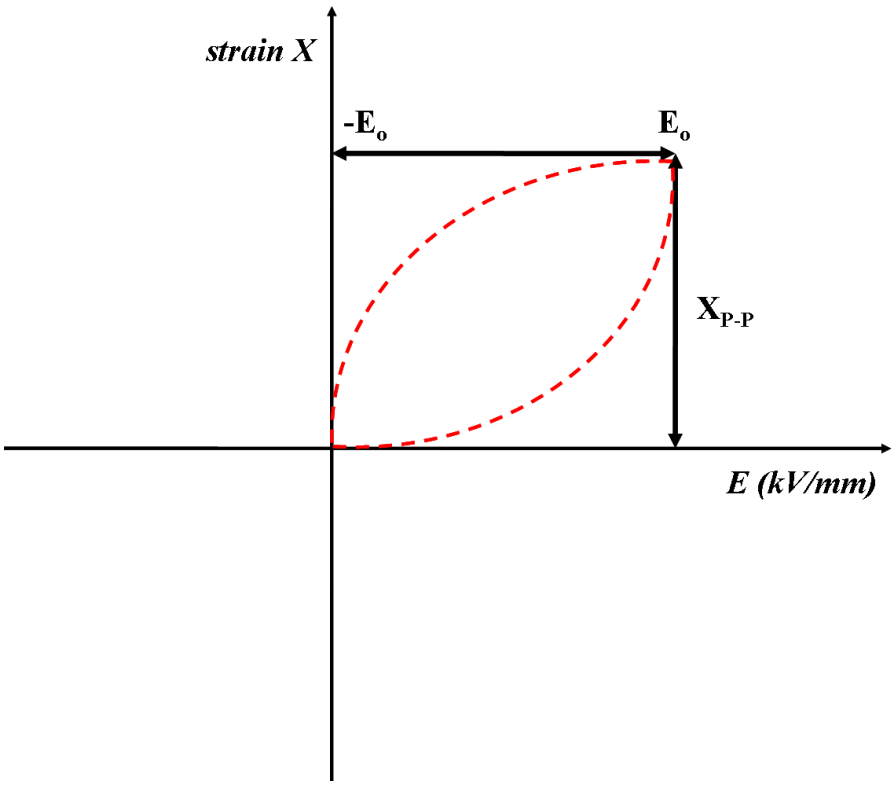

B

Figure 4-1. Experimental Set-up For Strain Measurments. A.) Strain Hysteresis Measurement System Schematic B.) The piezoelectric coefficient d_{33} was calculated using the measured peak-to-peak longitudinal strain, indicated as $X_{p\text{-}p}$, using equation 4-3.

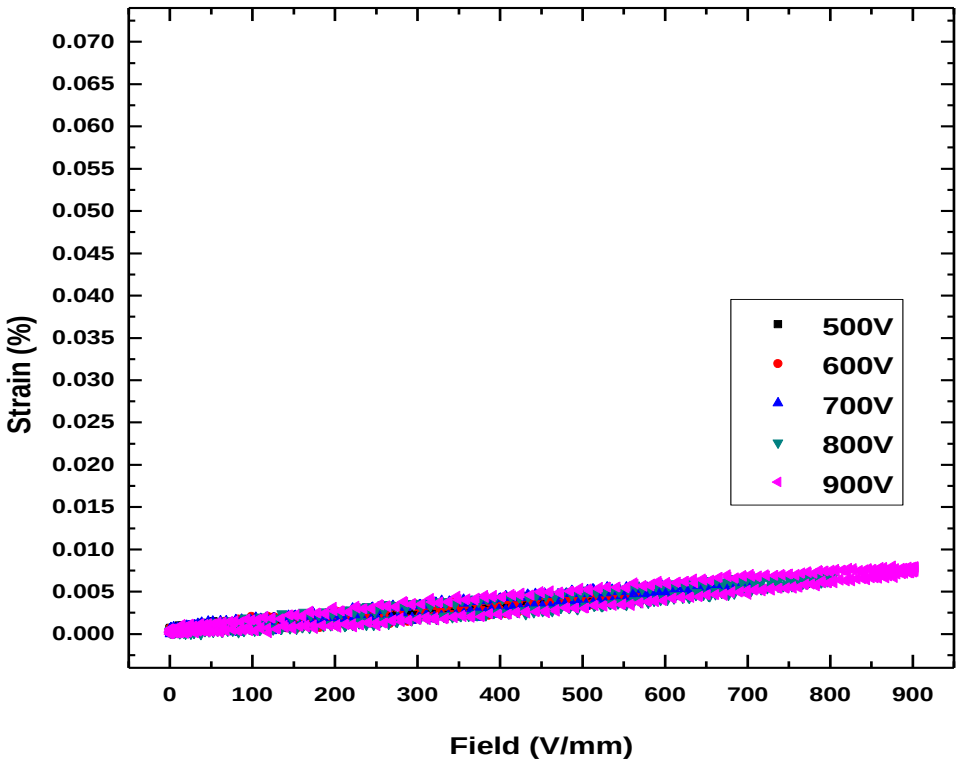

A

Figure 4-2. K350 poled at various poling conditions. A) 0.75 kV/mm, B) 1 kV/mm, and C) 2 kV/mm all at 50°C

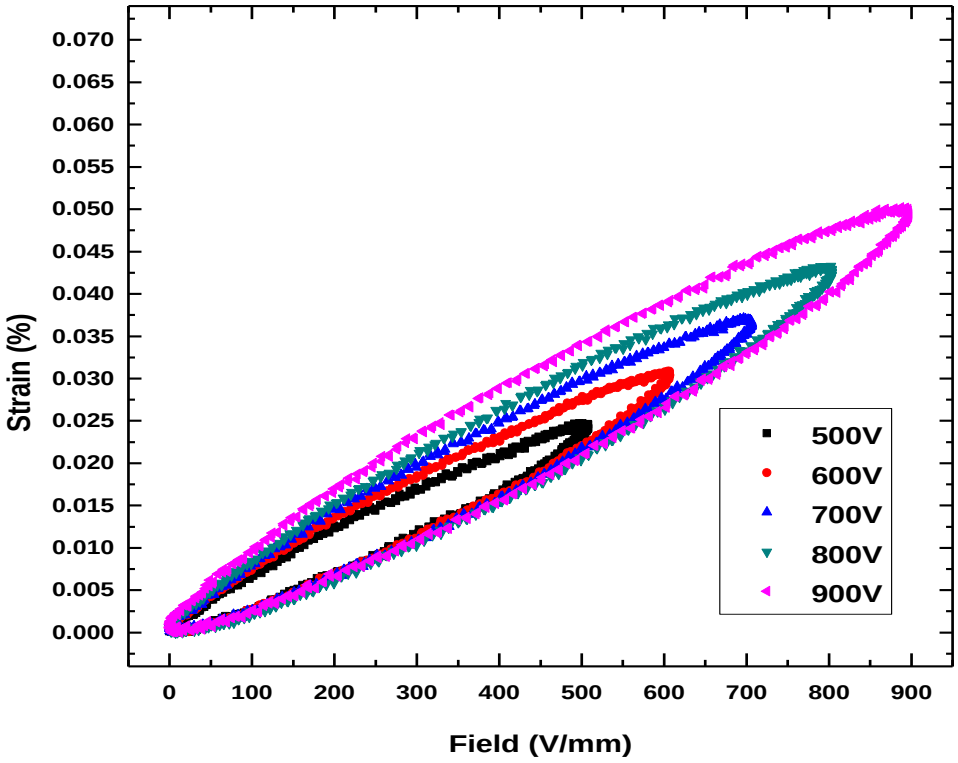

B

Figure 4-2. Continued

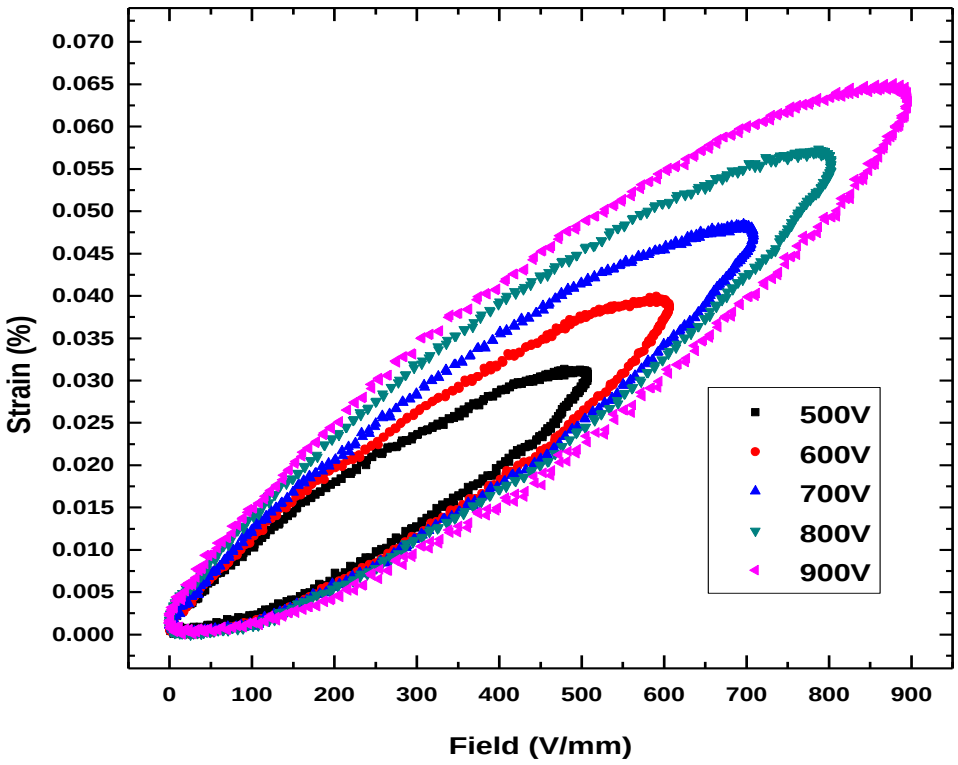

C

Figure 4-2. Continued

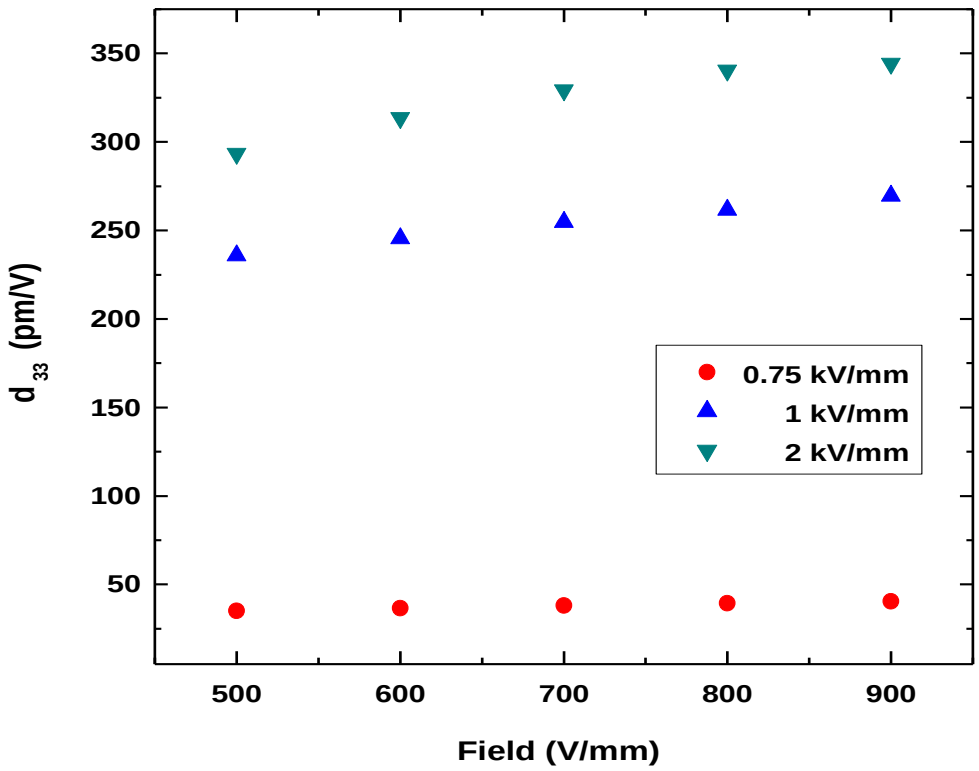

Figure 4-3. Converse piezoelectric coefficients of K350 PZT as a function of applied sinusoidal electric field amplitudes for the samples poled at a field of 0.75 kV/mm, 1 kV/mm, and 2 kV/mm and at a temperature of 50°C

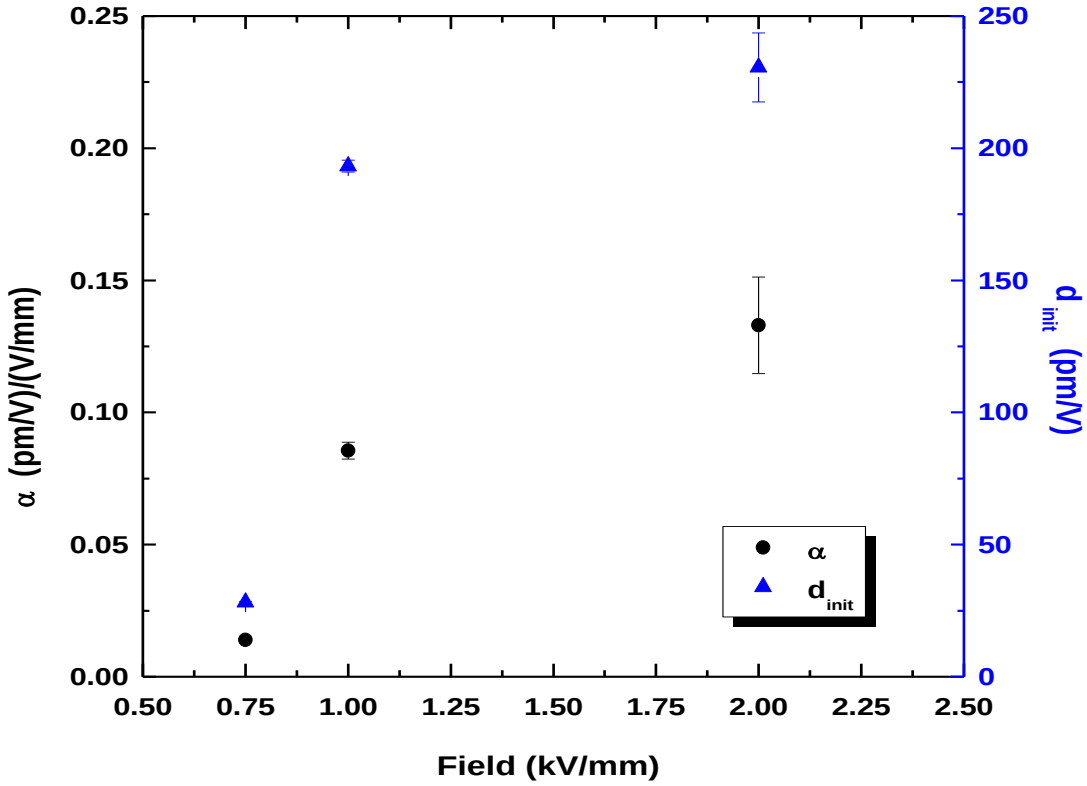

A

Figure 4-4. Values for α and d_{init} calculated for K350 poled at a constant temperature of 50°C and at electric field amplitudes of 0.75 kV/mm, 1 kV/mm, and 2 kV/mm.

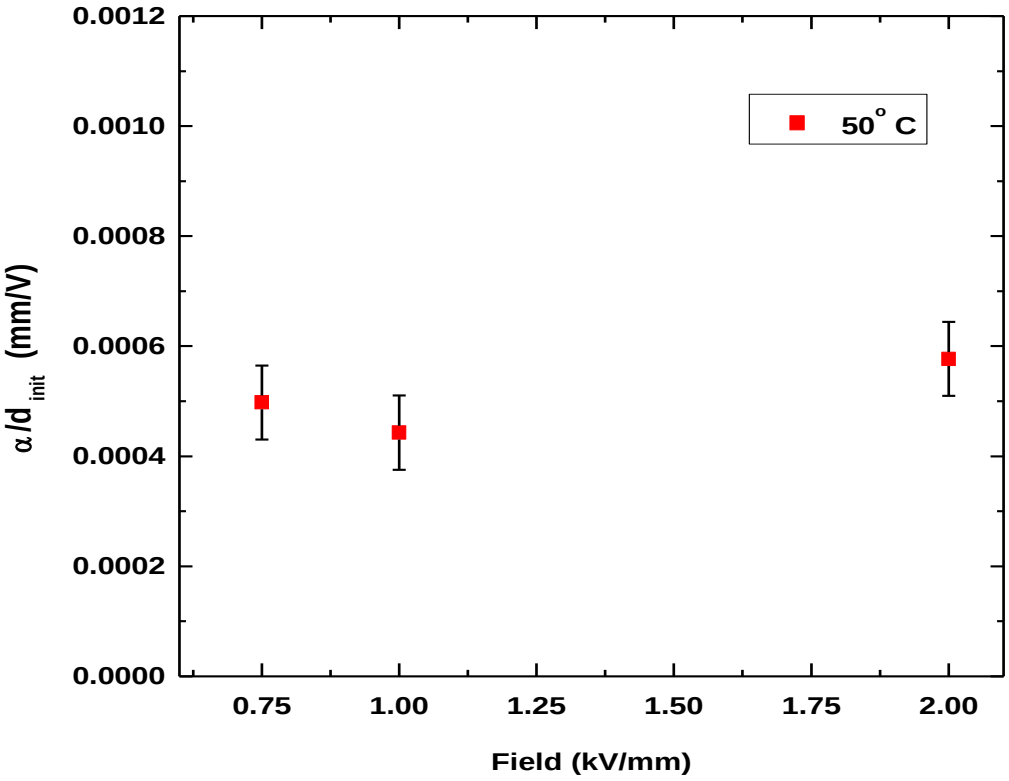

B

Figure 4-4. Continued

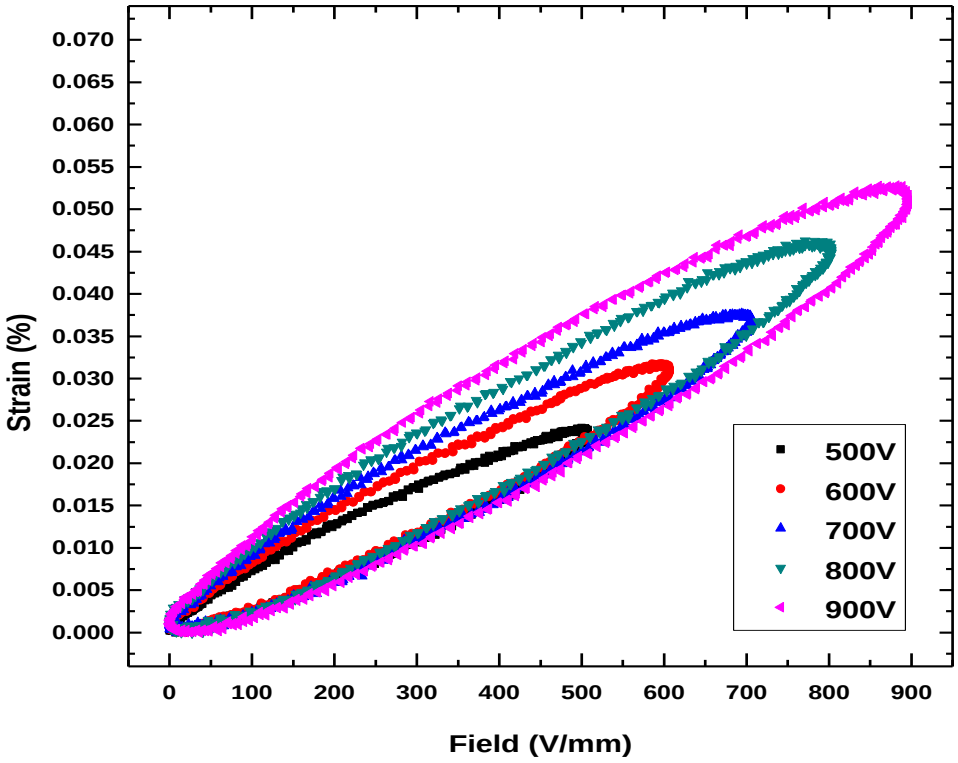

A

Figure 4-5. K350 poled at a field of 1 kV/mm and at temperatures of A) 25°C B) 50°C and C) 100°C.

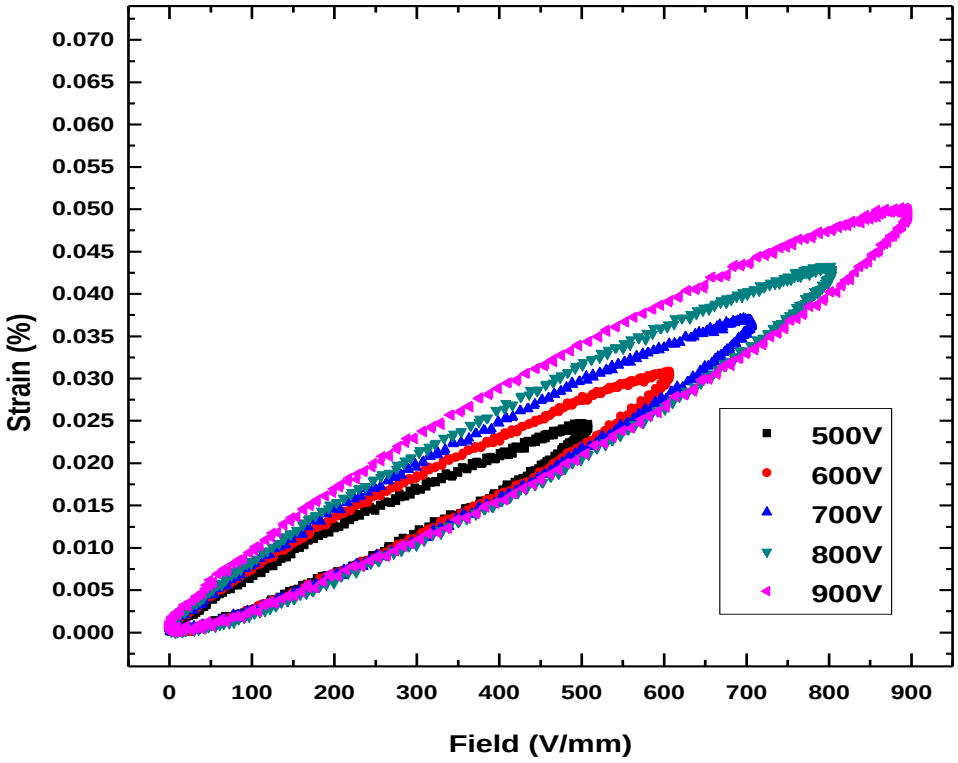

B

Figure 4-5. Continued

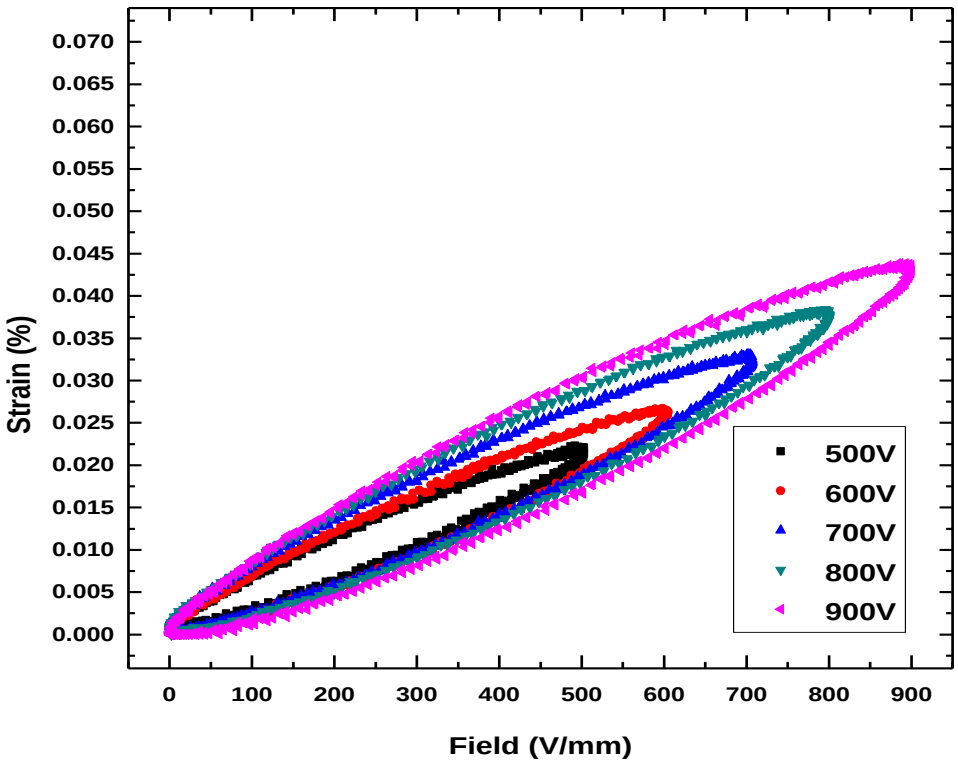

C

Figure 4-5. Continued

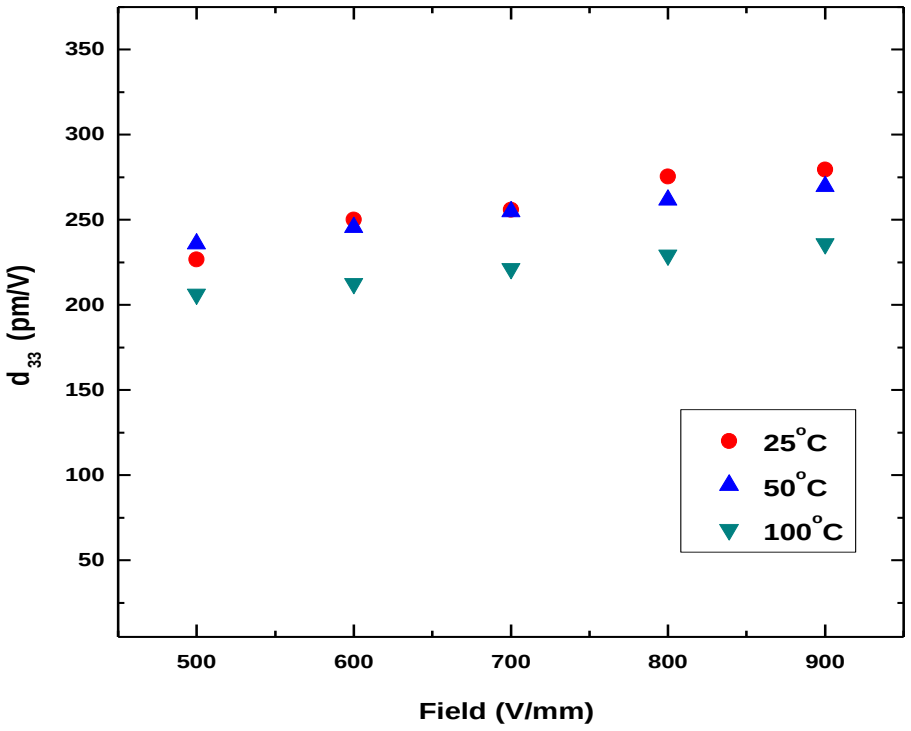

Figure 4-6. Converse piezoelectric coefficients of K350 PZT as a function of applied sinusoidal electric field amplitudes for the samples poled at temperatures of 25°C, 50°C, and 100°C and at the same poling field of 1 kV/mm.

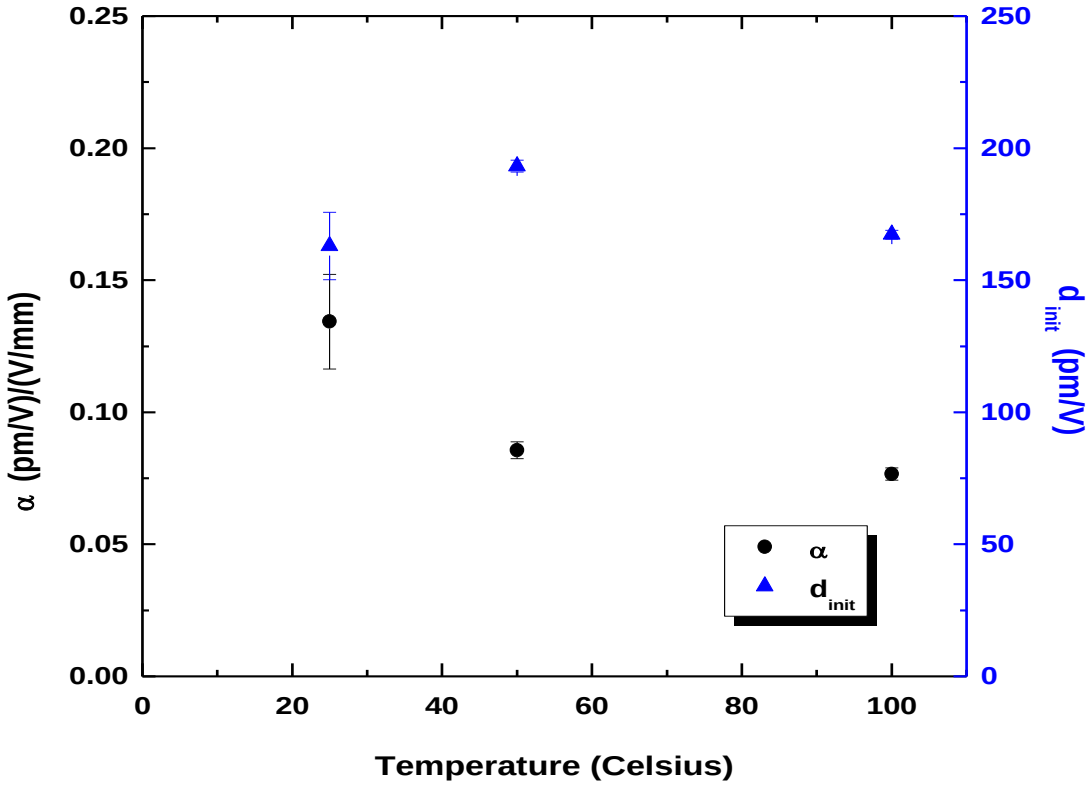

A

Figure 4-7. Values for α and d_{init} calculated for K350 poled at a constant electric field amplitude of 1 kV/mm and temperatures of 25°C, 50°C, and 100°C.

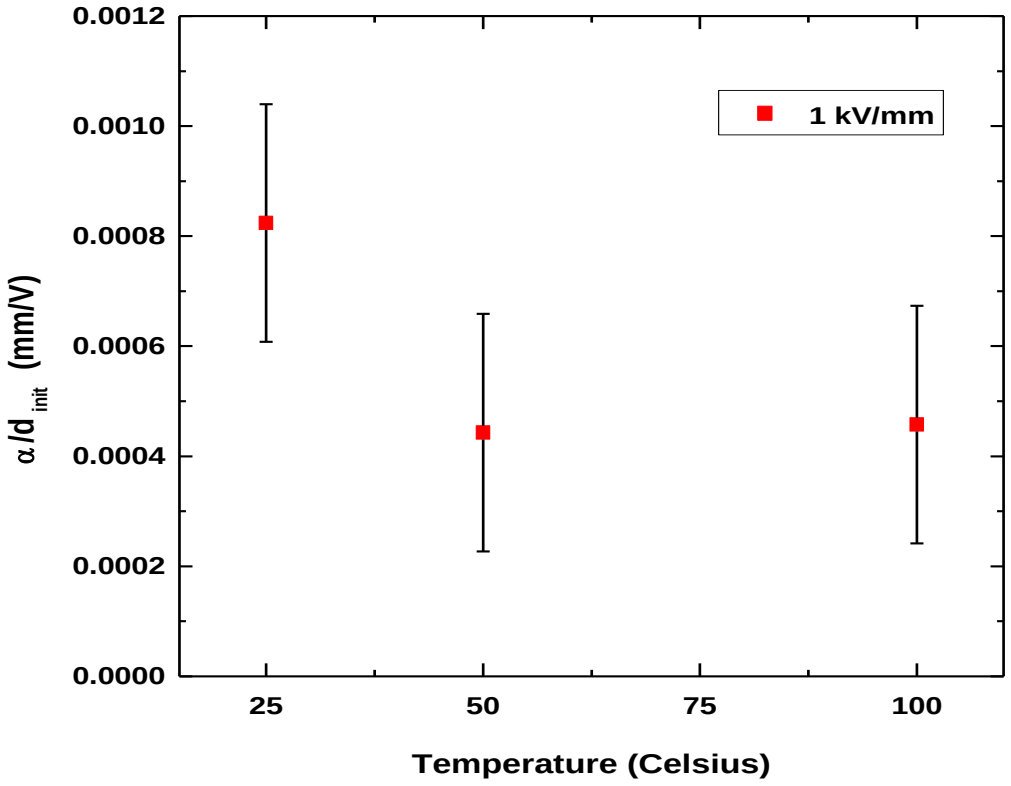

B

Figure 4-7. Continued.

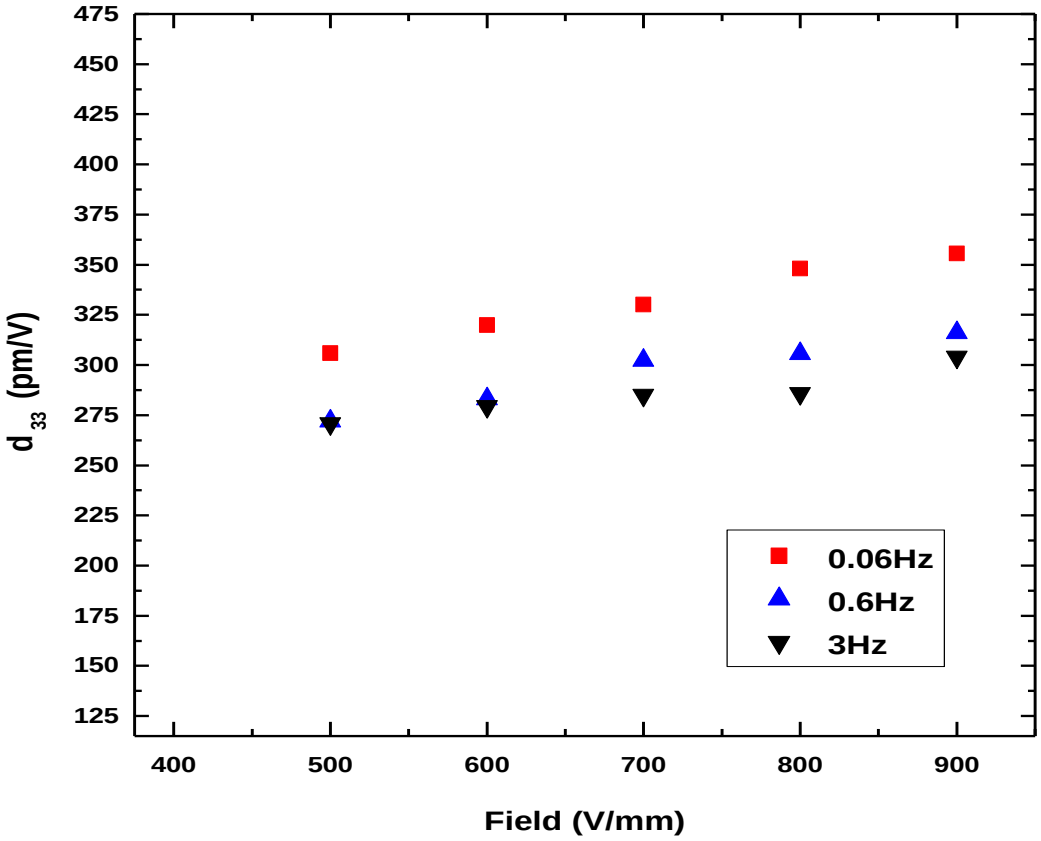

Figure 4-8. Converse piezoelectric coefficients of K350 PZT as a function of applied sinusoidal electric field amplitudes for frequencies of 0.06 Hz, 0.6 Hz, and 3 Hz. The sample was poled at temperatures of 25°C and at a poling field of 2 kV/mm.

Table 4-1. List of Measured Samples and Electrical Poling Conditions

Sample Designation	Poling Field (kV/mm)	Poling Temperature (°C)
K350	1	100
K350	0.75	50
K350	1	50
K350	2	50
K350	0.75	25
K350	1	25
K350	2	25

Table 4-2. K350 Values of α, d_{init}, and $α/d_{init}$ for samples poled at different poling conditions. Poling field was 1 kV/mm.

Frequency [Hz]	25 [°C]			50 [°C]			100 [°C]		
	α (pm/V) /(V/mm)	d_{init} pm/V	$α / d_{init}$ mm/V	α (pm/V) /(V/mm)	d_{init} pm/V	$α / d_{init}$ mm/V	α (pm/V) /(V/mm)	d_{init} pm/V	$α / d_{init}$ mm/V
0.06	0.147	179	8.2E-4	0.079	223	3.5E-4	0.081	198	4.1E-4
0.6	0.102	206	5.0E-4	0.075	215	3.5E-4	0.083	180	4.6E-4
3	0.134	163	8.2E-4	0.086	193	4.4E-4	0.077	167	4.6E-4

Table 4-3. K350 Values of α, d_{init}, and $α/d_{init}$ for samples poled at different poling conditions. Poling field was 50°C.

Frequency [Hz]	0.75 [kV/mm]			1 [kV/mm]		
	α (pm/V)/(V/mm)	d_{init} pm/V	$α / d_{init}$ mm/V	α (pm/V)/(V/mm)	d_{init} pm/V	$α / d_{init}$ mm/V
0.06	0.013	34	3.7E-4	0.079	223	3.5E-4
0.6	0.015	30	5.0E-4	0.075	215	3.5E-4
3	0.014	28	5.0E-4	0.086	193	4.4E-4

CHAPTER 5
FIELD AND FREQUENCY DEPENDENCE OF PERMITTIVITY

The experiments in this chapter were intended to determine how the degree of poling affects the extrinsic contribution to dielectric properties of a piezoelectric material by taking polarization versus electric field hysteresis measurements and calculating the dielectric response. Some of the extrinsic contributions to permittivity are calculated and discussed as well as the intrinsic and reversible contributions.

5.1 Experimental Procedure

5.1.1 Electrical Poling Conditions

The samples were prepared by sputter coating gold electrodes on the parallel faces of the commercial PZT ceramics of designations K350 (Piezo Technologies, Indianapolis, IN, USA) and EC65 (EDO Ceramics Inc., Salt Lake City, Utah, USA) with sample dimensions of 4x3.5x1 mm (±0.01 mm) and 5x5x1 mm (±0.01 mm), respectively. For both types of samples, electrodes were placed on parallel sides of the longest dimension. The various samples were poled at a constant poling time of 5 minutes and electric field amplitudes from 0.75-2kV/mm and at constant temperatures from 25-100°C in a silicone oil bath. The poling conditions are listed in table 5-1. The samples were poled using a high voltage source (Matsusada, AU-30P1). The samples were first connected to electrodes with the power supply turned off then the specified electric field was applied at constant temperature. The electric field was then set to zero and the connection was shorted to ground. The samples were then subsequently removed from the oil bath. All subsequent measurements were taken at least 24 hours after poling.

5.1.2 Polarization Hysteresis Measurement

To determine how the degree of poling affects the extrinsic contribution to dielectric properties of a material, polarization versus ac electric field hysteresis measurements were taken and the dielectric permittivity ε_{33} response was calculated. Electric field [E=V/l] sine waves [$V = V_o \sin(\omega t)$] of differing amplitudes ranging from 200 V to 900 V were used and the response was measured. The measurements were taken at different frequencies. The applied electric field E_o vs the polarization P was measured using a measurement system for acquisition of P-E hysteresis curves. The frequencies selected were 0.6Hz, 3Hz, 50Hz, and 500Hz.

5.1.3 Calculation of Rayleigh Behavior

The Rayleigh law can be used to describe the dependence of dielectric permittivity ε' on the electric field for differently poled ferroelectric materials[5]. Originally, the Rayleigh law was applied to ferromagnetic materials, but it has been very useful in describing the relative extrinsic and intrinsic contributions to the piezoelectric behavior in ferroelectric ceramics [4],[13],[14]. The Rayleigh law for dielectric permittivity is expressed as

$$\varepsilon'(E_o) = \varepsilon'_{init} + \alpha \cdot E_o, \qquad (5\text{-}1)$$

where the real value of the dielectric permittivity, ε', can be expressed as a function of the applied electric field E_o. The irreversible Rayleigh coefficient (α) in equation 5-1 represents a quantitative measure of the irreversibility of domain wall displacement and describes the field dependence of the dielectric permittivity (α). The absolute extrinsic contribution due to the irreversible displacement of domain walls is described by the quantity $\alpha \cdot E_o$. Examples of

extrinsic contributions could include 180° and non-180° domain wall motion. The total dielectric permittivity, ε', is the sum of an irreversible extrinsic contribution, $\alpha \cdot E_o$, and the reversible plus intrinsic component ε'_{init}. By calculating the α coefficient values, quantitative information about the extrinsic response of a particular material can be calculated. The value of ε' for each P-E loop can be calculated by applying the equation

$$\varepsilon' = \frac{P_{pp}}{2 * E_o} \tag{5-2}$$

where P_{pp} is the peak to peak value of the polarization and E_o is the applied cycling field. All permittivity values reported here are relative to vacuum (i. e. $\varepsilon_{33} = \varepsilon'/\varepsilon_o$).

5.2 Results

5.2.1 Effect of Electrical Poling Field on Dielectric Response

5.2.1.1 Poling field amplitude dependence of permittivity

For K350, polarization was measured as a response to electric field amplitude and is shown in Figure 5-1 A, Figure 5-1 C, and Figure 5-1 E for the samples poled at 0.75 kV/mm, 1 kV/mm and 2 kV/mm, respectively. At the conditions measured, for lower poling fields (e.g. Figure 5-1 A) the P-E loops have a larger area than those measured on samples poled with higher poling fields (e.g. Figure 5-1 E). The coercive field of K350 extracted from polarization and strain measurements at room temperature is ~1 kV/mm[25]. The relevant Rayleigh region for the materials tested is likely at values less than 1/3 to 1/2 of the coercive field [32], [33]. Using equation 5-2, the relative dielectric permittivity calculated from the slope of the loops yields the points in Figure 5-2. By fitting the

results to a line, the Rayleigh parameters can be calculated and are displayed in the accompanying graphs on the right side of Figure 5-1, B, D, and F, for the K350 samples poled at 0.75 kV/mm, 1 kV/mm and 2 kV/mm, respectively. The values of ε_{init} appear to increase as higher initial poling fields are applied.

Hysteresis loops of polarization versus electric field amplitude for EC65 are shown in Figure 5-3 A, Figure 5-3 C, and Figure 5-3 E for the samples poled at 0.75 kV/mm, 1 kV/mm and 2 kV/mm, respectively. Again, it is clear that the field at which the material was poled affects the shape of the measured hysteresis loop. The coercive field for EC65 is ~ 0.8 kV/mm[18]. Again, assuming the Rayleigh region extends up to 1/3 to 1/2 of the coercive field, the Rayleigh coefficients can be calculated by fitting a line to the values of the slopes of the hysteresis loops. Figure 5-3 B, D, and F show the Rayleigh parameters for EC65 samples poled at 0.75 kV/mm, 1 kV/mm and 2 kV/mm, respectively. The α values for the EC65 samples are higher for the samples poled above the coercive field when compared to the sample poled at 0.75 kV/mm, and they seem to saturate at ~ 3.0 mm/V. A plot of the Rayleigh region and the relative dielectric permittivity calculated from the slope of the loops using equation 5-2 can be seen in Figure 5-4.

In both K350 and EC65 materials qualitative changes in the shape of the hysteresis loops can be observed for increasing poling field amplitudes. This indicates that the amplitude of the applied poling field clearly affects the behavior of the material at the cyclic voltages applied, which are generally in the operating region of these materials for many applications.

5.2.1.2 Frequency dependence of dielectric response

A graph showing the frequency response of K350 samples initially poled at a constant temperature of 50°C and initial poling field values of 0.75 kV/mm, 1 kV/mm, and 2 kV/mm can be seen in Figure 5-5. For K350, a definite decrease occurs in the calculated value of the permittivity as the measurement frequency increases for all of the poling conditions measured. Additionally, the sub-coercively poled sample (poled at 0.75 kV/mm) has the lowest permittivity values. The ε_{33} values for the samples poled at or above the coercive field for this material seem to be approximately equal for the given measurements. Figure 5-6 shows the differences in permittivity as a function of field for samples poled at different fields and measured at different frequencies.

Figure 5-7 shows the ε_{33} versus frequency plot for EC65 poled at 25°C and the given poling field amplitudes. Similarly to the behavior of K35o, EC65 exhibits a decrease in the calculated value of the permittivity as the measurement frequency increases for all of the poling conditions and the sub-coercively poled sample has the lowest permittivity values. EC65 also seems to exhibit ε_{33} values approximately equal for the given measurements. Figure 5-8 shows plots of the ε_{33} values versus measurement field at various frequencies for the different poling field amplitudes of 0.75 kV/mm, 1 kV/mm, and 2 kV/mm. All of these measurements were taken at 25°C.

5.2.2 Permittivity as a function of poling state

Table 5-2 shows the calculated values of the Rayleigh parameters for the various poling conditions of the K350 samples poled at a temperature of 50°C.

Table 5-3 shows the calculated values of the Rayleigh parameters for the various poling conditions of the EC65 samples poled at a temperature of 25°C.

5.3 Discussion

The Rayleigh region is likely 200V-400 V/mm for both EC65 and K350. Both are considered to be soft PZT and a discernable trend seems to occur. Figure 5-2 shows a general increase of ε_{33} for K350 with measurement field E_o for all poling conditions. Figure 5-4 shows similar results for EC65. For both materials, samples poled above the coercive field had ε_{33} values higher than values at the corresponding testing frequency for the samples poled at 0.75 kV/mm, below the coercive field. The 1 kV/mm and 2 kV/mm values of ε_{33} differ from each other by less than 3% for both EC65 and K350. Above 500V, the EC65 samples poled above E_c continue to only slightly vary by ~3% or less, however the K350 samples no longer seem to follow a discernable trend. This could be due solely to this measurement no longer being in the relevant region for Rayleigh like behavior, but it is possible that there was also experimental error due to poling one of the K350 samples in a different set-up than the others.

The frequency dependence of the behavior of the permittivity can be observed as values of ε_{33} decrease with increasing measurement frequencies for K350 and EC65, Figure 5-5 and Figure 5-7, respectively.

Figure 5-6 shows the frequency dispersion of the K350 samples poled at 50°C and the given poling fields. The corresponding data for the Rayleigh parameters for these plots is given in Table 5-2. The data shows that for K350, there is less frequency dependence of the total ε_{33} response for more fully poled samples. Interestingly, the α values for each poling state decrease at higher

frequencies while the ε_{init} values remain relatively constant. This suggests that the amount of irreversible domain wall motion decreases at higher frequencies, yet the reversible component is independent of frequency. The ratio of $\alpha/\varepsilon_{init}$ is a way of semi-quantitatively assessing nonlinear (e.g. irreversible) to linear response (e.g. reversible or effects of180° domain walls). Table 5-2 also shows that the ratio of $\alpha/\varepsilon_{init}$ decreases at higher degrees of poling and at higher measurement frequencies. Since α and $\alpha/\varepsilon_{init}$ both decrease and ε_{init} does not appear to change as significantly, it is likely that α, which represents the degree of irreversible domain wall motion is dominating the frequency response. It is likely that at low frequencies a lot of irreversible 180° domain walls are present which give rise to the nonlinear effects.

In the case of EC65, Figure 5-8 shows the frequency dispersion of the samples measured at 25°C and the given poling fields. For EC65, α values appear to decrease at higher frequencies, but increase or saturate at higher degrees of poling, as evidenced in Table 5-3. However, ε_{init} values are again relatively constant, indicating little change occurs in the reversible domain wall motion response of EC65 to frequency, though it is likely the intrinsic response is higher in different poling states. This trend is consistent with work by Bassiri-Gharb et al. who have shown similar trends for Rayleigh parameters in ferroelectrics as a function of frequency [34]. In contrast to K350, the value of $\alpha/\varepsilon_{init}$ increases at higher degrees of poling, though the value still decreases at higher frequencies. The dynamic poling model has been used to describe a mechanism whereby an ac electric field-induced strain can cause 180° domain

walls to contribute to the total strain of a material[27]. In K350, the Rayleigh values are roughly half of what they are for EC65. It is possible that the fact that K350 and EC65 exhibit different degrees of “softness” may mean that the excess domain wall motion is more prevalent in the softer material, EC65, causing the discrepancies in the amplitudes of the Rayleigh responses.

The results from Table 5-2 and Table 5-3 suggest that 180° (vs non-180°) domain walls may behave differently in different materials. In addition, it is likely that defect chemistry plays an important role in the material behavior as well.

5.4 Conclusions

These results suggest that EC65 and K350 have different extrinsic responses depending on how they are poled. The extrinsic response of both materials decreases at higher frequencies. Though both EC65 and K350 are commercially available soft PZT materials they exhibit different extrinsic responses as a result of the degree of poling. For K350 the value of $\alpha/\varepsilon_{init}$ decreases at higher degrees of poling yet the value increases with degree of poling for EC65.

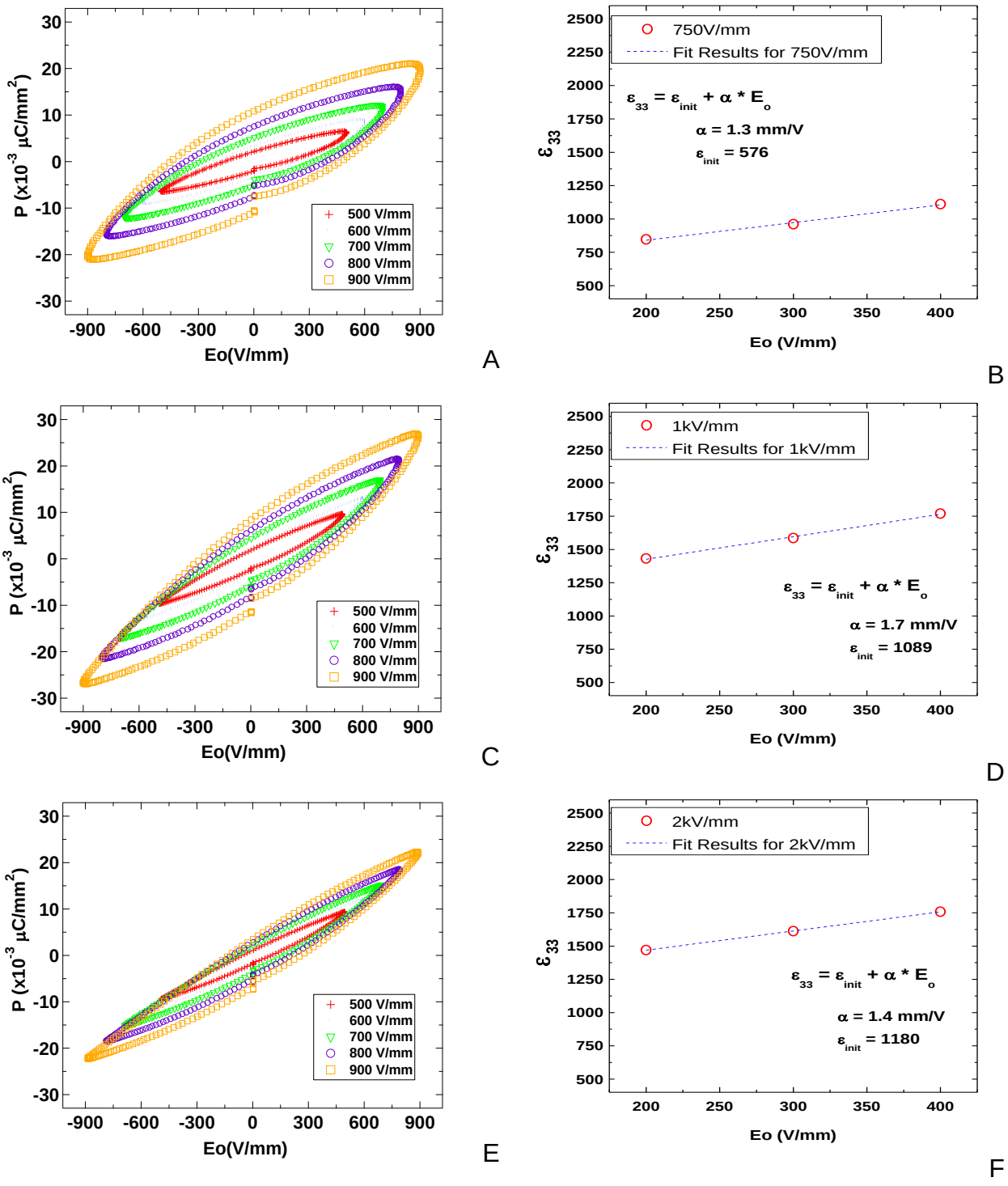

Figure 5-1. Polarization of K350 samples as a function of electric field amplitude. Figures A, C, and E represent samples poled at 0.75 V/mm, 1 kV/mm, and 2 kV/mm, respectively. The samples were all poled at 50°C and measured at a frequency of 3Hz.

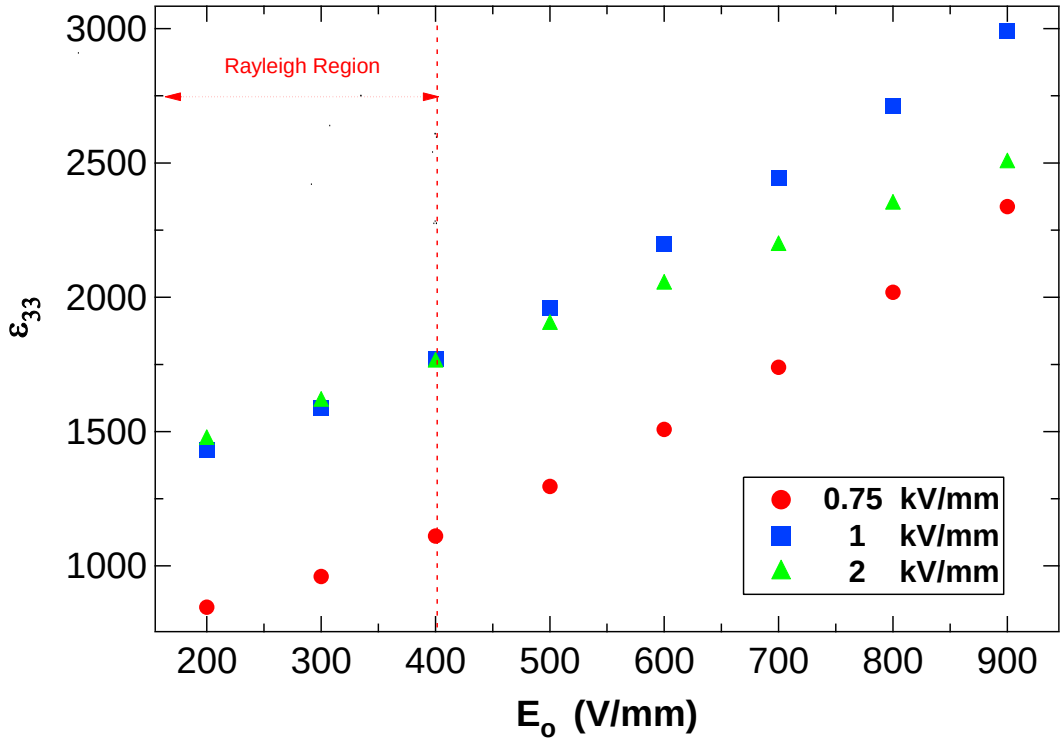

Figure 5-2. K350 poled at 50°C and measurement taken at 3Hz. Rayleigh values for differently poled samples showing the effect of poling field amplitude on the response of the material.

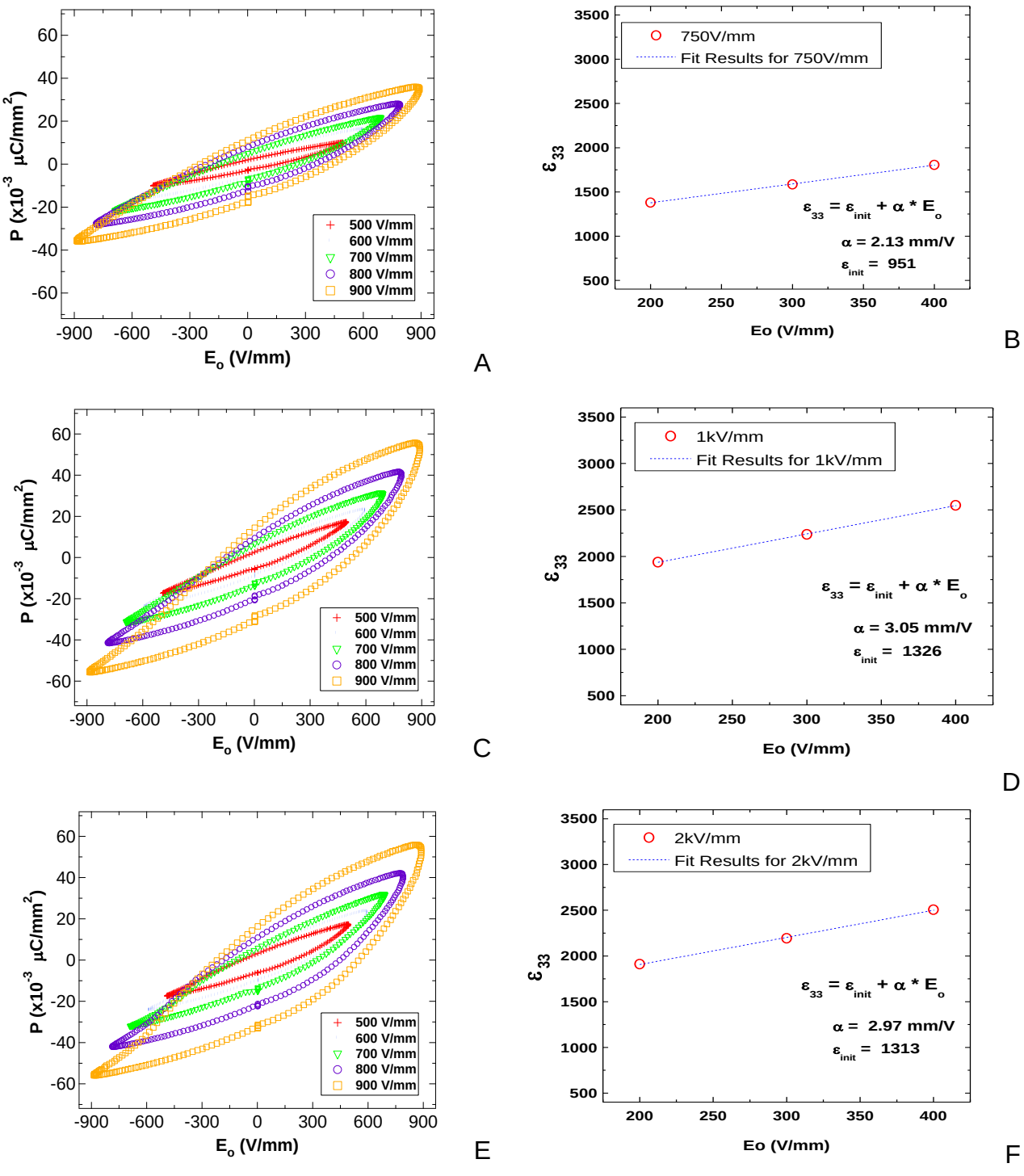

Figure 5-3. Polarization of EC65 samples as a function of electric field amplitude. Figures A, C, and E represent samples poled at 0.75 kV/mm, 1 kV/mm, and 2 kV/mm, respectively. The samples were all poled at 25°C and measured at a frequency of 3Hz.

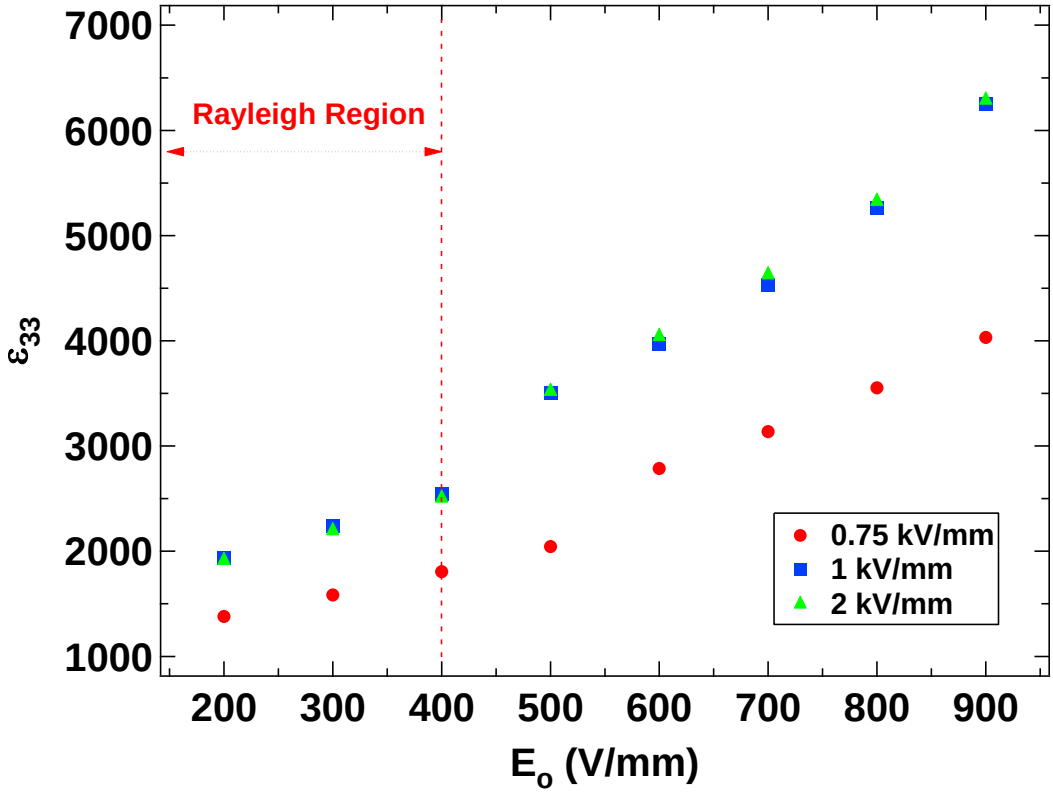

Figure 5-4. EC65 poled at 25°C and Measured at 3Hz Rayleigh values for differently poled samples showing the effect of poling field amplitude on the response of the material

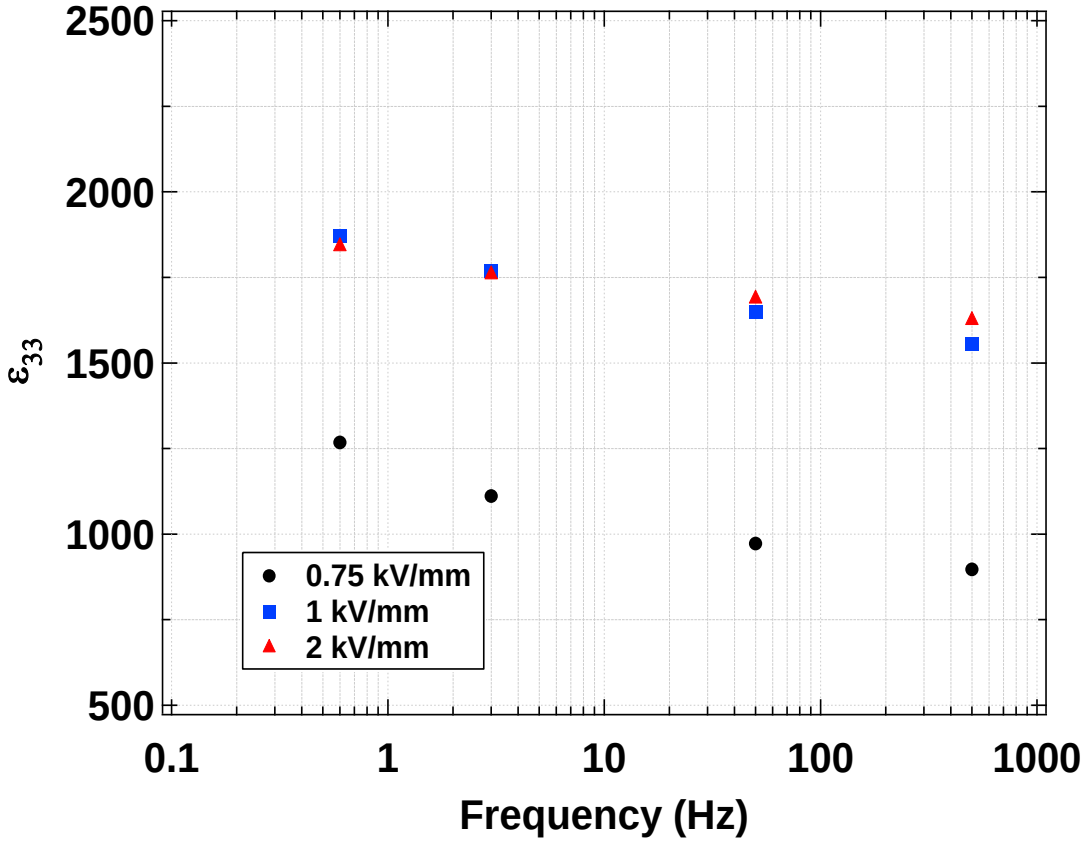

Figure 5-5. K350: Constant temperature plots showing the frequency dispersion of ε_{33} vs E_o. The samples used were initially poled at 50°C and a 400 V/mm measurement field amplitude was used.

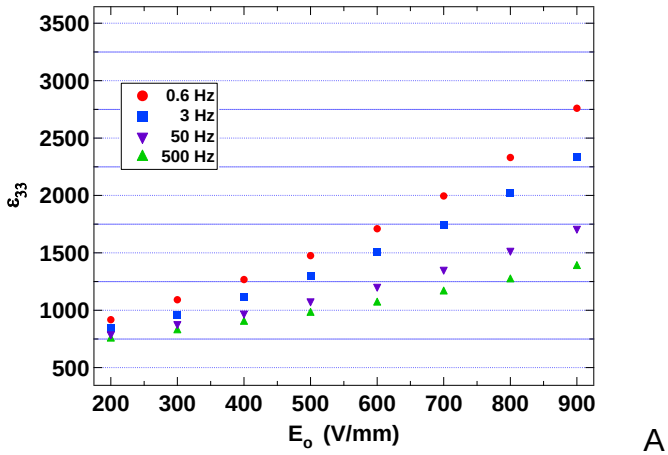

Figure 5-6. K350: Constant Temperature Plots showing the frequency dispersion of ε_{33} vs Eo. A.) 0.75 kV/mm, B) 1 kV/mm, and C.) 2 kV/mm

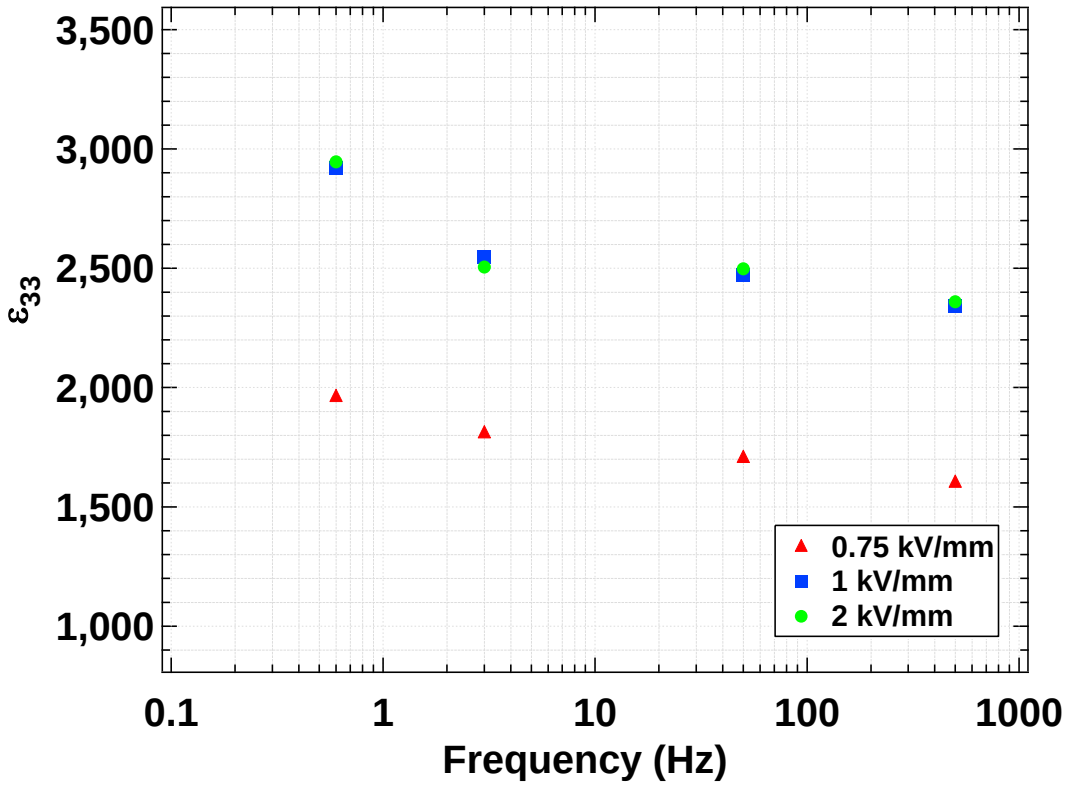

Figure 5-7. Permittivity of EC65 poled at 25°C and measured at 400V as a function of frequency. Constant Temperature Plots showing the frequency dispersion of ε_{33} vs E_o.

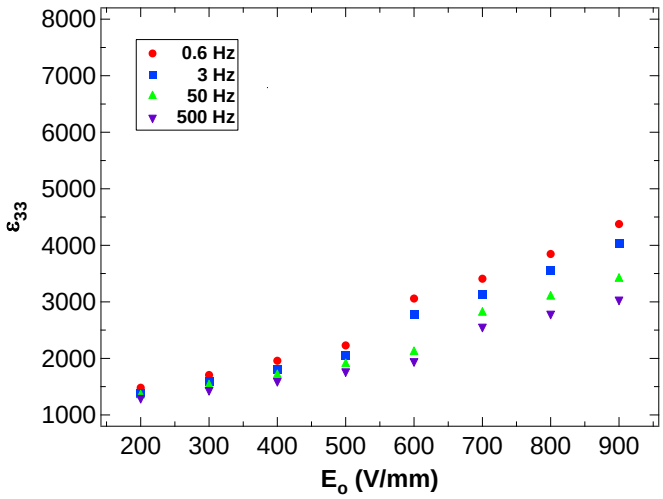

A

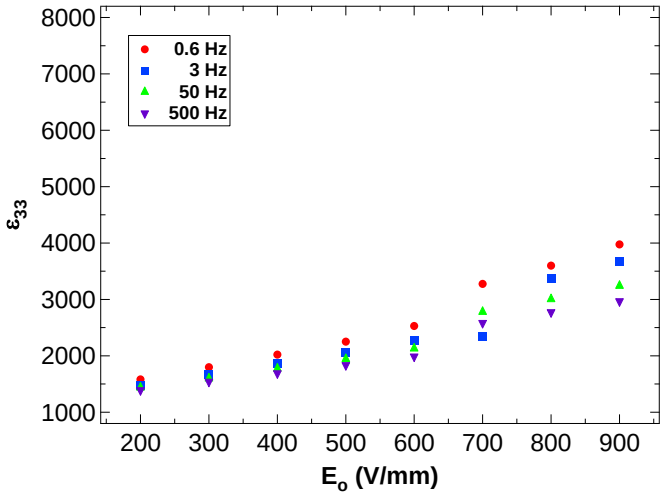

B

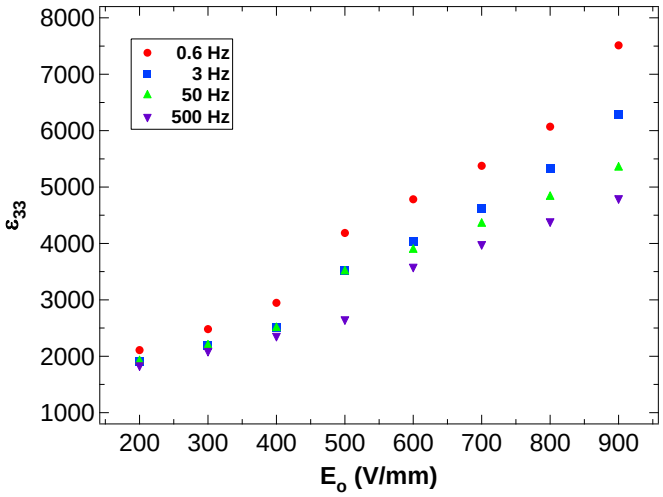

C

Figure 5-8. EC65: Constant Temperature Plots showing the frequency dispersion of ε_{33} vs E_o. A.) 0.75 kV/mm, B.) 1 kV/mm, C. 2 kV/mm.

Table 5-1. Poling conditions for the measured PZT samples.

Sample Designation	Poling Field (kV/mm)	Poling Temperature (°C)
EC65	0.75	25
EC65	1	25
EC65	2	25
K350	0.75	50
K350	1	50
K350	2	50

Table 5-2. K350 Values of α, ε_{init}, and $\alpha/\varepsilon_{init}$ for samples poled at different poling conditions. Poling temperature was 50°C.

Frequency [Hz]	0.75 [kV/mm]			1 [kV/mm]			2 [kV/mm]		
	α mm/V	ε_{init}	α / ε_{init} mm/V	α mm/V	ε_{init}	α / ε_{init} mm/V	α mm/V	ε_{init}	α / ε_{init} mm/V
0.6	1.8	567	0.0031	1.9	1110	0.0017	1.6	1217	0.0013
3	1.3	576	0.0023	1.7	1089	0.0016	1.4	1180	0.0012
50	0.9	609	0.0015	1.4	1094	0.0013	1.3	1159	0.0011
500	0.7	605	0.0012	1.2	1059	0.0012	1.2	1130	0.0011

Table 5-3. EC65 Values of α, ε_{init}, and $\alpha/\varepsilon_{init}$ for samples poled at different poling conditions. Poling temperature was 25°C.

Frequency [Hz]	0.75 [kV/mm]			1 [kV/mm]			2 [kV/mm]		
	α mm/V	ε_{init}	α / ε_{init} mm/V	α mm/V	ε_{init}	α / ε_{init} mm/V	α mm/V	ε_{init}	α / ε_{init} mm/V
0.6	2.4	998	0.0024	3.9	1360	0.0029	4.2	1257	0.0032
3	2.1	951	0.0022	3.0	1326	0.0023	3.0	1313	0.0023
50	1.8	988	0.0018	2.8	1330	0.0021	2.9	1320	0.0022
500	1.5	997	0.0015	2.4	1359	0.0018	2.6	1312	0.0020

CHAPTER 6
INFLUENCE OF MECHANICAL STRESS ON DOMAIN SWITCHING

This chapter investigates the response of domain walls to large scale stresses as a function of degree of poling. After electrical poling at various conditions, mechanical pressure was applied during *in situ* neutron diffraction measurements. The goal is to better understand the influences of electrical poling and stress on the movement of domain walls.

6.1 Experimental Procedure

6.1.1 Electrical Poling and Piezoelectric Measurements

Commercial PZT ceramic samples of designation EC65 (ITT Corporation., Salt Lake City, Utah, USA) and sample dimensions of 5x5x10mm (±0.01 mm) were sputter coated on the 5x10mm faces with gold electrodes. The samples were first connected to electrodes with the power supply switched off then the specified electric field was applied at constant temperature. The various samples were poled at different electric field amplitudes at 25°C in a silicone oil bath at a constant poling time of 5 minutes. The poling conditions and sample designations are listed in Table 6-1. The samples were poled using a high voltage source (Matsusada, AU-30P1). The electric field was then set to zero after poling and the connection was shorted to ground. The samples were subsequently removed from the oil bath. After poling, the longitudinal direct piezoelectric coefficient d_{33} was measured using a Berlincourt d_{33} meter (APC International Ltd, Mackeyville, PA, USA).

6.1.2 *in situ* Neutron Diffraction and Mechanical Compression

Neutron diffraction was used for these experiments instead of laboratory x-ray diffraction because EC65 contains lead, which neutrons can penetrate. The poled materials were mechanically loaded on the Neutron Residual Stress Mapping Facility (NRSF2) instrument, located at the High Flux Isotope Reactor (HFIR) at Oak Ridge National Laboratory. Mechanical compression was applied perpendicular to the polarization axis of each poled sample as demonstrated in Figure 6-1(a). A monochromatic neutron beam of wavelength 2.27 Å was obtained from the 311 reflection of a doubly focusing Silicon wafer monochromator [35]. The slits for the incident beam were 3 mm wide and 7.5 mm high. In this geometry, the diffraction vectors for the measured peaks are perpendicular to the direction of the applied mechanical stress and parallel to the direction of electrical polarization. The detector measures an approximate 5° 2θ range and was set to measure the pseudo-cubic (002)-type reflection between 66° and 69° for this experimental set-up. During mechanical compression, *in situ* diffraction patterns were measured on the NRSF2 instrument [36].

The loading frame [37] mounted on the diffraction instrument is shown in Figure 6-1b. An example of the stress loading profile is shown in Figure 6-1c. Diffraction patterns from the sample were measured for approximately 11 minutes at each mechanical compressive stress step.

An automated routine within the MATLAB (The MathWorks, 7.3.0.267 R2006b) framework was used to quantitatively interpret the diffraction data and fit the peaks of interest using two Pearson VII peak profile shape fitting functions

[38]. From the best fits, the peak center positions and intensities of the 002 and 200 peaks were determined.

6.2 Results

6.2.1 Effect of Electrical Poling

6.2.1.1Effect of electrical poling on piezoelectric response

Electric field amplitudes used to pole the samples were 0.5 kV/mm, 1 kV/mm and 2 kV/mm for the EC65 samples A, B, and C, respectively. Table 6-2 shows the resulting values of piezoelectric coefficient d_{33} for all poled samples.

For the samples tested, the d_{33} coefficient increases as the poling field amplitude increases. The coercive field of this type of soft PZT is ~0.8 kV/mm [18], and it is evident that the sample poled at subcoercive conditions (EC65-A) had a d_{33} value that was less than half that of the other two samples which were poled above the coercive field.

6.2.1.2 Effect of poling on initial diffraction pattern

The analysis of the initial diffraction patterns of each poled sample show the effect of electrical poling on the materials. The effects of poling on the initial diffraction patterns are shown in Figure 6-2 A-D. Throughout the remainder of this chapter Miller Indices are referenced according to the pseudo cubic tetragonal system. A tetragonal phase is noticeably predominant in all samples because distinct 002 and 200 diffraction peaks are present. The unpoled sample EC65-0 is shown in Figure 6-2A. An increase in the intensity of the 002 peak is observed after poling at the sub-coercive field conditions of sample EC65-A (Figure 6-2B), compared to the unpoled sample. The switching behavior is readily apparent and can be observed in the differences between Figure 6-2B

and Figure 6-2C, the sample poled at a field amplitude below the coercive field (EC65-A) and the first sample poled above the coercive field (EC65-B), respectively. In the unpoled sample of PZT shown in Figure 6-2A it is evident that there is a difference in the intensity of the (002)-type diffraction peaks, with a greater intensity in the 200-peak. In Figure 6-2B, the sample partially poled at 0.5 kV/mm was electrically polarized at a lower electric field than required for ferroelectric switching and the 200-peak at higher 2θ values is initially larger than the 002-peak at a lower 2θ value. In Figure 6-2C, the sample poled at 1 kV/mm and Figure 6-2D, poled at 2 kV/mm, the peak that is largest is the 002 peak at lower 2θ.

The integrated intensities were calculated for the 002 and 200 reflections using the Matlab fitting routine described above. A comparison of the integrated intensities for the differently poled samples are given graphically in Figure 6-3A. For the sample poled at 1 kV/mm, just above the coercive, the 002 intensity is significantly larger than the 200. Although at 2 kV/mm the difference between the 200 and 002 intensities is relatively high compared to the unpoled and partially poled samples, the greatest difference in the value of the 002 versus 200 integrated intensity occurs at 1 kV/mm.

6.2.2 Mechanical Compression After Poling

6.2.2.1 Intensity changes at various 2θ and stress values

An initial compressive stress of less than 7 MPa was used to hold the sample in place. Figure 6-4 shows plots of the 002/200 reflections of the poled samples from the *in situ* neutron diffraction during mechanical compression. Several differences in the material behavior as a function of the various poling

conditions can be observed. For example, in Figure 6-4A, the sample poled at a sub-coercive field, the intensity changes more significantly than the intensities in Figure 6-4B or Figure 6-4C, from the samples poled above the coercive field. The intensity changes considerably less as the degree of poling increases. Intensity redistribution appears to occur in the weakly poled sample (0.5 kV/mm) but not in well poled samples (poled at 1 kV/mm and 2 kV/mm).

Figure 6-5 shows plots of the calculated integrated intensities of the 002/200 peaks of the respective samples during *in situ* mechanical compression.

6.2.2.2 Peak shifts and lattice strain calculation

Lattice strain (ε_{hkl}) in the material can be calculated using information about the changes in *d*-spacing of a particular (hkl) plane. From Bragg's Law, the *d*-spacing, d_{hkl}, is given by:

$$d_{hkl} = \frac{\lambda}{2\sin\theta} \tag{6-1}$$

where λ is the wavelength of the incident neutrons, and θ is the diffraction angle of the (hkl) plane. The lattice strain of the (hkl) plane was calculated using the equation:

$$\varepsilon_{hkl}(\%) = \frac{d_{hkl}(\sigma) - d_{hkl}(\sigma_0)}{d_{hkl}(\sigma_0)} \times 100 \tag{6-2}$$

where $d_{hkl}(\sigma)$ is the interplanar spacing of the (hkl) plane at a given mechanical stress, σ. The pre-stress, σ_0, applied to hold the sample in place was between 4.1 and 6.8 MPa. The results of the lattice strain calculations are given in Figure 6-6.

6.2.2.3 Domain volume fraction calculations

Domain wall motion leads to a change in the intensities of certain peaks and diffraction can be used to study changes in the volume fractions of non-180° domains [39]. The volume fraction of 002-oriented domains (η_{002}) can be calculated for tetragonal perovskite materials using:

$$\eta_{002} = \frac{\dfrac{I_{002}}{I_{002,unpoled}}}{\dfrac{I_{002}}{I_{002,unpoled}} + 2\left(\dfrac{I_{200}}{I_{200,unpoled}}\right)} - \frac{1}{3} \qquad (6\text{-}3)$$

where I_{002} and $I_{002,unpoled}$ are the poled and unpoled values of integrated intensity values, respectively. η_{002} describes the fraction of (200)-to-(002) domain switching at a certain stress or electric field state with respect to the unpoled state, and can be described by η_{200} =1 - η_{002} . Figure 6-7 shows η_{002} calculated for the measured samples as a function of stress.

6.3 Discussion

6.3.1 Effect of Electrical Poling

The fact that the sample poled at subcoercive conditions (EC65-A) measured a significantly lower d_{33} value than either of the other 2 samples, both of which were poled above the coercive field for this material, suggest that higher d_{33} properties are achieved after the domain switching within the material has occurred via electrical polarization. For ferroelectric materials, the piezoelectric coefficient depends on poling state [40]. Additionally, the diffraction pattern of EC65-A in Figure 6-2B compared to the unpoled sample in Figure 6-2A shows a higher intensity in the 002 peak than the initial diffraction pattern and the 200-

peak on the right is initially higher than the 002-peak on the left, indicating that a significant amount of switching has not yet occurred. This is expected in the context of the materials and conditions investigated since 0.5 kV/mm is below the coercive field of the material. The EC65-B and EC65-C diffraction patterns of samples poled at 1 kV/mm and 2 kV/mm, respectively, have the highest intensity at lower 2θ in the 002 peak, which indicates that ferroelectric switching has occurred. In Figure 6-3A, the calculated integrated intensity value for 002 peak of the 2 kV/mm poled sample I =(820) is higher than the integrated intensity measured for the 1 kV/mm poled sample I =(695) suggesting that more ferroelectric switching has occurred in the sample poled at a higher electric field. Based on previous neutron experiments with this material it has been shown that the 002 and 200/020 peaks should be the only peaks present for this particular material composition [16].

The 002 domains in electrically poled samples have a preferred orientation parallel to the direction of initial poling [39]. In the unpoled sample the 200 domains represent the largest volume fraction in the sample, though it is unlikely that there is any actual preferred orientation in this case. This is reasonable because the 200 reflections represent both the 200 and 020 planes and therefore combine to be approximately twice the intensity of 002 domains. As a sub-coercive electric field is applied, some domains begin to reorient, which is observed in the distinct decrease in the difference between the 002 and 200 peak intensities. It is noteworthy that both reflections increase in intensity for the unpoled and the 0.5 kV/mm poled samples but the 200 domains are still slightly

more dominant. Since the sample was only partially poled (sub-coercively), significant switching has not yet occurred. Comparison of the 0.5 kV/mm poled sample with the 1 kV/mm poled sample shows another significant difference in the 200 and 002 intensities. At 1 kV/mm, just above the coercive field, the 002 intensity is significantly greater than the 200. This is most likely due to the fact that ferroelastic switching has occurred. Interestingly, the difference between the integrated intensities of the 002 and 200 peaks is highest in the sample poled at 1 kV/mm, as shown in Figure 6-3B. This result is unexpected because the d_{33} value is highest in the sample poled at 2 kV/mm.

In Figure 6-3, the 002 integrated intensity increases for all cases, however, the 200 intensity values do not increase although there is an overall decrease in the integrated intensities of the 200 peaks of the unpoled sample versus the value of the 200 peak intensity for the 2 kV/mm poled sample. This suggests that the electrical poling process primarily affects only the 002 domains and the 200 type domains solely react to the reorientation of the 002 domains.

6.3.2 Effect of Mechanical Compression After Electrical Poling

6.3.2.1 002 and 200 reflections during mechanical compression

Evolution of the intensities of the 002 and 200 diffraction peaks during application of static mechanical stresses for all of the samples poled at the conditions given is shown in Figure 6-4.

Peak position shifts to lower 2θ values (Figure 6-4A and Figure 6-4B), indicating lattice expansion and positive strain, occur as a response to mechanical stress. Obviously, a more dramatic shift seems to occur for Figure 6-4A, the sample poled initially at 0.5 kV/mm. The 002 peak at 2θ≈67° shifts

towards lower 2θ values, corresponding to higher d-spacing, lattice expansion and strain in the c-direction in response to the macroscopic compressive stress perpendicular to the poling axis. This occurs because the c-axis is perpendicular to the compression axis and parallel to the poling direction of the samples.

Switching in response to the mechanical load occurs in the weakly poled sample (0.5 kV/mm) but does not seem to occur in well-poled samples, such as the samples which were poled above the coercive field. In Figure 6-4(A), an abrupt change in the 200 and 002 peak intensities is observed for the EC65-A sample at an applied stress of ~40 MPa during initial loading. In partially poled samples (EC65-A), the intensity of the 002 peak initially increases with increasing mechanical stress, but becomes constant after about ~90MPa. The fully poled samples in Figure 6-4(B) and Figure 6-4(C) have intensity values that remain relatively unchanged, indicating switching has already occurred in these samples (EC65-B and EC65-C) during the electrical poling process.

Previous work has shown that a majority of the 002 switching occurs below ~90MPa stress. Additionally, the 002 domains generally reorient in a plane perpendicular to the mechanical loading direction and have been observed to disappear completely when measured parallel to the stress axis [16]. In the samples poled above the coercive field (EC65-B and EC65-C), the intensity remains unchanged with stress, similar to the behavior of the partially poled sample above ~90MPa.

Integrated intensities decrease for the 200 reflection in the EC65-A and EC65-B samples but appear to remain relatively constant for EC65-C. This

suggest that perhaps EC65-C is fully saturated after the electrical poling. This is consistent with work by others (e.g. Marsellius *et al*.) who have suggested that a fully electrically poled material may have approximately the same response as a material poled electrically and mechanically[41].

6.3.2.2 Comparison of reflections before and after compression

Examining the behavior of the samples before and after compression, various changes in the response of the differently poled samples is observed.

In this experiment electrical poling was done *ex situ* prior to compression. Others have shown that mechanical compression in conjunction with electrical poling can dramatically influence the domain configuration of a ferroelectric [9], [10], [41]. More specifically, the way in which electric field and stress are applied heavily influences the domain configuration and resulting properties of ferroelectric materials. Granzow *et al*. and others [42][9] have shown that certain combinations of field **and** stress can cause non-180° domains to switch into the poling direction that normally might not have switched if exposed only to a stress **or** a field.

The present experimental set-up has successfully been used by others [16][43] to investigate domain structure in various ferroelastic ceramics in response to mechanical compression. In this case, the response of the diffraction peaks of the differently poled samples to mechanical compression can be observed.

Figure 6-2B shows that for a partially poled sample, switching does not occur initially, yet Figure 6-2E shows that switching occurs after significant mechanical compression. This suggests that mechanical compression after

partial electrical poling may allow additional domain states to be reached which could lead to more extensive poling [42].

6.3.2.3 Domain volume fraction before and after compression

In tetragonal PZT, changes in the observed intensity of the 002 and 200 diffraction peaks can be related to volume fractions of the ferroelastic domains [39].

Clear differences can be observed for the volume fraction of crystallographic domains before and after mechanical compression shown in Figure 6-7. Before mechanical compression, the values of η_{002} are different depending on the poling condition. The sample poled at 0.5 kV/mm has the lowest η_{002} value of 0.15, while the 1 kV/mm poled sample has the highest η_{002} value of the samples tested, 0.29. With a value of 0.25, the 2 kV/mm poled sample has a higher η_{002} value than the 0.5 kV/mm poled sample but a lower value than the 1 kV/mm poled sample. As previously discussed, the integrated intensity values measured also followed a similar trend, i.e. the EC65-B sample had the highest initial integrated intensity for the 002-peak and the EC65-C sample poled at 2 kV/mm had a lower intensity, but the highest overall d_{33} value. Table 6-3 summarizes these results.

The sample poled at 0.5 kV/mm has an initial η_{200} value of 0.85, the highest overall value for 200 domains. The 1 kV/mm sample has the lowest initial η_{200} value compared to the other samples, 0.71. The 2 kV/mm poled sample has a η_{200} value of 0.75, higher than the 1 kV/mm sample but less than the 0.5 kV/mm sample.

After compression the values of η_{002} for all poling conditions are higher than values before mechanical compression. The greatest change occurs in the 0.5 kV/mm poled sample, where the value of η_{002} increases to 0.23, a change of 0.08 compared to the value before mechanical compression. The value of η_{002} after mechanical compression for the 0.5 kV/mm poled sample is still lower than the values for both the poled samples prior to compression. The 1 kV/mm poled sample has a higher final η_{002} value than starting value, increasing by 0.01, and it has the highest domain volume fraction of all poling conditions tested, 0.30. The 2 kV/mm poled sample has a calculated η_{002} value after compression of 0.27, increasing by 0.02.

The values of η_{200} decrease for all poling conditions with increasing stress as a result of mechanical compression. The 0.5 kV/mm poled sample has a lower η_{200} value following compression, 0.77 compared to its value prior to compression, a decrease of 0.08. The final η_{200} value for the sample poled at 0.5 kV/mm is higher than the starting intensity values for the other samples poled above the coercive field. The 1 kV/mm poled sample has a lower final η_{200} value than beginning η_{200} value, decreasing by a factor 0.01. The η_{200} value of 0.70 has the lowest η_{200} value of all the samples measured under the different poling conditions. The 2 kV/mm poled sample has an η_{200} value of 0.73 after mechanical compression, 0.02 lower than the beginning value for that sample.

The η_{002} values before mechanical compression represent the domain volume fraction as a result of the initial electrical poling. In all cases there are more 002 domains than 200 domains following both electrical poling and

mechanical compression. Mechanical compression further increases the amount of 002 domains for all samples. For the sample poled at 0.5 kV/mm, the greatest change in the amount of 002 domains before and after mechanical compression occurs. Differences were less for the samples poled above the coercive field, at 1 kV/mm and 2 kV/mm. However, both samples showed higher η_{002} values after mechanical compression, with the highest value for all poling conditions occurring for the sample poled at 1 kV/mm.

The greatest change in the amount of 200 domains before and after mechanical compression occurs in the sample poled at 0.5 kV/mm, below the coercive field. For the samples poled above the coercive field, 1 kV/mm and 2 kV/mm, very little not much change occurs in the domain volume fraction, indicating the prior electrical poling at sufficiently high fields to cause switching may have saturated the domain structure in this material inhibiting further switching as a response to mechanical compression. With increasing stress, greater amounts of 200-to-002 domain switching occurs leading to increasing volume fraction of 002 domains perpendicular to the mechanical loading direction and parallel to the electrical poling axis. The implications of these results suggest that electrical poling alone can saturate domain switching whereas mechanical compression even above 250 MPa cannot align domains much better.

6.3.2.4 Effect of mechanical compression on lattice strains

The (200) lattice strains, ε_{200}, parallel to the loading direction and the (002) lattice strains, ε_{002}, perpendicular to the loading direction are shown in Figure 6-6 for the differently poled samples. Reorientation of the 200 domains away from the loading direction and contraction of the (200) lattice planes initially consumes

most of the energy input for the material during mechanical compression. For all poling conditions, an increase in applied compressive stress produced increasingly negative strains for ε_{002}. During the application of compressive stress to all poled samples, the ε_{200} values are within the fit error at all stress amplitudes. The 200 plane is parallel to the compression axis and the 200 and 020 domains are perpendicular to the diffraction vector. The 200 and 020 domains are indistinguishable, which accounts for the large error bars associated with the lattice strain in the 200 direction since the compression of the 200-axis as well as any expansion of the 020-axis is included in the measurement of that particular reflection.

Previous work has indicated that contraction parallel to the polarization axis and reorientation of non-180° domains occurs more readily than elastic strains perpendicular to the crystallographic polarization axis [16]. After non-180° domain switching is exhausted as a mechanical strain accommodation mechanism, the (200) planes undergo elastic contraction in response to the applied compressive stress. If it is assumed that the x-direction (the 200) is the compression axis, the domain reorientation as a result of compression will occur primarily in the y-direction (the 020 plane), or in the z-direction (the 002 plane). The amount of 200 domains will decrease and the amount of 020 domains and 002 domains will increase due to the direction of compression. This is reflected in the change of slope of the (002) lattice strains with increasing stress amplitudes for all poled samples.

6.4 Conclusions

In conclusion, for the samples measured, the electric field initially used to pole the materials has a significant effect on the domain volume fractions. The electric field appears to lock in the texture of the sample after poling regardless of mechanical stress. The electrical poling process seems to primarily affect the 002 domains as evidenced by comparing the initial integrated intensities. The behavior of the 200 type domains is possibly a reaction to the reorientation of the 002 domains. Application of the mechanical compressive stress is parallel to the 200 plane. This work suggests that purely electrical poling can fully saturate the domain structure of a material. However, unique domain states may be achieved by unique electromechanical loading pathways, e.g. 0.5 kV/mm poling followed by mechanical compression.

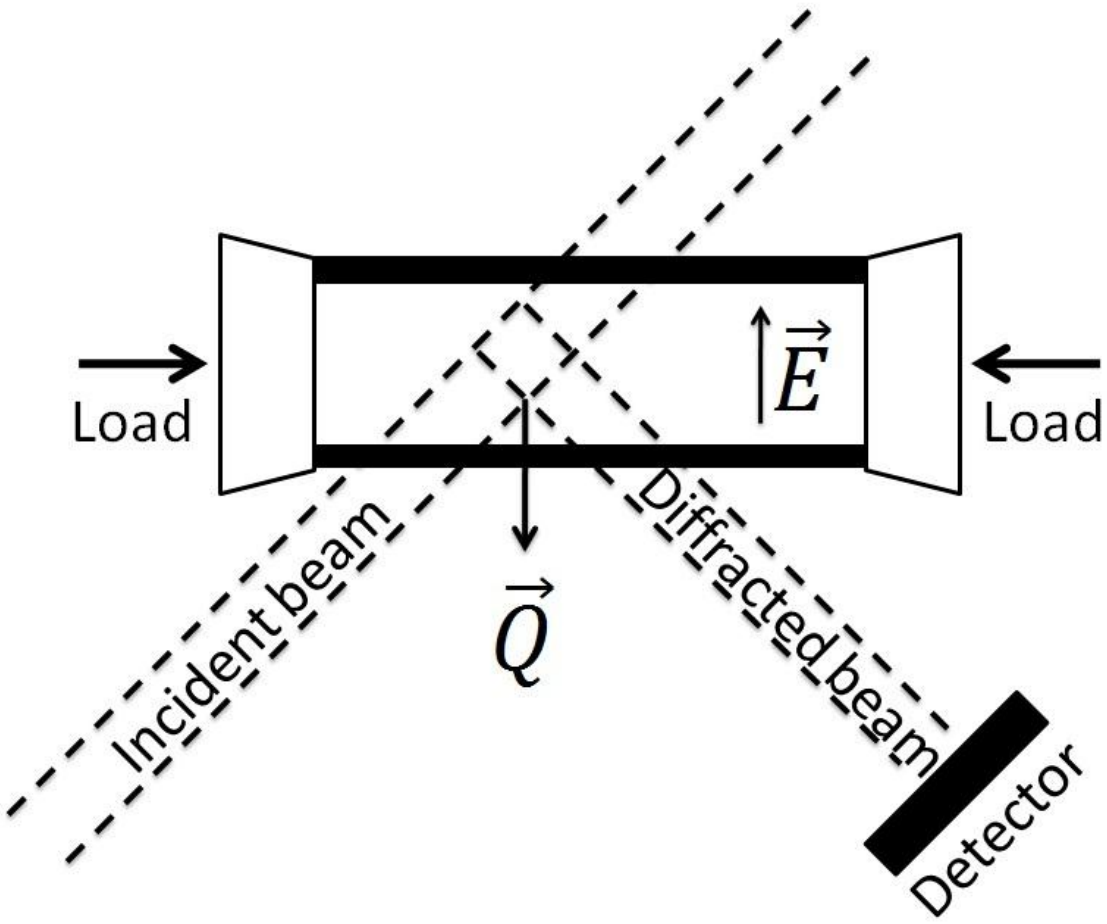

A

Figure 6-1. Diffraction Measurement Experimental Setup. A) Schematic of sample orientation showing $\vec{E}$ and $\vec{Q}$, the respective poling and diffraction directions, and the direction of compression (top down view). B) Photograph of the mechanical loading device on the NRSF2 instrument on HFIR at ORNL. C) Example of the stress loading profile used in the experiments. Diffraction patterns were measured at each value of constant stress.

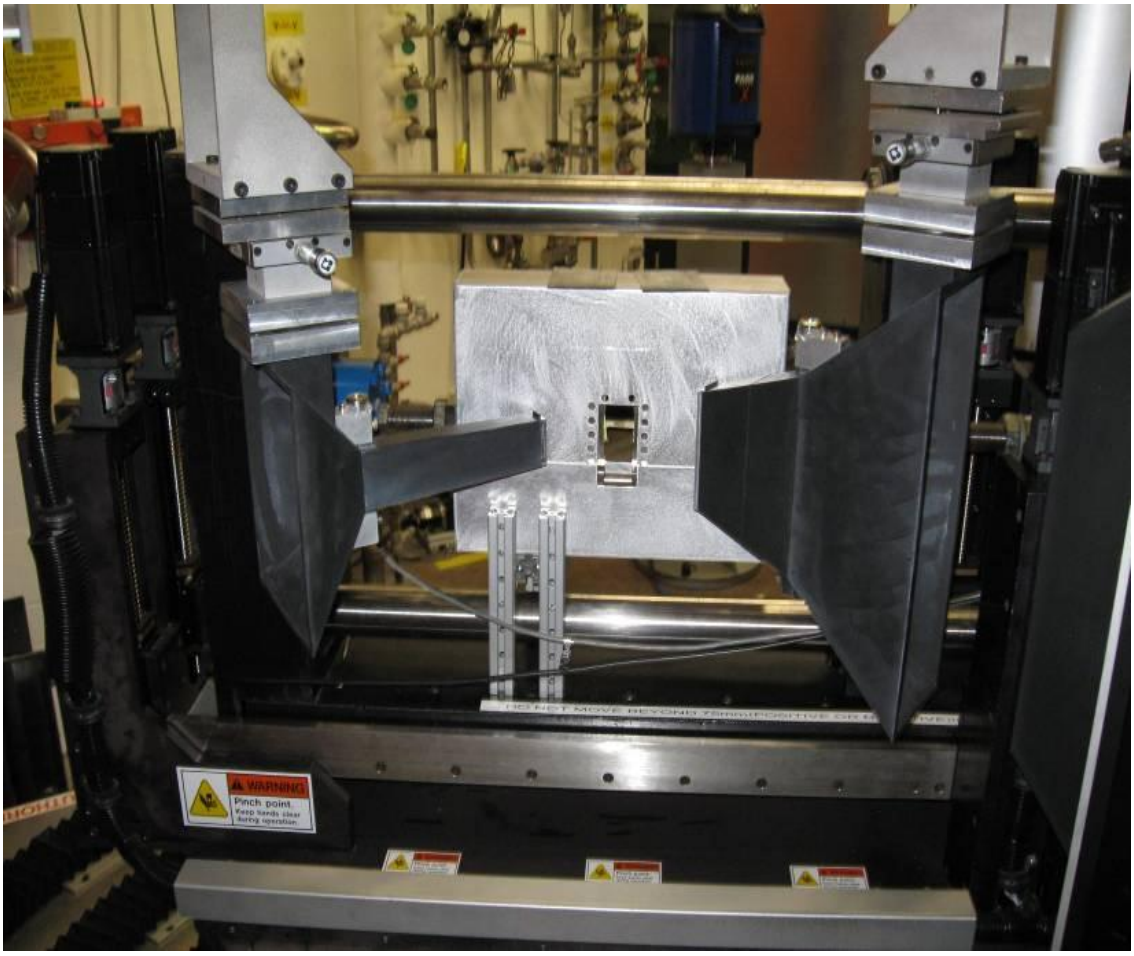

B

Figure 6-1. Continued.

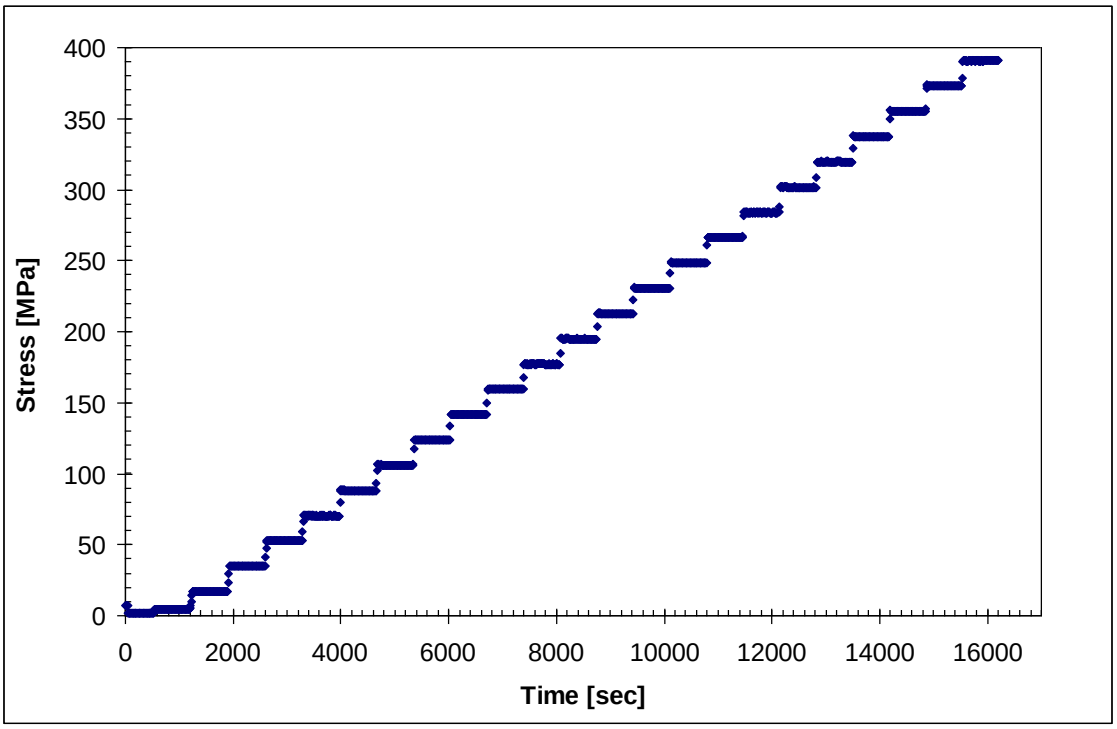

C

Figure 6-1 Continued.

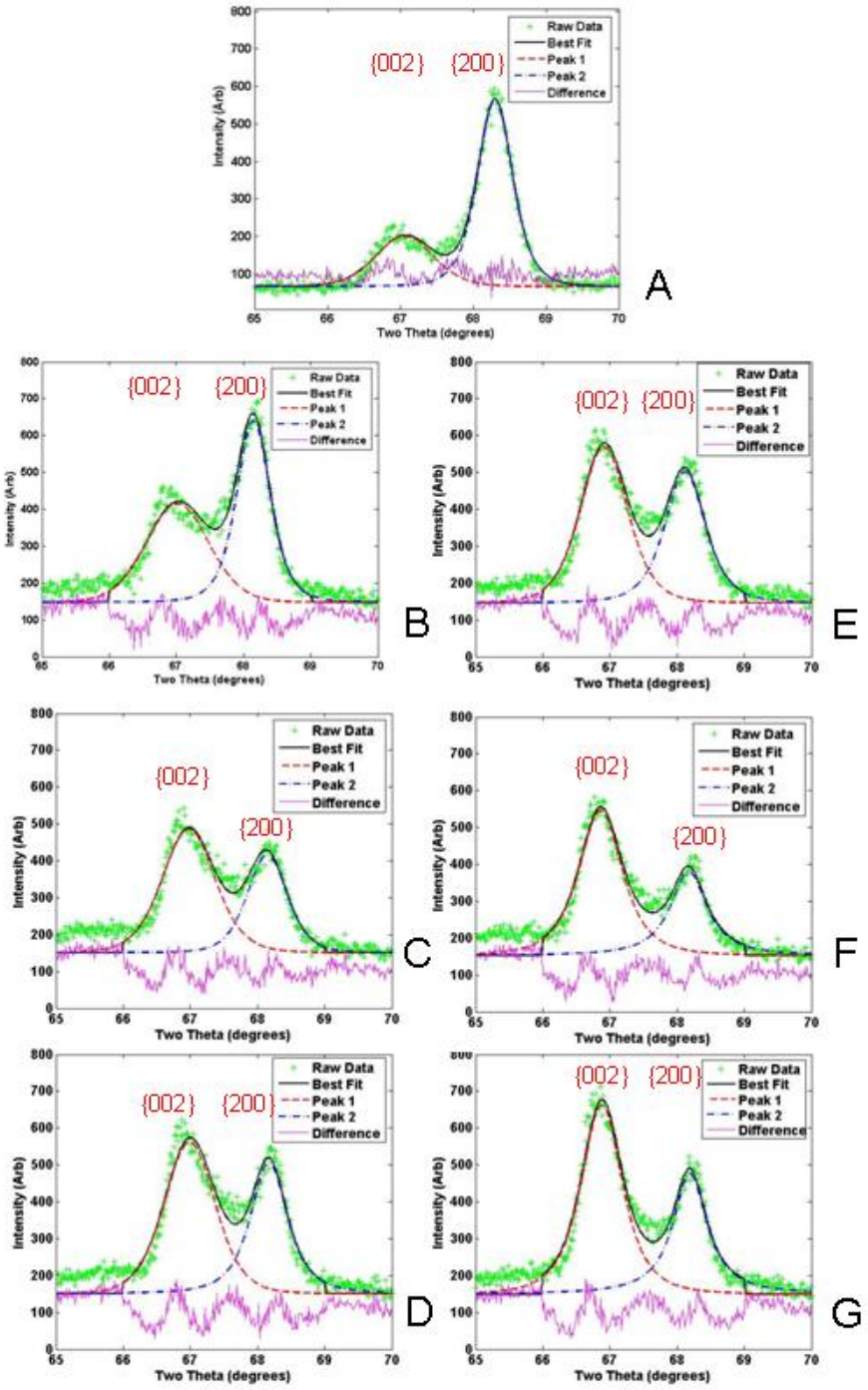

Figure 6-2. Initial diffraction patterns of EC65 samples. A) the unpoled sample, B) the sample poled at 0.5 kV/mm, before compressive stress and E) after compressive stress; C) 1 kV/mm before compressive stress and F) after compressive stress; and D) 2 kV/mm before and G) after compressive stress. All patterns were recorded after an initial compressive pre-load was applied.

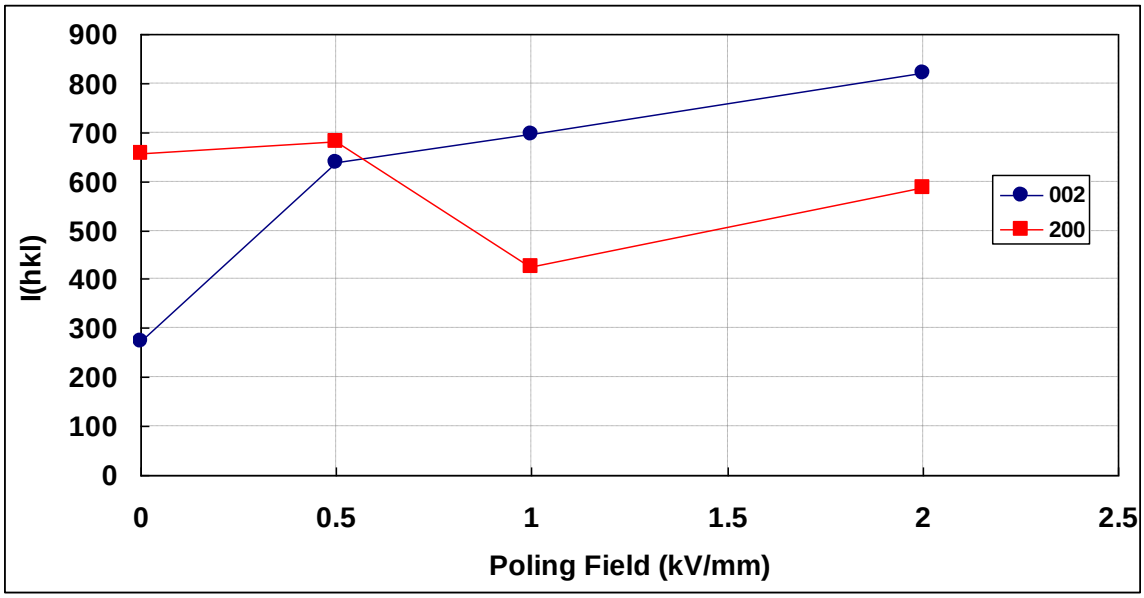

A

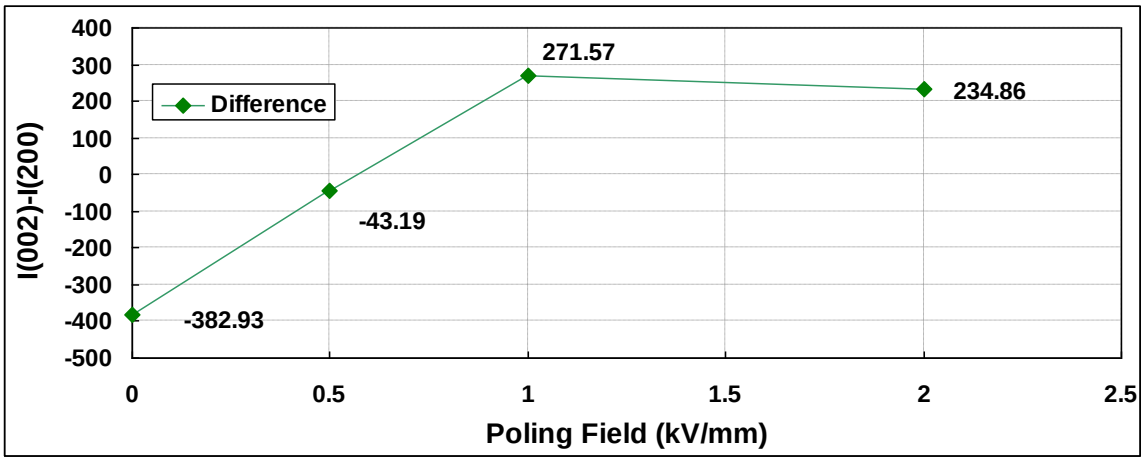

B

Figure 6-3. Comparison of the integrated intensities for the differently poled samples. A) Before the application of compressive stress. The integrated intensities of the 002 peaks (blue) and 200 peaks (red) are affected by the degree of poling. The samples were all poled at room temperature. B) The difference in the integrated intensities of the 002 peaks and 200 peaks.

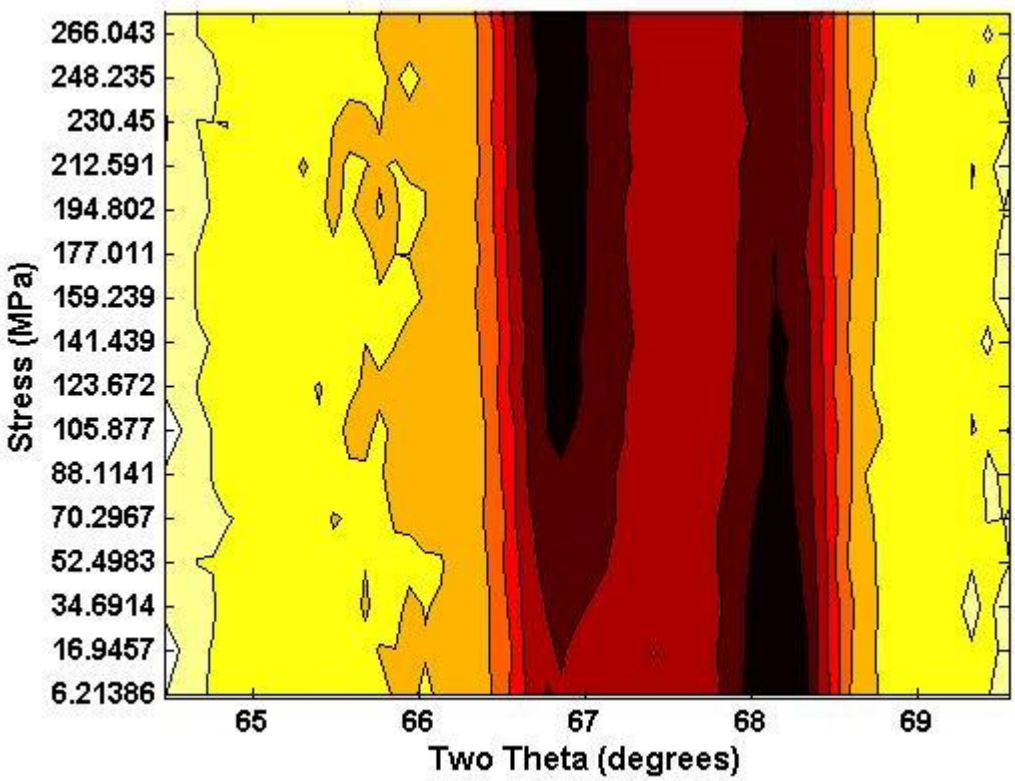

A

Figure 6-4 Plots of the (002)-type diffraction peaks under static mechanical stresses for samples poled at room temperature and electric field values of A) 0.5kV/mm, B) 1kV/mm and C) 2kV/mm. The z-scale for all plots is the square root of the measured intensity and contour lines are drawn at constant intervals of square root of intensity.

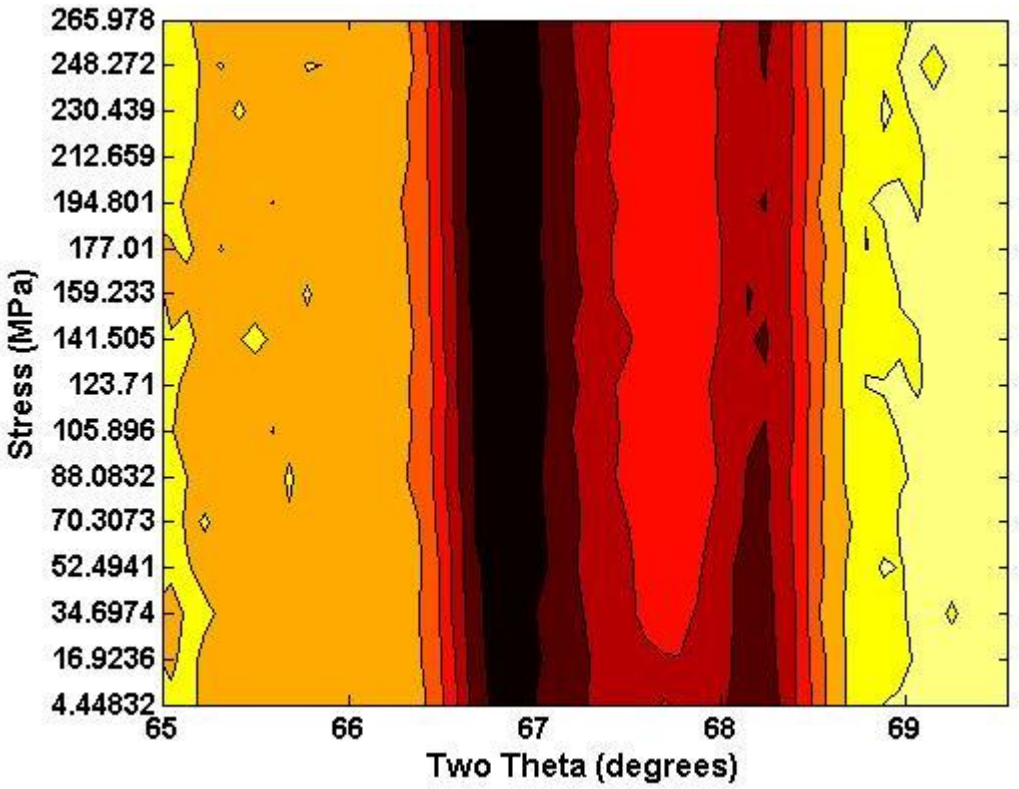

B

Figure 6-4 Continued.

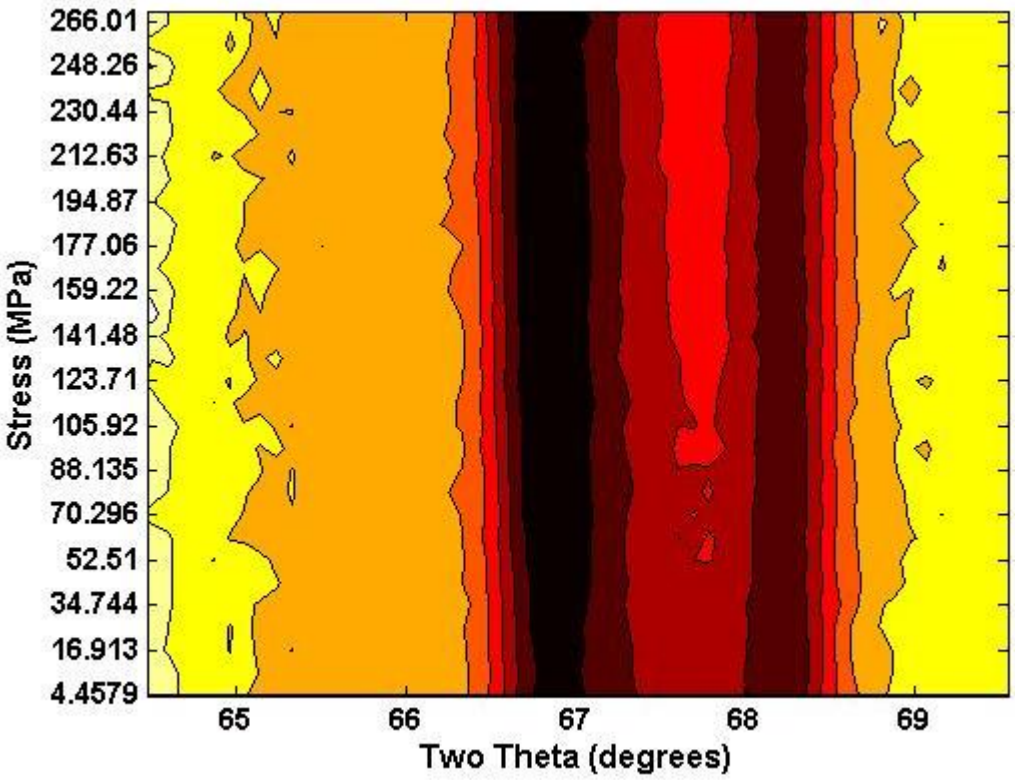

C

Figure 6-4 Continued.

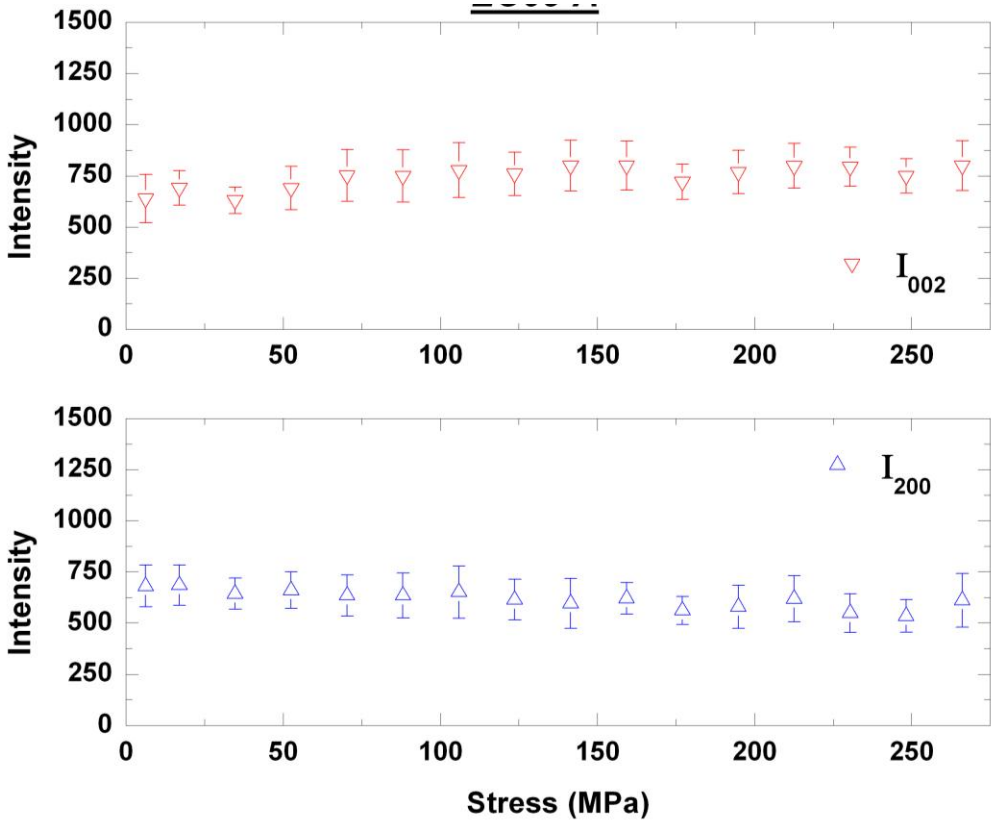

A

Figure 6-5 Integrated Intensity values calculated from the applied mechanical stress of the (002)-type diffraction peaks for the EC65 PZT samples poled at room temperature and electric field values of A) EC65-A, B) EC65-B and C) EC65-C.

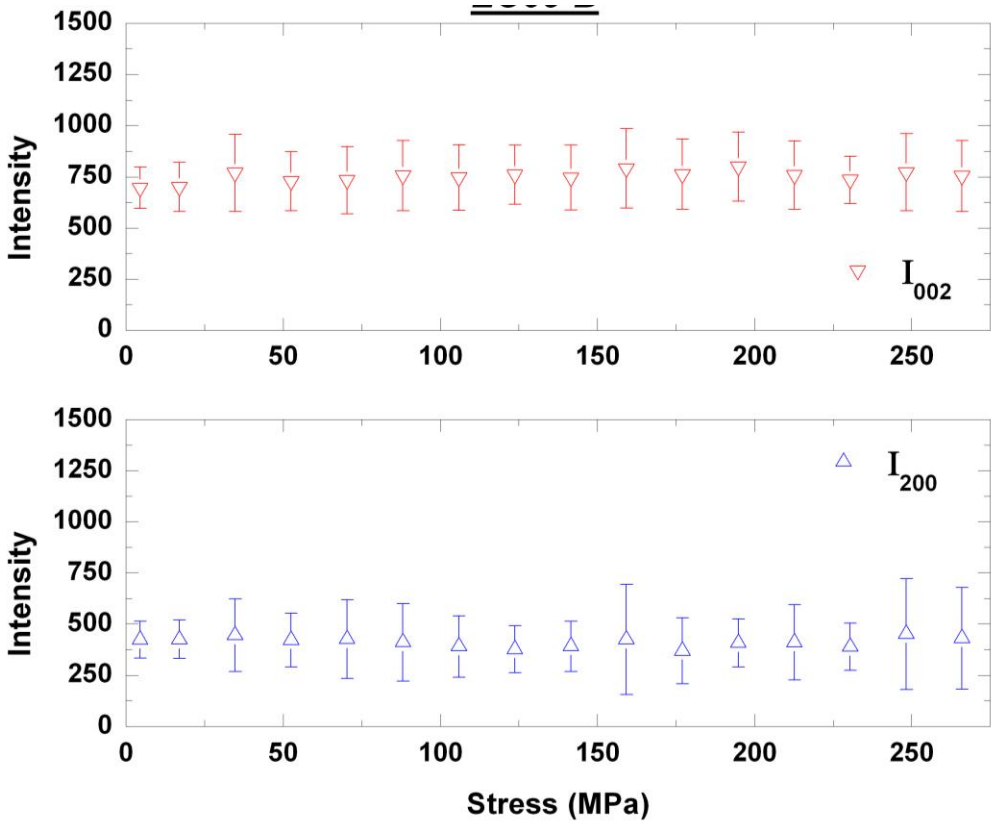

B

Figure 6-5 Continued.

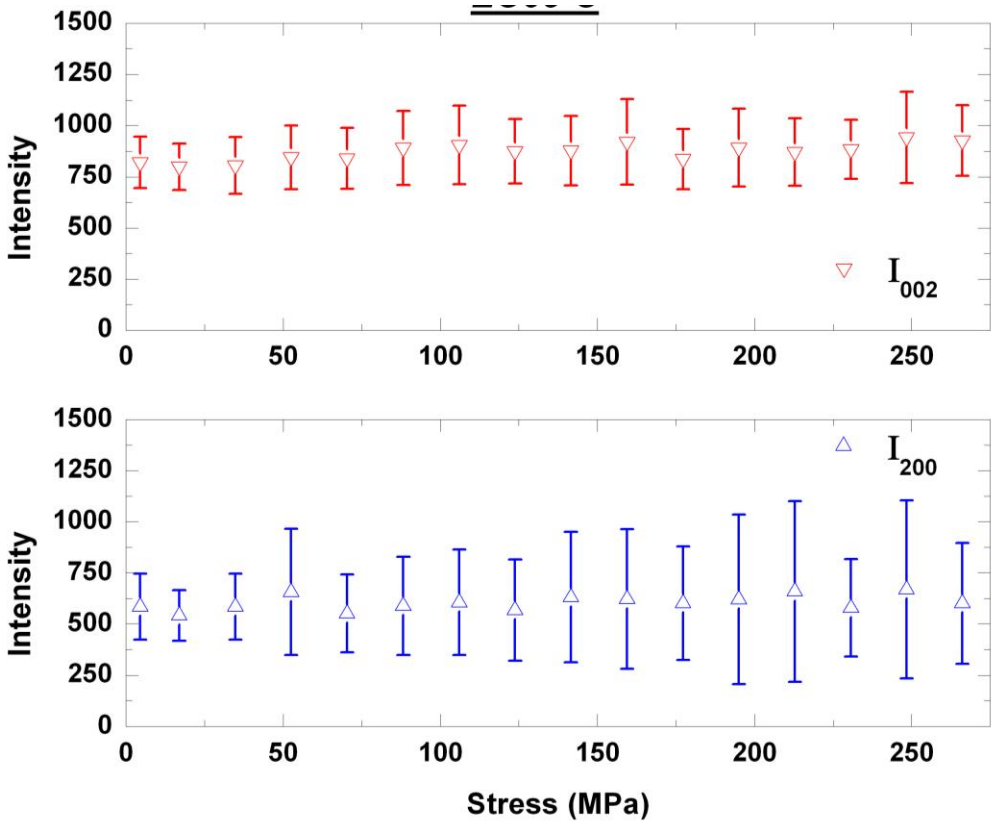

C

Figure 6-5 Continued.

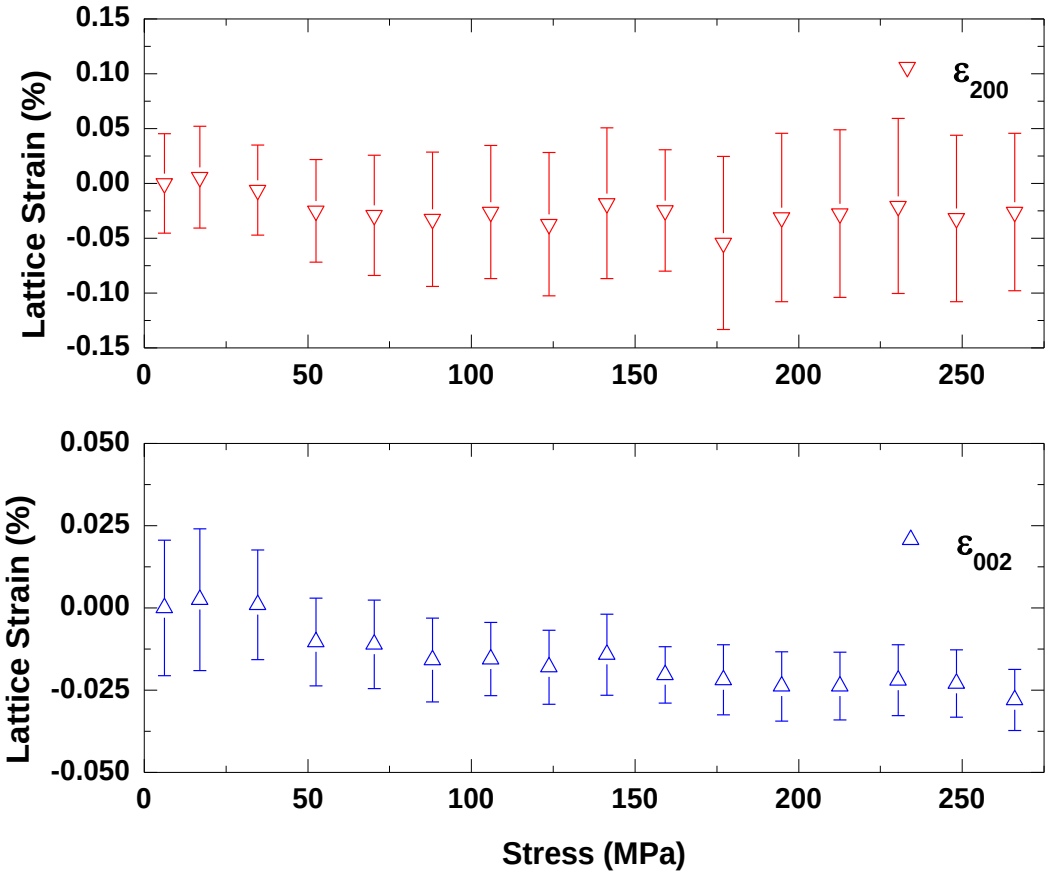

A

Figure 6-6 Lattice strain calculated from the (002)-type diffraction peaks for the given samples poled at electric field values of A) 0.5kV/mm, B) 1kV/mm and C) 2kV/mm.

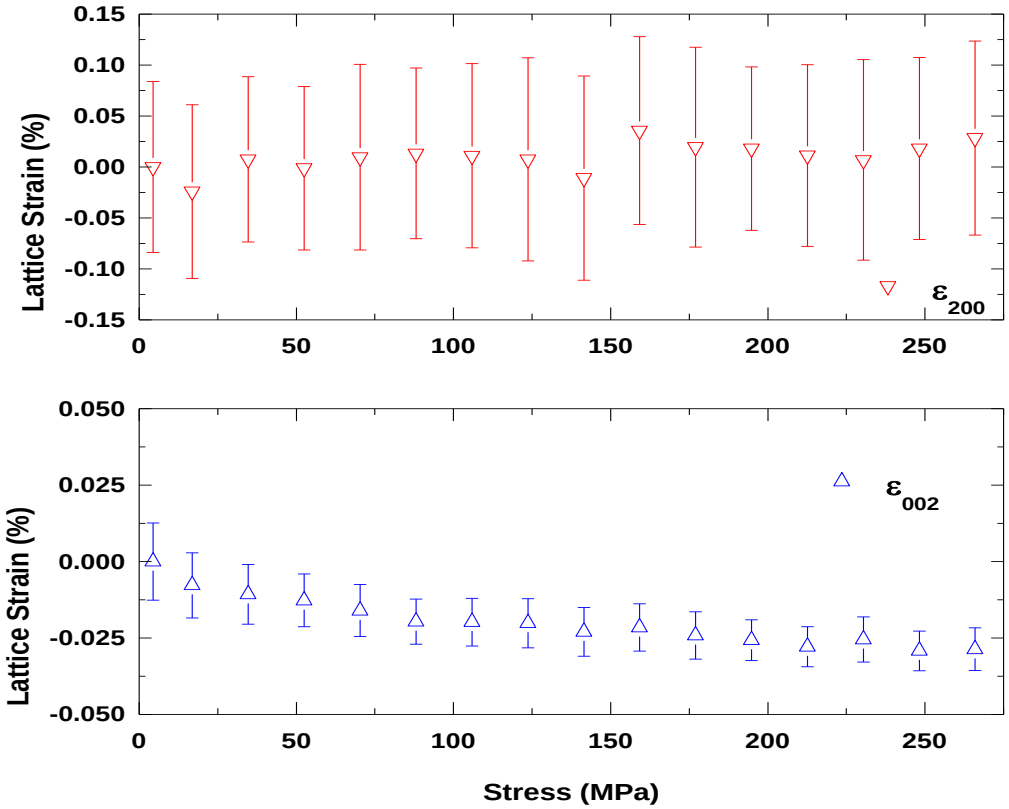

B

Figure 6-6 Continued.

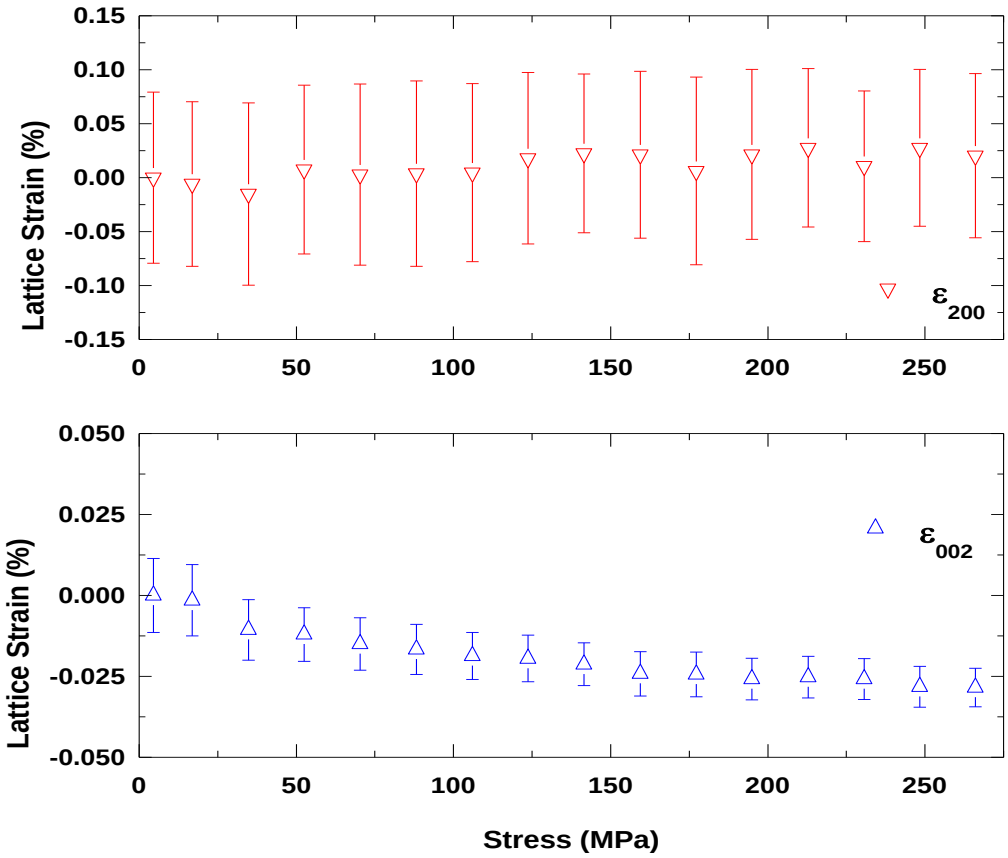

C

Figure 6-6 Continued.

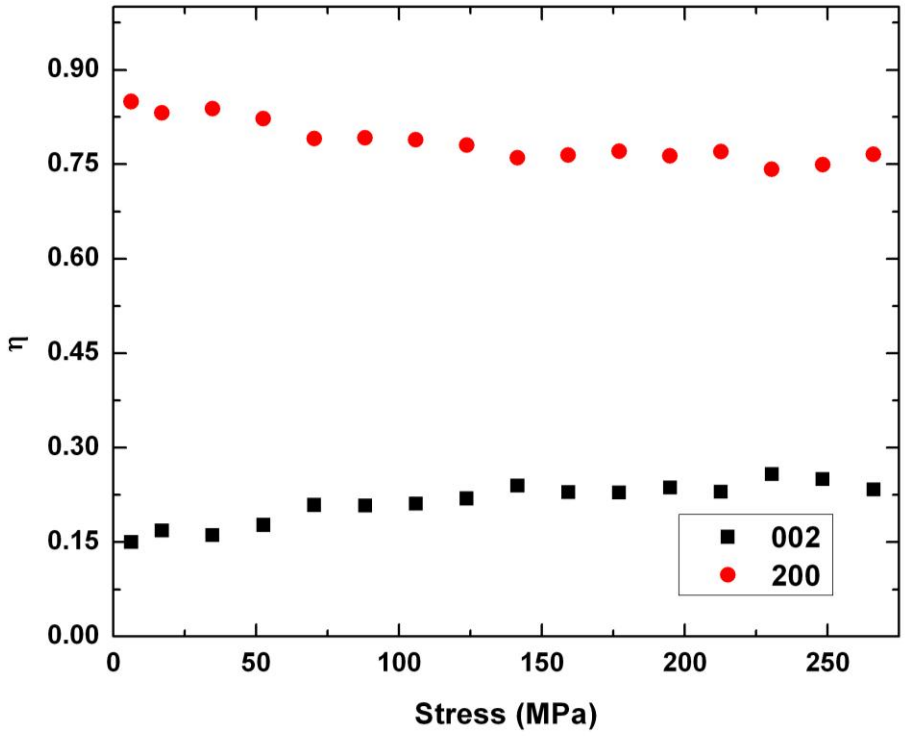

A

Figure 6-7 Plots of measured structural changes (η) during the application of applied mechanical stress from the (002)-type diffraction peaks for the given samples poled at room temperature and electric field values of A) 0.5 kV/mm, B) 1 kV/mm and C) 2 kV/mm.

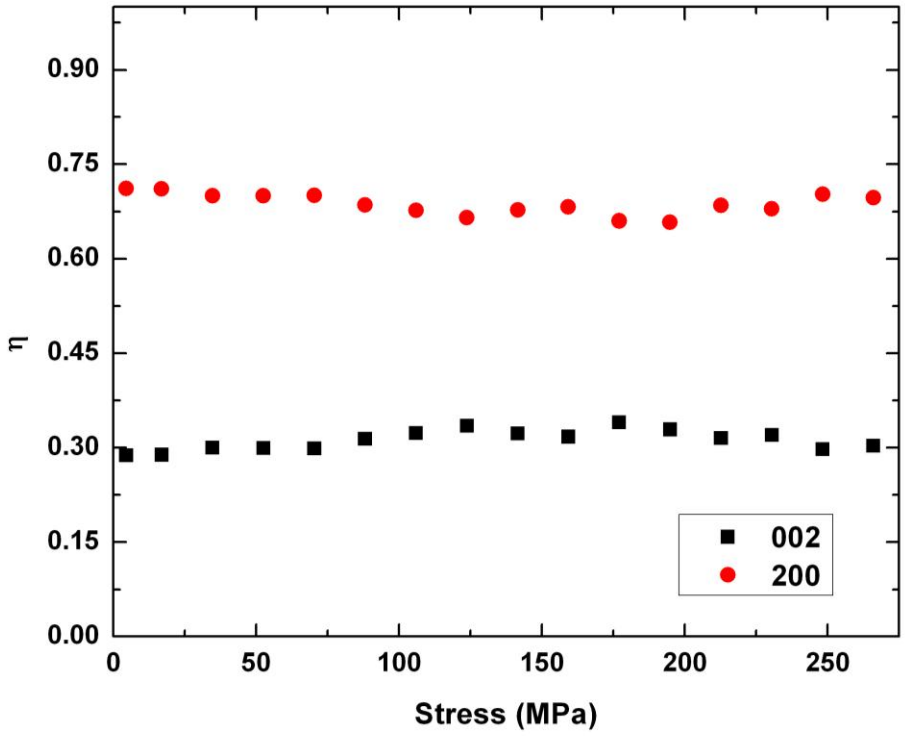

B

Figure 6-7 Continued.

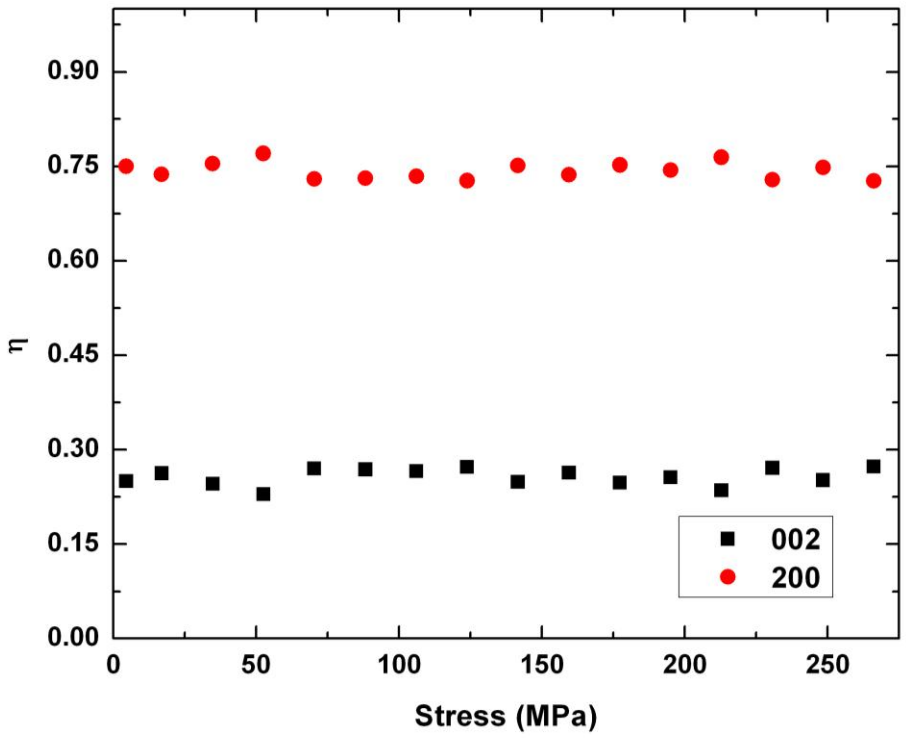

C

Figure 6-7 Continued.

Table 6-1. Poling conditions and sample designations of measured PZT samples

Sample Designation	Poling Field (kV/mm)	Poling Temperature (°C)
EC65-0	Unpoled	Unpoled
EC65-A	0.5	25
EC65-B	1	25
EC65-C	2	25

Table 6-2. Piezoelectric coefficient values of the measured sample designations.

Sample Designation	d_{33} (pC/N)
EC65-A	204
EC65-B	435
EC65-C	485

Table 6-3 Table of measured structural changes (η) before and after the application of applied mechanical stress for the 002 domains and the 200 domains.

Sample Designation	η_{002} Begin	η_{002} End	η_{200} Begin	η_{200} End
EC65-A	0.15	0.23	0.85	0.77
EC65-B	0.29	0.30	0.71	0.70
EC65-C	0.25	0.27	0.75	0.73

CHAPTER 7
FIELD AND FREQUENCY DEPENDENCE OF DIRECT d_{33}

In this chapter the direct piezoelectric coefficient is used in order to study the effects of small scale stresses on the motion of domain walls. The direct piezoelectric coefficient of materials poled at various conditions is investigated as a function of frequency and stress amplitudes.

7.1 Experimental Procedure

7.1.1 Electrical Poling and Piezoelectric Measurements

In order to conduct electrical poling and piezoelectric measurements the samples were sputter coated using gold electrodes on the parallel faces of the commercial PZT ceramics of designation EC65 (ITT Ceramics Inc., Salt Lake City, Utah, USA) with sample dimensions of 5x5x1 mm (±0.01 mm). Electrodes were placed on the parallel sides of dimension 5x5mm. The various samples were poled at a constant poling time of 5 minutes and electric field amplitudes from 0.75-2kV/mm and at a constant temperature of 25°C in a silicone oil bath. The poling conditions are listed in table 7-1. The samples were poled using a high voltage source (Matsusada, AU-30P1). The samples were first connected to electrodes with the power supply turned off then the specified electric field was applied at constant temperature. The electric field was then set to zero and the connection was shorted to ground. The samples were then subsequently removed from the oil bath. After poling, the longitudinal direct piezoelectric coefficient d_{33} was measured using a Berlincourt d_{33} meter (APC, YE2730A). Measurements were taken at least 24 hours after poling.

7.1.2 Cyclic Pressure Measurement

To determine how the degree of poling affects the extrinsic contribution to piezoelectric properties of a material, charge versus cyclic applied pressure hysteresis measurements were taken and the direct d_{33} response was calculated. Uniaxial sinusoidal mechanical pressure was applied to the samples in order to measure the direct, longitudinal piezoelectric charge coefficient. A stepper motor was used to provide a DC offset force and a piezoactuator was used to provide the AC force.

The frequency dependence of the piezoelectric charge coefficient d_{33} was measured under fixed cyclic pressure of 5 MPa and in order to examine the dependence of d_{33} on the amplitude of the pressure, a driving frequency of 3 Hz was selected. An illustration of the set-up for these experiments can be seen in Figure 7-1.

7.1.3 Phase Lag and Rayleigh Behavior

7.1.3.1 Rayleigh behavior

The Rayleigh law can be used to describe the dependence of the piezoelectric coefficient d_{33} on the applied ac pressure for different materials at sufficiently low amplitudes of pressure or electric field[5]. Originally, the Rayleigh law was applied to ferromagnetic materials, but it has been very useful in describing the relative extrinsic and intrinsic contributions to the piezoelectric behavior in ferroelectric ceramics [4], [13], [27].The Rayleigh law for the piezoelectrically induced charge density Q_o and the piezoelectric coefficient is expressed as

$$Q_o(X_o) = d_{init} X_o + \alpha \cdot (X_o)^2 \qquad (7\text{-}1)$$

$$d_{33}(X_o) = d_{init} + \alpha \cdot X_o \qquad (7\text{-}2)$$

where the value of the piezoelectric coefficient, d_{33}, can be expressed as a function of the applied ac pressure X_o, and the quantities d_{init} and α represent the Rayleigh parameters. The Rayleigh parameters d_{init} and α in Eqns. 7-1 and 7-2 represents a quantitative measure of the irreversibility of extrinsic mechanisms (for example domain wall displacement), and describes the field dependence of the piezoelectric coefficient. The absolute extrinsic contribution due to the irreversible extrinsic mechanisms (e.g. displacement of domain walls) is described by the quantity $\alpha \cdot X_o$. Examples of extrinsic contributions could include 180° and non-180° domain wall motion. The total piezoelectric coefficient, d_{33}, is the sum of an irreversible extrinsic contribution, $\alpha \cdot X_o$, and the reversible plus intrinsic component d_{init}. By calculating the α coefficient values, quantitative information about the extrinsic response of a particular material can be calculated. The value of the piezoelectric coefficient d_{33} can be calculated from $d_{33}=Q_o/X_o$ from a measurement of the Charge versus Pressure as seen in Figure 7-2.

7.1.3.2 Phase lag

When the piezoelectrically induced electric charge C lags in phase by an angle δ behind an applied sinusoidal force F, the piezoelectric coefficient (d=C/F) may be expressed as a complex number:

$$F = F_o \cdot e^{(i\omega t)}$$

$$C = C_o \cdot e^{[\,i\,(\omega t - \delta)]}$$

$$d = d_o \cdot e^{(-i\delta)} \qquad (7\text{-}3)$$

where F_o is the amplitude of the force applied force, ω is the angular frequency, and C_o represents the amplitude of the charge. By using Euler's identity ($e^{i\theta} = cos\ \theta + i\ sin\ \theta$), the piezoelectric coefficient can be expressed in terms of its real and imaginary components and subsequently the loss tangent. The expression is:

$$d = d_o \cdot (\cos \delta - i \sin \delta) = d' - id''$$

$$\tan \delta = d''/d' \qquad (7\text{-}4)$$

and the formalism used here is the same as that used to describe elastic compliance or dielectric permittivity [44], [45].

7.2 Results

7.2.1 Effect of Electrical Poling on Berlincourt d_{33}

Electric field amplitudes used to pole the samples were 0.75 kV/mm, 1 kV/mm and 2 kV/mm for the EC65 samples. The poling temperature was held constant at 25°C. Figure 7-2 shows the resulting values of piezoelectric coefficient d_{33} for all samples poled at 25°C.

A significant increase was observed in the value of the d_{33} coefficient at higher poling fields for the samples tested. The sample poled at 0.75 kV/mm had a the lowest d_{33} value of all the samples tested. The coercive field for this material is approximately 0.8 kV/mm.

7.2.2 Cyclic Pressure Experiments at Different Force Amplitudes

The values for the piezoelectric coefficient were calculated by taking the slope of the charge versus pressure curves that can be seen, for example, in Figure 7-3. The figure shows the hysteresis exhibited for a given applied pressure amplitude. The raw data for the sinusoidal applied pressure and charge response were fit to sinusoids of the form

$$y = y_0 + X_o * \sin(\pi*(t-tc)/\omega) \quad (7\text{-}5)$$

where y is either the applied pressure or measured charge. The adjusted R-squared value for all of the individual pressure fits was 0.999 or higher and the value for all of the charge fits was at least 0.998. Figure 7-4 (A.) shows the Charge density as a function of cyclic pressure amplitude, X_o. The charge density increases with initial poling field for all of the tested samples.

Figure 7-4 (B.) shows the resulting values of the piezoelectric coefficient d_{33} versus pressure amplitude for the samples poled at 25°C. As the initial poling field increases, the d_{33} values increase as well, consistent with trends in Fig 7-4(A). For example, the average d_{33} values for materials poled at 0.75 kV/mm and 25°C was 163 pC/N, while the average piezoelectric coefficient values for the samples poled at 1kV/mm and 2 kV/mm were 315 pC/N and 360 pC/N, respectively. A linear fit of the form y = a*x +b for the values of d_{33} as a function of pressure amplitude was obtained for samples of different poling conditions and the coefficients for each of those fits is given in Table 7-2. The slope of each line yields “a” for that particular poling condition and the y-axis intercept yields “b”. The ratio of a/b is also listed in the table.

The phase angle (δ)for each of the differently poled sample measurements was calculated by dividing the area of the hysteresis loop by the quantity $[\pi*d_{33}*X^2]$. A plot of the phase angle versus the amplitude of the applied pressure can be seen in Figure 7-5.

7.2.3 Cyclic Pressure Experiments at Different Frequencies

Figure 7-6 shows the values of d_{33} vs frequency for the samples poled at different electric field amplitudes. As the poling field increases, the value of the

piezoelectric coefficient increases as well. Regardless of initial poling field, at higher frequencies the value of the piezoelectric coefficient decreases.

The phase angle versus frequency for each of the differently poled samples is shown in Figure 7-7. The phase angle increases as the initial poling field increases.

7.3 Discussion

The sample poled at 25°C and 1 kV/mm had a Berlincourt d33 value of 460 pC/N, while the sample poled at the same temperature but twice the value of the electric field has a d33 value of 506 pC/N. The lowest Berlincourt d33 value was 425 pC/N for the sample poled at 0.75 kV/mm and 25°C. This directly illustrates the effect of initial poling field on apparent piezoelectric coefficient values. The values of d33 at 4 MPa from the charge versus pressure amplitude curves was 167 pC/N, 316 pC/N and 348 pC/N for the samples poled at 0.75 kV/mm,1 kV/mm, and 2 kV/mm, respectively. While the d33 values increase with poling field as well, the measured values and calculated averages between the Berlincourt and direct d33 measurements differ significantly. This could be due to a number of factors such as sample geometry or measurement frequency, which can have a significant effect on the effective Berlincourt d33 values[46]. However, the values measured for d33 seem to be in reasonable agreement with the literature (values between 100 pC/N and 400 pC/N) for the given materials compared to literature on similarly measured PZT ceramics[44], [47], [48].

A linear fit of the d_{33} for the differently poled samples can give the Rayleigh parameters (d_{init} and α) for the samples measured, if they are truly exhibiting Rayleigh behavior. The Rayleigh law is only valid for the low field regime and it is

possible that the pressures used in these experiments (>4MPa) were outside of the Rayleigh regime. The value of the y-axis intercept increases for each of the poling conditions from 175 ± 1 pC/N for the 0.75 kV/mm poled sample, to 320 ± 3 pC/N for the 1 kV/mm poled sample, to 344 ± 8 pC/N for the 2 kV/mm poled sample. These values represent the combination of the the intrinsic d_{33} response of the measured piezoelectrics and the reversible component of their response when Rayleigh is valid. The values for the slope increase with increasing initial poling field amplitude, going from -1.8 ± 0.15 (10^{-18} m^2 C N^{-2}) for the 0.75 kV/mm poled sample, to -0.75 ± 0.44 (10^{-18} m^2 C N^{-2}) for the 1 kV/mm poled sample, to 2.5 ± 1.2 (10^{-18} m^2 C N^{-2}) for the 2 kV/mm poled sample. The negative slope could be a result of partial versus full poling and domain back switching or deaging effects that may be occurring during the mechanical compression.

A comparison of the charge density versus pressure amplitude and d_{33} versus pressure amplitude plots, Figure 7-3 and Figure 7-4, respectively, yields interesting observations. The charge density for each poling condition apparently increases as the applied sinusoidal pressure increases for each of the initial poling states investigated. The response of the piezoelectric coefficient seems relatively flat as a function of applied pressure amplitude for the measured samples, yet the values of the piezoelectric coefficients increase as a function of initial poling condition, the sample poled at 0.75 kV/mm has the lowest d_{33} values and the sample poled at 2 kV/mm has the highest.

If Rayleigh is applicable, then the increase in the y-intercept (d_{init}) with increasing initial poling field would indicate that the intrinsic and reversible

response of the material was directly proportional to the degree of poling and the extrinsic response is highest for the most fully poled sample. However, the error for the values obtained from these linear fits is relatively high and though the 0.75 kV/mm sample's fit has an R^2 value of .97, the 1 kV/mm and 2 kV/mm samples had R^2 values of 0.42 and 0.54, respectively. This indicates that a linear fit of the data for the more fully poled samples may not be the best fit and that the Rayleigh equations might not be applicable.

Furthermore, in Figure 7-5, the phase angle is plotted versus the amplitude of the applied pressure and as the initial degree of poling increases the phase angle increases as well.

Natterman et al. [49] proposed a model for the nature of interface or domain wall pinning in random systems by imperfections. Though the model was presented and explained for magnetic systems, it was generalized in such a way that it could be applied generally to ferroic systems, i.e. ferroelastic or ferroelectric. Natterman describes the relationship between both the length scale of interaction and subsequently the time scales involved. In his model, at lower frequencies and shorter length scales, interfaces are able to react more quickly, effectively independent of frequency. At longer length scales there are more opportunities for pinning of the interface to occur and the material reacts more slowly, resulting in a frequency dependence of the response. He found that the magnetic susceptibility, χ, could be calculated as $\chi(\omega) = Fo + F * \ln [1/(\omega * t_o)]^{\theta}$ where Fo and F are constants and t_o is a time constant. The exponent θ is associated with the roughness of the interface.

The work of Damjanovic goes on to further support the previously mentioned model [47]. Damjanovic directly applies the generalized model in terms of magnetic susceptibility to the specific case of the piezoelectric coefficient in a ferroelectric and finds that as a function of frequency, $d_{33}(\omega) = Fo + F * \ln [1/(\omega)]$. In this case the interface roughness exponent, $\theta = 1$. Additionally, Damjanovic found that the frequency dependence of d_{33} is due to the frequency dependence of the reversible and irreversible Rayleigh parameters and that the pinning of domain walls in a ferroelectric system and the field and frequency dependence of d_{33} behave similarly to of the magnetic domain walls and the field and frequency dependence of susceptibility in ferromagnetic materials.

The frequency response of the samples' piezoelectric coefficient can be seen in Figure 7-6. Again as in the previous plots, it is apparent that the higher the degree of poling the higher the material response, i.e. the piezoelectric coefficient. As frequency increases, the d_{33} values appear to decrease. For all poling conditions, the piezoelectric coefficient decreases monotonically with the logarithm of frequency and can be represented with a linear equation of the form $d_{33}(\omega) = 193 - 2.3 \ln(\omega)$ for the 0.75 kV/mm sample, $d_{33}(\omega) = 330 - 4.9 \ln(\omega)$ for the 1 kV/mm sample, and $d_{33}(\omega) = 365 - 6.8 \ln(\omega)$ for the 2 kV/mm sample. This result is consistent with the model presented by Natterman and supported by the work of Damjanovic that describes pinning and interface effects in ferroic systems [47], [50].

Figure 7-7 shows the Phase Angle of the measured samples versus the measurement frequency. Though the values of the Phase Angle seem to be fairly

constant as a function of frequency, the δ_p values do increase as the degree of poling increases.

7.4 Conclusions

In conclusion, it has been shown that a logarithmic frequency dependence exists for the piezoelectric coefficient of the differently poled samples and d_{33} decreases monotonically with the log of frequency. A higher degree of poling consistently increased the value of the piezoelectric coefficient.

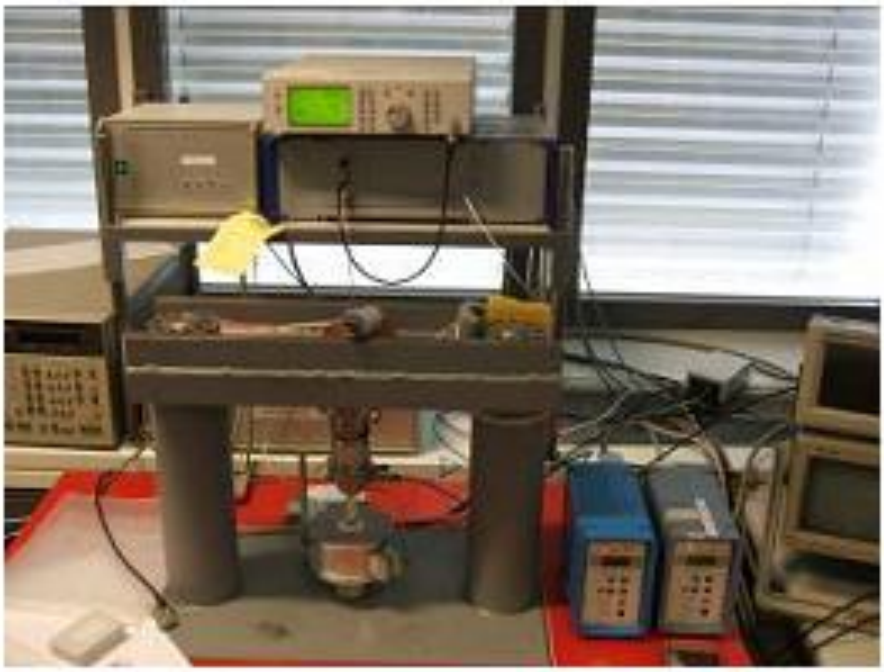

A

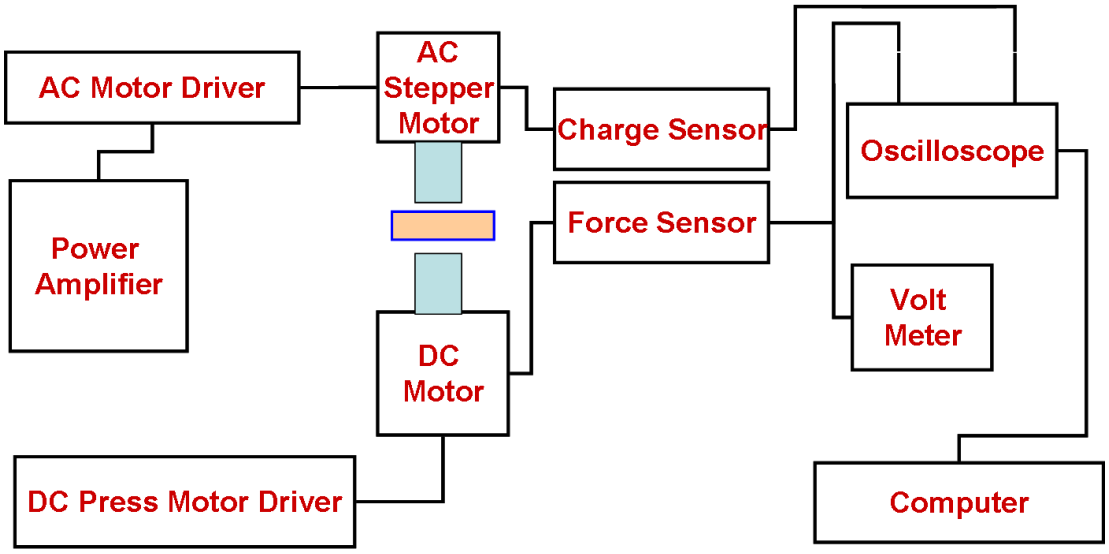

B

Figure 7-1. AC press experimental set-up.

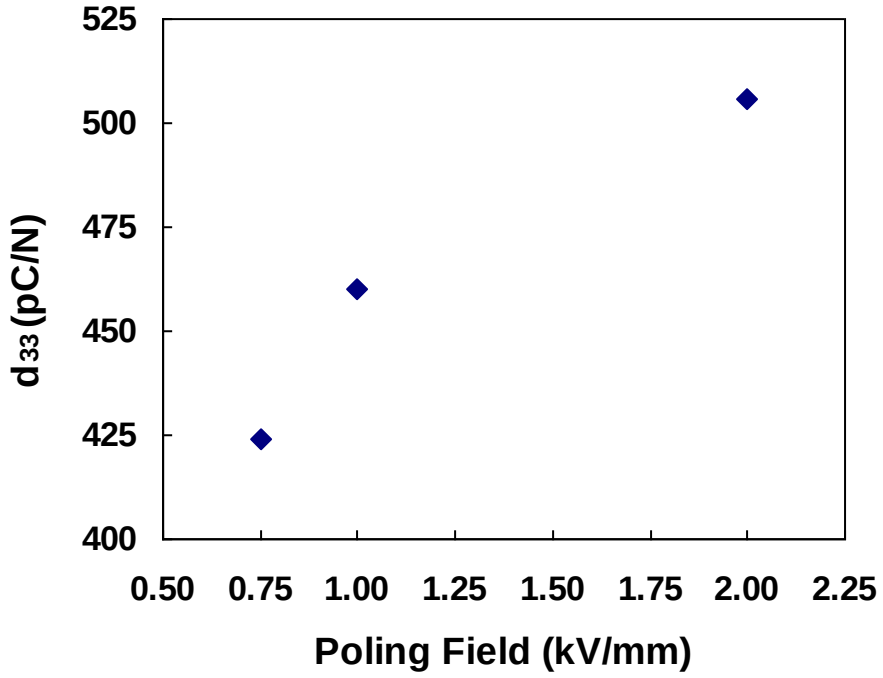

Figure 7-2. The measured Berlincourt d_{33} values at a constant poling temperature of 25°C.

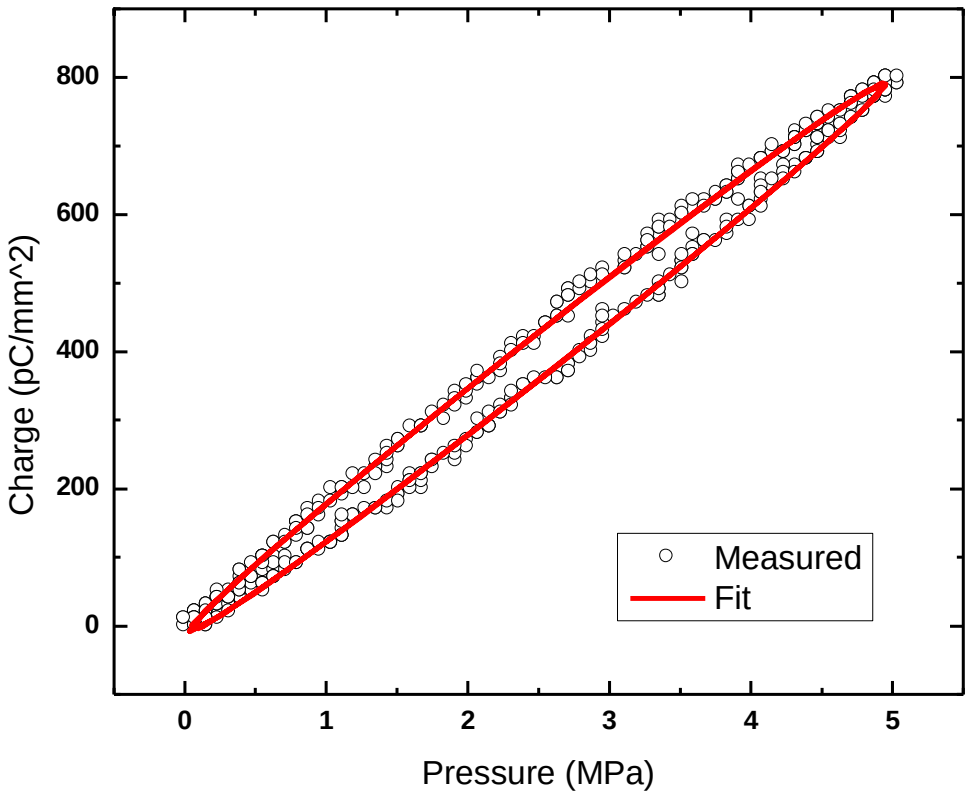

Figure 7-3. Representative hysteresis loop and data fit using Eqn (7-5).

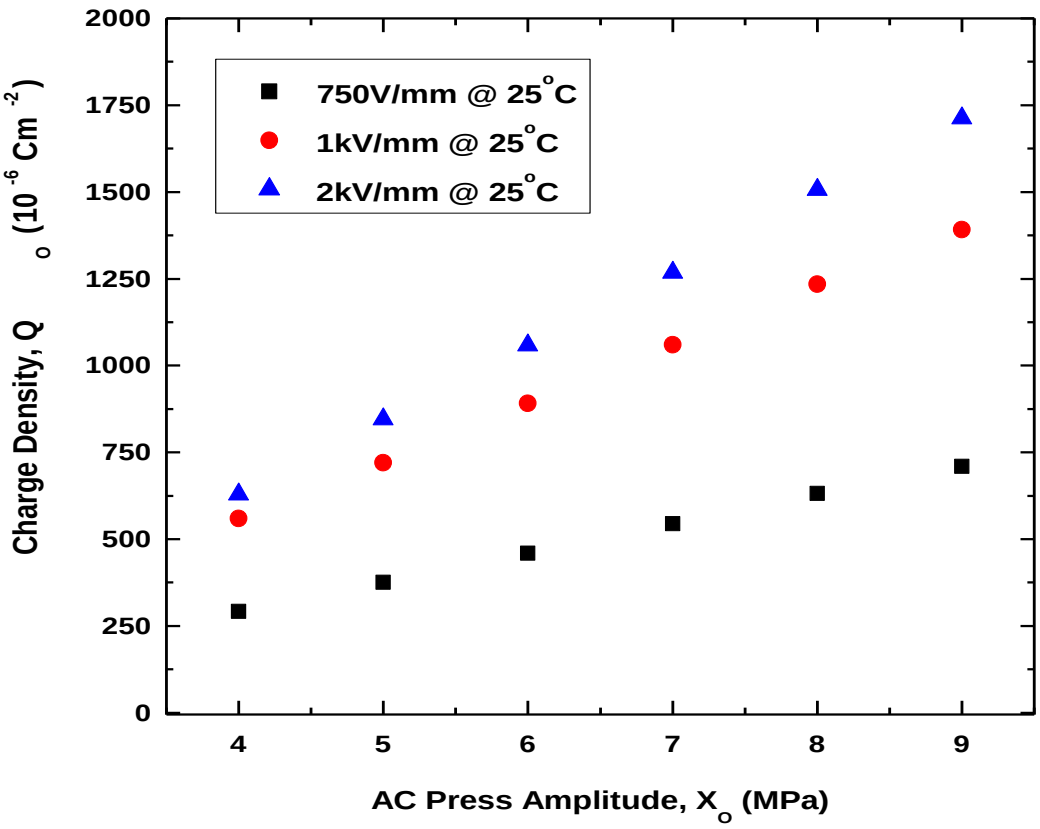

A

Figure 7-4. EC65 poled at constant temperature. A) Constant poling temperature: Charge density response to cyclic pressure B) Constant poling temperature: Piezoelectric response to cyclic pressure

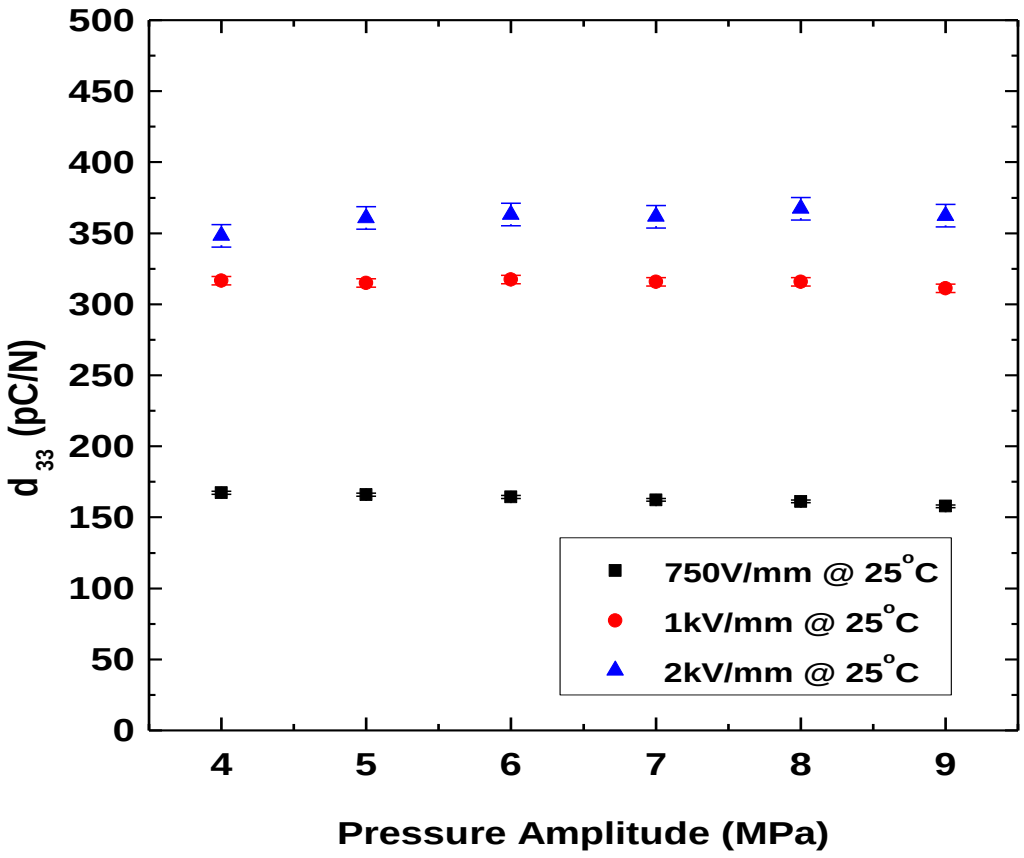

B

Figure 7-4. Continued.

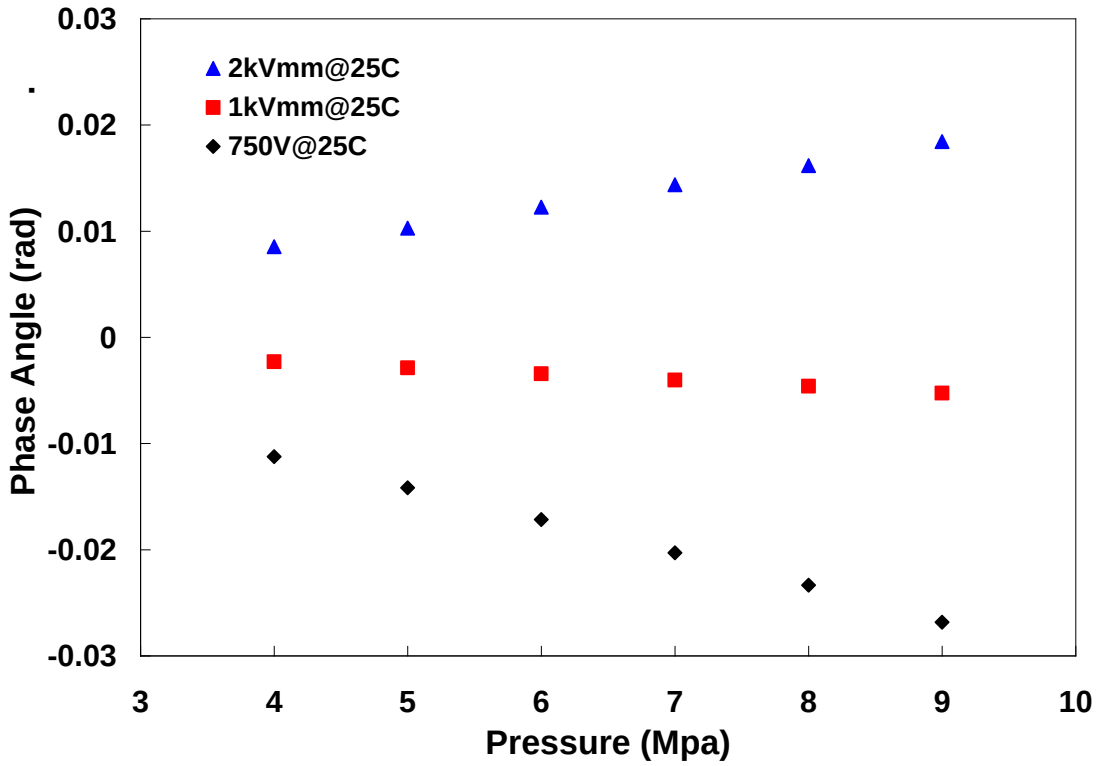

Figure 7-5. Phase Angle vs. Pressure amplitude for samples with initial poling conditions of 0.75 kV/mm, 1 kV/mm, and 2 kV/mm for these measurements.

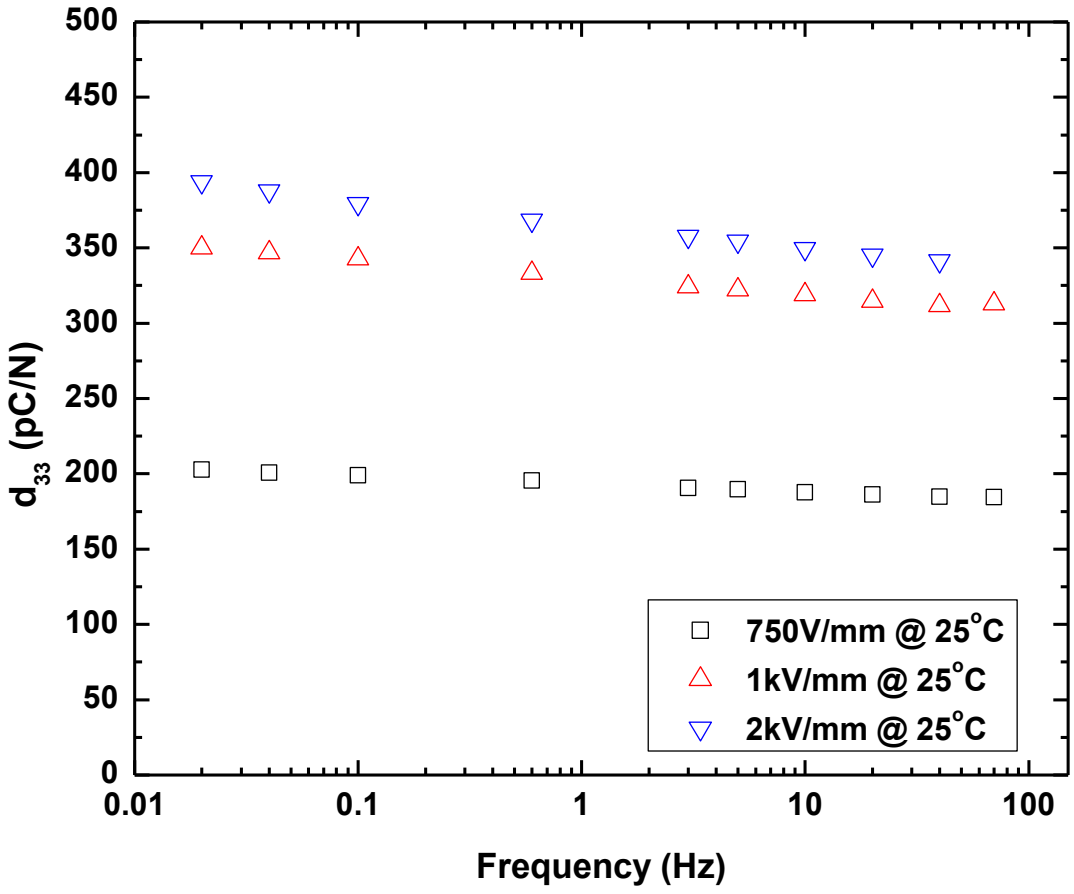

Figure 7-6. Constant poling temperature: piezoelectric frequency response to cyclic pressure

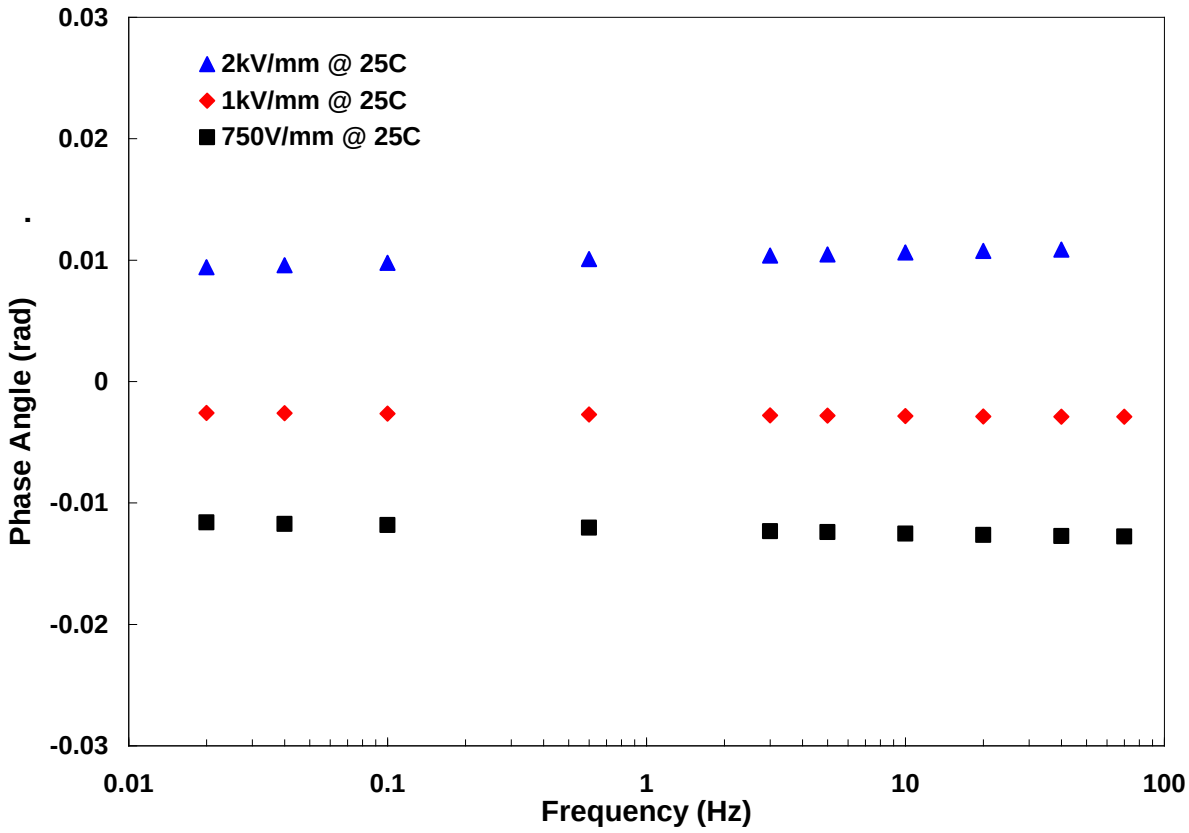

Figure 7-7. Phase angle vs. frequency graph for samples with initial poling conditions of 750 V/mm, 1 kV/mm, and 2 kV/mm for these measurements,

Table 7-1. List of samples and electrical poling conditions

Sample Designation	Poling Field (kV/mm)	Poling Temperature (°C)
EC65	0.75	25
EC65	1	25
EC65	2	25

Table 7-2. Values for samples poled at 25°C and fit to Eqn 7-2

Poling Condition	d_{init} or Intercept (pC/N)	α or Slope (10^{-18} m^2 C N^{-2})	α/d_{init} (10^{-6} Pa^{-1})
0.75 kV/mm 25°C	175 ± 1.01	-1.8 ± 0.15	-0.010
1 kV/mm 25°C	320 ± 2.94	-0.75 ± 0.44	-0.002
2 kV/mm 25°C	344 ± 7.92	2.5 ± 1.2	0.007

CHAPTER 8
SUMMARY

8.1 Discussion

Ferroelectric materials are used in a wide variety of sensor and memory applications due to their electromechanical coupling ability and polarization memory. This functionality requires a polar crystal structure in which the internal dipole is directionally biased. The thermodynamics of this polarization bias are typically described using a potential energy well versus displacement plot such as that shown in Figure 8-1. In Figure 8-1A, the equilibrium position of the B ion in an ABO_3 unit cell is at the center of the unit cells, resulting in no polarity, and is the structure of the material in the high-temperature, non-ferroelectric state. As temperature is lowered and the ferroelectric phase becomes stable, the B cation is displaced in one of the [001] directions in order to lower its energy. Figure 8-1 B shows the type of “double-well” potential that can be expected in this state in a ferroelectric unit cell. The response of a ferroelectric material to an electric field can also be described using the energy schematics in Figure 8-1. In Figure 8-1 C, the position of a B cation and the change in the energy profile is shown schematically. The detailed physical models for this type of behavior have been described by others [51][33].

The regions of uniform polarization in a ferroelectric are called ferroelectric domains, and they are generally formed in an attempt to minimize the free energy of the system. The interface between two domains is a domain wall. Tetragonal perovskite structured PZT materials have possible polarization directions and available orientations that are either antiparallel or perpendicular, referred to as 180° or 90° domain walls, respectively. The 180° domain walls generally contribute primarily to the dielectric

properties and are purely excited by electric fields, while 90° (non-180°) domain walls contribute to the strain and polarization and are excited by stress and electric fields [13], [33], [34].

In real ferroelectric materials, many unit cells constitute the ferroelectric domains, meaning that the response is governed by the collective effects of numerous unit cells and domain walls. The intrinsic response, leading to both polarization and elongation, involves the distortion of the crystallographic unit cell which includes small local B-cation displacements (illustrated in Figure 8-1 B). The extrinsic response involves the movement of domains and domain walls, or the collective reorientation of unit cells.

Electrical poling involves the application of an electric field to a ferroelectric material after processing and results in an overall polarity bias in the entire material that mimics the polarity bias in the unit cell. Domains can be reoriented and domain wall positions are changed by the poling process and numerous factors affect the degree of poling and thus the resultant properties in the biased state. For example, it is well known that the coercive field of a ferroelectric is influenced by chemical modification of the structure, or doping, since doping affects the point defect structure in a material[6]. Thus, donor modification through the doping process can be thought of energetically as lowering the energy barrier for dipolar reorientation shown in Figure 8-1 C. In acceptor-modified materials, defects or defect dipoles are known to restrict the motion of domain walls [4], and the energy barrier to domain wall motion can be described as increasing. Moreover, domain walls can become pinned or clamped by defects and imperfections. These pinning centers can inhibit the motion of domain walls. Mechanical stress has

also been shown to influence the degree of domain wall motion that occurs during the poling process [9], [10].

In many ferroelectrics, the piezoelectric and dielectric properties have a field-dependence. For instance, Figure 8-2 shows an example of the relative permittivity versus electric field measurements for a ferroelectric sample. A low field region of approximately constant ε'_r can be clearly distinguished from a region above the threshold field E_t where ε'_r increases linearly with the applied field E_o, but below the coercive field. This intermediate field region is known as the Rayleigh region. At the high field region, above the coercive field E_c, switching occurs and the ε'_r versus E_o behavior becomes non-linear. The graph in Figure 8-2 is a representation of the general nonlinear behavior in ferroelectric ceramics.

Domain-wall displacement in a polycrystalline medium with pinning centers can be expressed as a combination of reversible movement around an equilibrium position at the minimum of a potential well and irreversible displacement across potential barriers as shown in Figure 8-3. The irreversible displacement into a new equilibrium position occurs when the driving field is large enough to overcome potential barriers around the original position.

When domain wall displacement is considered in a medium which contains randomly distributed defects, these defects act as pinning centers for domain walls and the potential energy of the domain walls becomes an irregular function of the wall position [4],[52]. An example of this type of energy profile is shown in Figure 8-3 A. Nonuniformities in the lattice (e.g. random pinning centers) produce a distribution of free energy profiles which can produce differing saturation behavior after dipole switching

and can be manifested as variations in the local coercive field and remnant polarization (Smith et al 2003 “A Free Energy Model for Hysteresis in Ferroelectric Materials”). As domain walls move in the medium a field dependence of the piezoelectric charge and the piezoelectric coefficient occurs. This field dependence can be expressed by the Rayleigh relations [5].

Originally, the Rayleigh law was applied to ferromagnetic materials, but it has been very useful in describing the relative extrinsic and intrinsic contributions to the piezoelectric behavior in ferroelectric ceramics[4],[13],[14]. The generalized Rayleigh law for the piezoelectric materials is expressed as

$$p(F_o) = p_{init} + \alpha_p \cdot F_o, \qquad (8\text{-}1)$$

where the material property coefficient $p = \varepsilon \text{ or } d$ (permittivity or piezoelectric coefficient), the general driving force $F = \Pi \text{ or } E$ (stress or electric field) and p_{init} is the zero-field value of the permittivity or the converse or direct piezoelectric coefficient. The Rayleigh coefficient (α_p) in Equation 8-1 represents a quantitative measure of the irreversibility of domain wall displacement and describes the field dependence of the direct piezoelectric coefficient (α_{dp}), the converse piezoelectric coefficient (α_{cp}), or the dielectric permittivity (α_ε). The absolute extrinsic contribution due to the irreversible displacement of domain walls is described by the quantity $\alpha_p \cdot F_o$. Examples of extrinsic contributions could include 180° and non-180° domain wall motion. The total material coefficient, $p(F_o)$, is the sum of an irreversible extrinsic contribution, $\alpha_p \cdot F_o$, and the reversible plus intrinsic component p_{init}. By calculating the α_p coefficient values, quantitative information about the extrinsic response of a particular material can be calculated.

8.1.1 Electrical Driving Force

8.1.1.1 Strength of poling

The field-induced domain wall motion in the commercial PZT designated K350 demonstrated independent effects of 180° and non-180° domain wall contributions to the dielectric and piezoelectric properties. The Rayleigh parameters for the dielectric (ε_{init} and α_{ε}) and converse piezoelectric (d_{init} and α_{cp}) responses of the material are calculated in previous chapters and introduced in order to compare these effects.

Table 8-1 shows how permittivity varies with the strength of the electric poling field. The coefficient ε_{init} is a measure of the collective intrinsic and reversible contributions to permittivity for the polycrystalline material with multiple domains. Table 8-1 shows that ε_{init} increases with the strength of poling independent of measurement frequency. For example the ε_{init} value at 3 Hz increases from 567 to 1180. This likely indicates that the intrinsic contribution to the permittivity increases for the entire polycrystal since the value ε_{init} represents the reversible and intrinsic contribution.

Table 8-2 shows the piezoelectric coefficient increases independent of frequency for all poling strengths (e.g. from 28 to 193 pm/V for 3 Hz). The parameter d_{init} represents a combination of the intrinsic contribution and the reversible contribution to the piezoelectric response. The substantial increase in the d_{init} coefficient as seen in Table 8-2 is likely associated with the intrinsic contribution to the piezoelectricity increasing with a higher degree of poling.

More insight into the intrinsic coefficients can be garnered by comparing d_{init} and ε_{init}, since the intrinsic contribution to domain wall motion is described quantitatively through these coefficients. The ε_{init} value increases by a factor of 2 as the poling field increases from 0.75 to 1.0 kV/mm. Across similar strengths in poling and measured at

the same frequency, the d_{init} value increases by a factor of 7. The dramatic increase in d_{init} when compared to ε_{init} is likely due to the fact that before they are poled, ceramics have a d_{init} value of zero and already have a finite ε_{init} value, so while the poling process will contribute to some of the dielectric response it influences all of the piezoelectric response.

The quantity α can describe the extrinsic contribution due to the irreversible displacement of domain walls. Table 8-2 shows that the values for the converse piezoelectric α_{cp} coefficient increase from approximately 0.014 to 0.086 (pm/V)/(V/mm) as poling strength increases. For the converse piezoelectric response the α_{cp} coefficient, which represents the irreversibility of domain wall motion, increases significantly. Prewitt et al [31] reported that more irreversible domain wall motion occurs at higher degrees of poling, and these results seem consistent.

It is interesting that the piezoelectric α_{cp} coefficient increases with increased poling significantly more than the dielectric α_{ε} coefficient. The energy landscape for 180° and non-180° domain walls can differ significantly even in the exact same material (see Figure 8-3 A). Since α_{cp} is a measure of the irreversibility of non-180° domain walls (as measured in d_{33}) and α_{ε} is a measure of the irreversibility of 180° domain walls (as measured in ε_{33}) it is possible that irreversible motion of non-180° domain walls are more affected by poling strength than the irreversibility of 180° domain walls.

8.1.1.2 Frequency dispersion

At the strongest poling conditions, the ε_{init} value and α_{ε} for permittivity both decrease with frequency, as seen in Table 8-1. It is expected that both reversible and irreversible domain wall contributions will be reduced at higher frequencies. Interestingly, at weaker poling conditions the α_{ε} value decreases as frequency increases

yet the ε_{init} value increases with increasing frequency. This may occur if the sample is experiencing fatigue or deaging [53]. This effect cannot be observed to the same degree at the stronger poling conditions. The d_{init} values decrease for all of the poling conditions listed in Table 8-2. The decrease of the d_{init} value at higher frequencies is likely a result of either the reversible or the intrinsic response, since d_{init} describes both the reversible and the intrinsic contribution to the piezoelectric response, The intrinsic contribution to the piezoelectric effect is primarily independent of frequency at the frequency ranges measured here, so it is likely the frequency effects are exclusively a result of the reversible domain wall motion associated with d_{init}. Since the d coefficient is primarily associated with non-180° domain wall motion in the system described, reversible non-180° domain wall motion contributions likely are decreasing at increased frequencies.

8.1.2 Mechanical Driving Force

Next, stress-induced domain wall motion was investigated on another soft PZT, EC-65 in order to understand the effects of strong forces on large-scale domain switching and weak forces on small-scale domain wall motion. Neutron diffraction measurements as well as direct piezoelectric response measurements were taken on soft PZT EC-65 to study the response of domain walls due to mechanical stress. Both large static forces and dynamic weak forces are used in order to better understand the energetic landscape of the material, specifically how the forces affect domain wall motion across various types of pinning centers.

8.1.2.1 Domain switching measured during application of strong forces

In order to get a general understanding of how the electrical poling process affected the samples the direct piezoelectric coefficient was measured using a

traditional Berlincourt d_{33} meter. The initial piezoelectric coefficient of the samples (Berlincourt) is shown in Table 8-3. An increase in d_{33} with increased strength of initial electrical poling is observed. This indicates that the domain walls are moving and the sample is becoming polarized due to the poling process. In order to see if the degree of domain wall alignment could be increased using large stresses beyond that obtained during the initial electrical poling process, additional forces were applied to poled samples. Specifically, a longitudinal stress was applied in a direction transverse to the initial poling direction as shown in Figure 8-4 A. The goal of this measurement was to investigate the response of non-180° domain walls to large transverse stresses that attempt to reorient domain walls in the 'forward' direction because compressive stress creates 'positive' bias in transverse direction (e.g. stress applied in the x or y direction would result in some additional domain reorientation (polarization) in the z direction). The results of the *in situ* neutron diffraction measurements show that the degree of 002-domain alignment in the poling direction does not increase substantially beyond that achieved in the initial electrical poling process even under high transverse stresses. This likely means that on average, when describing all domain walls collectively, the motion of non-180° domain walls is predominately exhausted during the electrical poling process. This may be related to the non-180° domain walls being located next to very strong pinning centers in the poled state i.e. there are very high irreversible barriers in the energy landscape for the material that can not be further moved or overcome after the initial electrical poling field is applied.

8.1.2.2 Direct piezoelectric effect measured under weak cyclic forces

In order to measure the effect of non-180° domain wall motion to weak forces that are alternating (cyclic), a longitudinal stress was used to measure d_{33} during the direct

piezoelectric testing. The cyclic small-scale stress measurements show how domain walls respond to smaller longitudinal stress. Table 8-4 shows that d_{init} increases with increasing strength of poling (i.e., initial poling field). This is expected since the sample is becoming more well-poled, allowing more switching and therefore the intrinsic piezoelectric coefficient is expected to increase.

Table 8-4 also shows that α_d increases with strength of poling. Combined with the increase in d_{init} above, this makes a nice direct piezoelectric analogue to the previous section's converse piezoelectric measurements as well as results published in Prewitt et al [31]. The irreversibility in the direct piezoelectric coefficient increases with increased strength of poling even though the driving force (electric field versus stress) is different. This showcases one aspect of the material behavior that is similar for the two different types of soft PZT.

8.2 Conclusion

In general, the direct piezoelectric coefficient measurements show that irreversible non-180° domain wall contributions increase with increasing strength of poling. However, the application of strong forces shows that domain walls do not move over exceedingly large distances. It is possible that this occurs because domain walls are next to large pinning centers during poling as in Figure 8-3 B. Further mechanical stress to move them in the 'forward' direction is ineffective. However, small cyclic stresses in the 'reverse' direction may be able to overcome smaller pinning centers and move in a way which yields Rayleigh behavior. The changes in energy landscape in response to poling seems to have significant effects on domain wall motion by changing the way pinning centers move in the material.

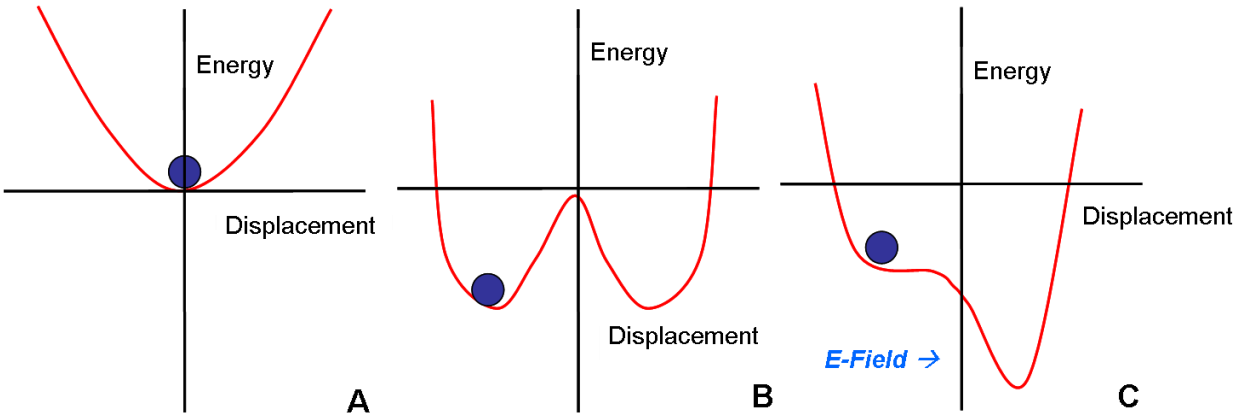

Figure 8-1. Energy profile for a simple PZT type unit cell. (A) Reversible Displacement or Paraelectric Phase. (B) Ferroelectric Phase with reversible and irreversible transitions. (C) Potential energy curve in the presence of electric field.

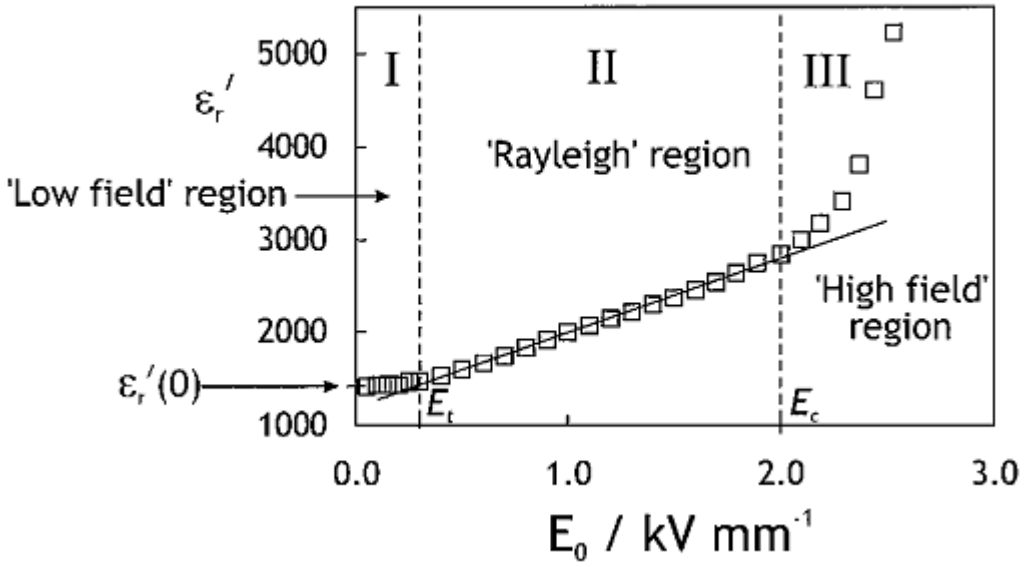

Figure 8-2. Schematic view of field dependence of dielectric permittivity in ferroelectric ceramics over a wide range of field strengths.Adapted from Reference [13]

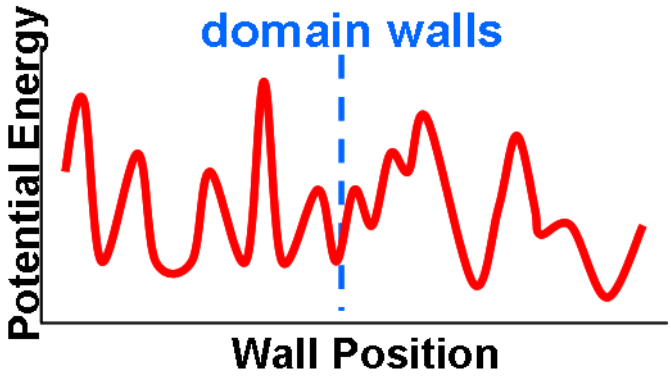

A

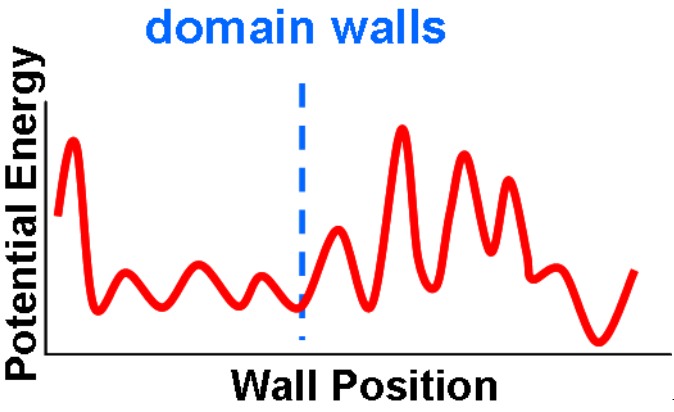

B

Figure 8-3. Schematic Diagrams of possible energy landscapes in a ferroelectric. (A) Normal energy landscape representing the potential of a domain wall with randomly distributed pinning centers. (B) Possible alternate energy landscape after application of electric field. Some of the pinning centers are moved while some are more rigid and remain.

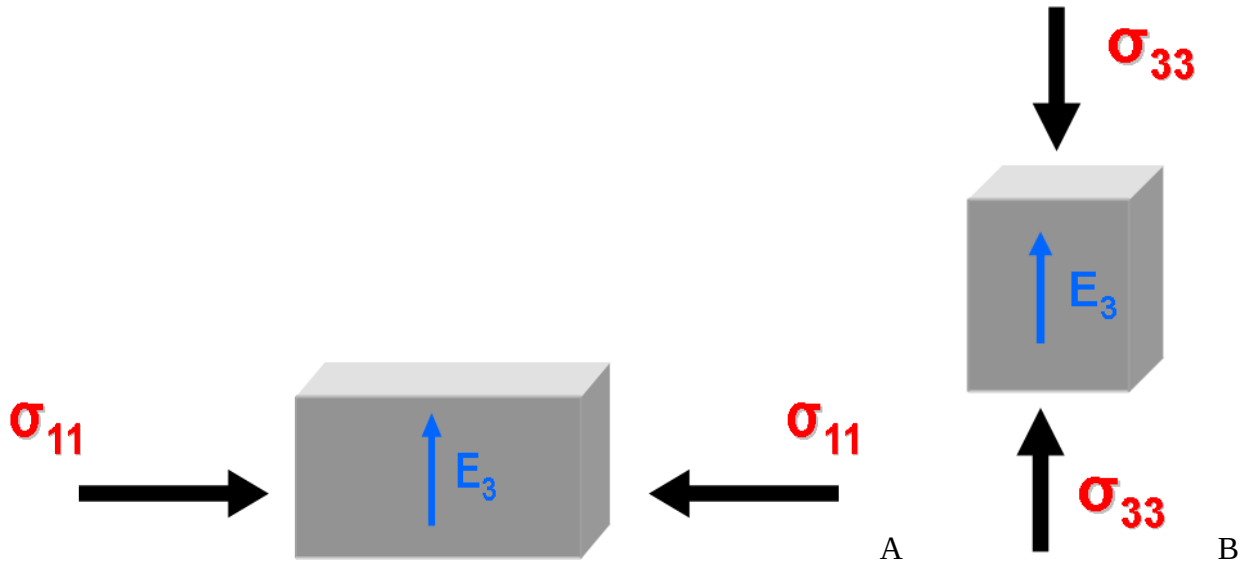

Figure 8-4. Poling direction and direction of applied stress. A.) Mechanical Compression during diffraction set-up. Stress was applied perpendicular to the electrical poling direction. B.) Direct d_{33} measurements. Stress was applied parallel to electrical poling direction.

Table 8-1. Values of α_ε, ε_{init}, and $\alpha_\varepsilon/\varepsilon_{init}$ for K350samples poled at different poling conditions. Poling temperature was 50°C.

Frequency [Hz]	0.75 [kV/mm]			1 [kV/mm]			2 [kV/mm]		
	α_ε mm/V	ε_{init}	α_ε / ε_{init} mm/V	α_ε mm/V	ε_{init}	α_ε / ε_{init} mm/V	α_ε mm/V	ε_{init}	α_ε / ε_{init} mm/V
0.6	1.8	567	0.0031	1.9	1110	0.0017	1.6	1217	0.0013
3	1.3	576	0.0023	1.7	1089	0.0016	1.4	1180	0.0012
50	0.9	609	0.0015	1.4	1094	0.0013	1.3	1159	0.0011
500	0.7	605	0.0012	1.2	1059	0.0012	1.2	1130	0.0011

Table 8-2. Values of α_{cp}, d_{init}, and α_{cp}/d_{init} for K350 samples poled at different poling conditions. Poling temperature was 50°C.

Frequency [Hz]	0.75 [kV/mm]			1 [kV/mm]		
	α_{cp} (pm/V)/(V/mm)	d_{init} (pm/V)	α_{cp} / d_{init} (mm/V)	α_{cp} (pm/V)/(V/mm)	d_{init} (pm/V)	α_{cp} / d_{init} (mm/V)
0.06	0.013	34	3.7E-4	0.079	223	3.5E-4
0.6	0.015	30	5.0E-4	0.075	215	3.5E-4
3	0.014	28	5.0E-4	0.086	193	4.4E-4

Table 8-3. Initial poling information for PZT samples measured at 25°C and mechanical stress results.

Poling Field (kV/mm)	Poling Temperature (°C)	d_{33} (pC/N)	η_{002} Begin	η_{002} End	η_{200} Begin	η_{200} End
0.5	25	204	0.15	0.23	0.85	0.77
1	25	435	0.29	0.30	0.71	0.70
2	25	485	0.25	0.27	0.75	0.73

Table 8-4. Values of α_{dp}, d_{init}, and α_{dp}/d_{init} for K350 samples poled at different poling conditions. Poling temperature was 25°C.

Poling Condition (kV/mm)	d_{init} or Intercept (pC/N)	α_{dp} or Slope (10^{-18} m^2 C N^{-2})	α_{dp}/d_{init} (10^{-6} Pa^{-1})
0.75	175	-1.8	-0.010
1	320	-0.75	-0.002
2	344	2.5	0.007

CHAPTER 9
FUTURE WORK

9.1 Continuation of Previous Research

9.1.1 Extension of Current Experiments

Continuation of the previous experiments for several intermediate poling fields and temperatures can be conducted for a more complete picture of how degree of poling affects properties. Eventually a full contour map of d_{33}, ε_{33}, and the corresponding Rayleigh parameters could be very informative. Additional experiments done at a broader frequency range could provide additional information on the effects of poling.

9.1.2 Additional Poling Experiments

Though the effect of poling time variation was beyond the scope of this thesis, there is evidence that poling time, in addition to field strength, can affect the response of ferroelectric materials [54],[55–57]. Previous work suggests that in addition to electric field dependence of ferroelectric properties, there is also a temporal dependence at certain time scales [58]. During small enough time scales, it has been shown that there is a relationship between the applied electric field and the time it takes for domain switching to occur and that strain and polarization occur over different time scales [59]. Additional experiments examining the effect of poling time (e.g. short pulsed fields) on material response may provide more insight on dielectric and ferroelectric behavior.

9.2 Suggestions for Future Work

9.2.1 Poling in Other Material Systems

Materials other than the commercial lead zirconate titanate investigated may be affected differently by the poling process. Using a similar methodology it may be

possible to decouple the intrinsic and extrinsic effects in other piezoelectric materials including chemically modified PZT as well as lead free materials.

9.2.2 Poling in Thin Films

There are numerous applications for ferroelectric materials to be used in thin film devices and structures and many factors influence their overall performance [4], [60] [61], [62]. For instance, the effects of substrate induced stresses significantly impact material and device performance. Investigation of how the inherent stresses in thin films are affected by the poling process could provide new insights into the behavior of piezoelectric films on a substrate.

In technologies such as ferroelectric random access memory (FRAM), there is significant interest in increasing storage density and performance through geometric scaling [63], [64]. Better understanding of how electric field, stress, and temperature affect properties at various size scales is essential to significantly advancing the currently available technology.

9.2.3 Enhanced Device Characterization

Extension of this work to investigate the proceeding systems described in this chapter could lead to novel characterization methodologies for advanced devices and materials. For instance, in semiconductor devices such as AlGaN/GaN transistors the piezoelectric effect (converse) can have a profound effect on device performance [65]. The effects of strain on device performance may be mitigated by sufficient pre-poling.

LIST OF REFERENCES

[1] M. E. Lines and A. M. Glass, *Principles and Applications of Ferroelectrics and Related Materials*, New Ed. Oxford University Press, USA, 2001.

[2] W. D. Callister Jr., *Materials Science and Engineering: An Introduction*, 7th ed. Wiley, 2006.

[3] D. R. Askeland and P. P. Fulay, *The Science & Engineering of Materials*, 5th ed. CL-Engineering, 2005.

[4] D. Damjanovic, “Ferroelectric, dielectric and piezoelectric properties of ferroelectric thin films and ceramics,” *Rep. Prog. Phys*, vol. 61, no. 1267–1324, pp. 97–98, 1998.

[5] D. Damjanovic and M. Demartin, “The Rayleigh law in piezoelectric ceramics,” *Journal of Physics D: Applied Physics*, vol. 29, no. 7, pp. 2057–2060, 1996.

[6] G. H. Haertling, “Ferroelectric Ceramics: History and Technology,” *J Am Ceram Soc*, vol. 82, no. 4, pp. 797–818, 1999.

[7] K. M. Rabe, C. H. Ahn, and J.-M. Triscone, *Physics of Ferroelectrics: A Modern Perspective (Topics in Applied Physics)*, 1st ed. Springer, 2007.

[8] N. Spaldin, “Analogies and Differences between Ferroelectrics and Ferromagnets,” *Physics of Ferroelectrics*, 2007.

[9] T. Granzow, A. B. Kounga, E. Aulbach, and J. Rödel, “Electromechanical poling of piezoelectrics,” *Applied Physics Letters*, vol. 88, p. 252907, 2006.

[10] A. B. Kounga Njiwa, E. Aulbach, T. Granzow, and J. Rödel, “Influence of radial stress on the poling behaviour of lead zirconate titanate ceramics,” *Acta Materialia*, vol. 55, no. 2, pp. 675–680, 2007.

[11] A. B. Kounga, T. Granzow, E. Aulbach, M. Hinterstein, and J. Rodel, “High-temperature poling of ferroelectrics,” *Journal of Applied Physics*, vol. 104, no. 2, p. 24116–24116, 2008.

[12] C. GANPULE, A. ROYTBURD, V. NAGARAJAN, B. HILL, S. OGALE, E. WILLIAMS, R. RAMESH, and J. SCOTT, “Polarization relaxation kinetics and 180 ° domain wall dynamics in ferroelectric thin films,” *Physical review B. Condensed matter and materials physics*, vol. 65, no. 1, p. 14101–14101, 2001.

[13] D. A. Hall, “Review Nonlinearity in piezoelectric ceramics,” *Journal of Materials Science*, vol. 36, no. 19, pp. 4575–4601, Oct. 2001.

[14] S. Trolier-McKinstry, N. B. Gharb, and D. Damjanovic, “Piezoelectric nonlinearity due to motion of 180° domain walls in ferroelectric materials at subcoercive fields: A dynamic poling model,” *Applied Physics Letters*, vol. 88, p. 202901, 2006.

[15] H. Jaffe, “Piezoelectric ceramics,” *Journal of the American Ceramic Society*, vol. 41, no. 11, pp. 494–498, 1958.

[16] A. Pramanick, A. D. Prewitt, M. A. Cottrell, W. Lee, A. J. Studer, K. An, C. R. Hubbard, and J. L. Jones, “In situ neutron diffraction studies of a commercial, soft lead zirconate titanate ceramic: response to electric fields and mechanical stress,” *Applied Physics A: Materials Science & Processing*, pp. 1–8, 2010.

[17] D. Viehland, “Effect of uniaxial stress upon the electromechanical properties of various piezoelectric ceramics and single crystals,” *Journal of the American Ceramic Society*, vol. 89, no. 3, pp. 775–785, 2006.

[18] X. Tan, Z. Xu, and J. K. Shang, “In situ transmission electron microscopy observations of electric-field-induced domain switching and microcracking in ferroelectric ceramics,” *Materials Science and Engineering A*, vol. 314, no. 1–2, pp. 157–161, 2001.

[19] J. L. Jones and M. Hoffman, “R-Curve and Stress-Strain Behavior of Ferroelastic Ceramics,” *Journal of the American Ceramic Society*, vol. 89, no. 12, pp. 3721–3727, 2006.

[20] J. L. Jones, B. J. Iverson, and K. J. Bowman, “Texture and Anisotropy of Polycrystalline Piezoelectrics,” *Journal of the American Ceramic Society*, vol. 90, no. 8, pp. 2297–2314, 2007.

[21] J. L. Jones, M. Hoffman, and S. C. Vogel, “Ferroelastic domain switching in lead zirconate titanate measured by in situ neutron diffraction,” *Mechanics of Materials*, vol. 39, no. 4, pp. 283–290, Apr. 2007.

[22] “EDO Ceramics EC-65 Lead Zirconium Titanate Piezoelectric.” [Online]. Available: http://www.matweb.com/search/datasheet.aspx?matguid=32ae532d308c4fd7b5bc779dfd3700ed&ckck=1. [Accessed: 11-Apr-2012].

[23] “K-350 - Lead Zirconate Titanate Piezoelectric Ceramic for Hydrophone and Accelerometer Applications.” [Online]. Available: http://www.piezotechnologies.com/k350.htm. [Accessed: 11-Apr-2012].

[24] “PI Ceramic | Leader in Piezoelectric Actuator Technology, PZT Material | Piezoelectric Ceramics / Piezo Materials | Overview.” [Online]. Available: http://www.piceramic.com/site/piezo.html. [Accessed: 11-Apr-2012].

[25] J. E. Daniels, T. R. Finlayson, A. J. Studer, M. Hoffman, and J. L. Jones, “Time-resolved diffraction measurements of electric-field-induced strain in tetragonal lead zirconate titanate,” *Journal of Applied Physics*, vol. 101, p. 094104, 2007.

[26] J. L. Jones, M. Hoffman, J. E. Daniels, and A. J. Studer, “Direct measurement of the domain switching contribution to the dynamic piezoelectric response in ferroelectric ceramics,” *Applied Physics Letters*, vol. 89, p. 092901, 2006.

[27] S. Trolier-McKinstry, N. B. Gharb, and D. Damjanovic, “Piezoelectric nonlinearity due to motion of 180° domain walls in ferroelectric materials at subcoercive fields: A dynamic poling model,” *Applied Physics Letters*, vol. 88, p. 202901, 2006.

[28] W. L. Warren, G. E. Pike, K. Vanheusden, D. Dimos, B. A. Tuttle, and J. Robertson, “Defect-dipole alignment and tetragonal strain in ferroelectrics,” *J. Appl. Phys.*, vol. 79, no. 12, pp. 9250–9257, Jun. 1996.

[29] L. E. Cross and T. W. Cline, “Contributions to the Dielectric response from charged domain walls in ferroelectric Pb5Ge3O11,” *Ferroelectrics*, vol. 11, no. 1, p. 333, 1976.

[30] G. Arlt and N. A. Pertsev, “Force constant and effective mass of 90[degree] domain walls in ferroelectric ceramics,” *J. Appl. Phys.*, vol. 70, no. 4, pp. 2283–2289, 1991.

[31] A. D. Prewitt and J. L. Jones, “Effects of the Poling Process on Piezoelectric Properties in Lead Zirconate Titanate Ceramics,” *FERROELECTRICS*, vol. 419, pp. 39–45, 2011.

[32] N. Bassiri-Gharb, I. Fujii, E. Hong, S. Trolier-McKinstry, D. V. Taylor, and D. Damjanovic, “Domain wall contributions to the properties of piezoelectric thin films,” *Journal of Electroceramics*, vol. 19, pp. 49–67, Mar. 2007.

[33] D. Damjanovic, “Hysteresis in Piezoelectric and Ferroelectric Materials,” in *The Science of Hysteresis*, vol. 3, I. Mayergoyz, and G. Bertotti, Eds. Chapter 4: Elsevier, 2005, pp. 337–465.

[34] N. B. Gharb, S. Trolier-McKinstry, and D. Damjanovic, “Piezoelectric nonlinearity in ferroelectric thin films,” *Journal of Applied Physics*, vol. 100, p. 044107, 2006.

[35] M. Popovici, A. D. Stoica, C. R. Hubbard, S. Spooner, H. J. Prask, T. H. Gnaeupel-Herold, P. M. Gehring, and R. W. Erwin, “Multiwafer focusing neutron monochromators and applications,” in *Neutron Optics*, San Diego, CA, USA, 2001, vol. 4509, pp. 21–32.

[36] B. C. Chakoumakos, J. A. Fernandez-Baca, V. O. Garlea, C. R. Hubbard, and X. L. Wang, “Diffraction at the HFIR,” *Neutron News*, vol. 19, no. 2, pp. 14–17, 2008.

[37] K. An, W. B. Bailey, S. O. Craig, H. Choo, C. R. Hubbard, and D. L. Erdman, “NRSF2 load frame: design, control, and testing,” *Journal of Neutron Research*, vol. 15, no. 3, pp. 207–213, Jan. 2007.

[38] J. E. Daniels, J. L. Jones, and T. R. Finlayson, “Characterization of domain structures from diffraction profiles in tetragonal ferroelastic ceramics,” *J. Phys. D: Appl. Phys.*, vol. 39, no. 24, pp. 5294–5299, Dec. 2006.

[39] J. L. Jones, E. B. Slamovich, and K. J. Bowman, “Domain texture distributions in tetragonal lead zirconate titanate by x-ray and neutron diffraction,” *Journal of Applied Physics*, vol. 97, p. 034113, 2005.

[40] J. L. Jones, M. Hoffman, and K. J. Bowman, “Saturated domain switching textures and strains in ferroelastic ceramics,” *Journal of Applied Physics*, vol. 98, p. 024115, 2005.

[41] M. Marsilius, T. Granzow, and J. Jones, “Effect of electrical and mechanical poling history on domain orientation and piezoelectric properties of soft and hard PZT ceramics,” *SCIENCE AND TECHNOLOGY OF ADVANCED MATERIALS*, vol. 12, no. 1, Feb. 2011.

[42] A. B. Kounga Njiwa, E. Aulbach, T. Granzow, and J. Rödel, “Influence of radial stress on the poling behaviour of lead zirconate titanate ceramics,” *Acta Materialia*, vol. 55, no. 2, pp. 675–680, 2007.

[43] T. Leist, K. G. Webber, W. Jo, E. Aulbach, J. Rödel, A. D. Prewitt, J. L. Jones, J. Schmidlin, and C. R. Hubbard, “Stress-induced structural changes in La-doped BiFeO3-PbTiO3 high-temperature piezoceramics,” *Acta Materialia*, vol. In Press, Corrected Proof.

[44] D. Damjanovic, “Stress and frequency dependence of the direct piezoelectric effect in ferroelectric ceramics,” *Journal of Applied Physics*, vol. 82, p. 1788, 1997.

[45] D. Damjanovic, M. Demartin, H. Shulman, M. Testorf, and N. Setter, “Instabilities in the piezoelectric properties of ferroelectric ceramics,” *Sensors and Actuators A: Physical*, vol. 53, no. 1–3, pp. 353–360, 1996.

[46] J. Erhart and L. Burianová, “What is really measured on a d33 meter?,” *Journal of the European Ceramic Society*, vol. 21, no. 10, pp. 1413–1415, 2001.

[47] D. Damjanovic, “Logarithmic frequency dependence of the piezoelectric effect due to pinning of ferroelectric-ferroelastic domain walls,” *Physical Review B*, vol. 55, no. 2, pp. 649–652, 1997.

[48] D. Damjanovic, “Hysteresis in Piezoelectric and Ferroelectric Materials,” in *The Science of Hysteresis*, Oxford: Academic Press, 2006, pp. 337–465.

[49] T. Nattermann, Y. Shapir, and I. Vilfan, “Interface pinning and dynamics in random systems,” *Phys. Rev. B*, vol. 42, no. 13, p. 8577, Nov. 1990.

[50] T. Nattermann, Y. Shapir, and I. Vilfan, “Interface pinning and dynamics in random systems,” *Physical Review B*, vol. 42, no. 13, pp. 8577–8586, 1990.

[51] O. Boser, “Statistical theory of hysteresis in ferroelectric materials,” *J. Appl. Phys.*, vol. 62, no. 4, pp. 1344–1348, Aug. 1987.

[52] D. V. Taylor and D. Damjanovic, “Domain wall pinning contribution to the nonlinear dielectric permittivity in Pb(Zr, Ti)O[sub 3] thin films,” *Appl. Phys. Lett.*, vol. 73, no. 14, pp. 2045–2047, Oct. 1998.

[53] G. Tutuncu, D. Damjanovic, J. Chen, and J. L. Jones, “Direct Observation of Asymetric Ferroelastic Domain Wall Motion to Symmetric Bipolar Electric Fields,” *Physical Review Letters*, Submitted 2011.

[54] E. Fatuzzo and W. J. Merz, “Switching Mechanism in Triglycine Sulfate and Other Ferroelectrics,” *©1959 The American Physical Society*, vol. 116, no. 1, 1959.

[55] M. Avrami, “Kinetics of Phase Change. I General Theory,” *The Journal of Chemical Physics*, vol. 7, no. 12, pp. 1103–1112, Dec. 1939.

[56] M. Avrami, “Kinetics of Phase Change. II Transformation- Time Relations for Random Distribution of Nuclei,” *The Journal of Chemical Physics*, vol. 8, no. 2, pp. 212–224, Feb. 1940.

[57] Y. Ishibashi and Y. Takagi, “Note on Ferroelectric Domain Switching,” *J. Phys. Soc. Jpn.*, vol. 31, pp. 506–510, 1971.

[58] S. Zhukov, Y. A. Genenko, O. Hirsch, J. Glaum, T. Granzow, and H. von Seggern, “Dynamics of polarization reversal in virgin and fatigued ferroelectric ceramics by inhomogeneous field mechanism,” *Phys. Rev. B*, vol. 82, no. 1, p. 014109, Jul. 2010.

[59] C. Dosch, T. Granzow, J. Daniels, A. Pramanick, and J. L. Jones, “Domain switching kinetics studied by application of instantaneous electric fields to lead zirconate titanate piezoelectric ceramics,” Undergraduate Honors Thesis, University of Florida, 2010.

[60] M. Okuyama and Y. Ishibashi, *Ferroelectric Thin Films: Basic Properties and Device Physics for Memory Applications*, 1st ed. Springer, 2005.

[61] G. L. Brennecka, J. F. Ihlefeld, J. Maria, B. A. Tuttle, and P. G. Clem, “Processing Technologies for High- Permittivity Thin Films in Capacitor Applications,” *Journal of the American Ceramic Society*, vol. 93, no. 12, pp. 3935–3954, Dec. 2010.

[62] S. Hiboux, P. Muralt, and T. Maeder, “Domain and Lattice Contributions to Dielectric and Piezoelectric Properties of Pb(Zr X, Ti1− x)O3 Thin Films as a Function of Composition,” *Journal of Materials Research*, vol. 14, no. 11, pp. 4307–4318, 1999.

[63] K. Maruyama, Masao Kondo, Sushil K. Singh, and Hiroshi Ishiwara, “New Ferroelectric Material for Embedded FRAM LSIs,” *Fujitsu Sci. Tech. J*, vol. 43, no. 4, pp. 502–507, 2007.

[64] K. R. Udayakumar, K. Boku, K. A. Remack, J. Rodriguez, S. R. Summerfelt, F. G. Celii, S. Aggarwal, J. S. Martin, L. Hall, L. Matz, and others, “Bit Distribution and Reliability of High Density 1.5 V Ferroelectric Random Access Memory Embedded with 130 nm, 5 lm Copper Complementary Metal Oxide Semiconductor Logic,” *Japanese journal of applied physics*, vol. 45, p. 3202, 2006.

[65] J. A. del Alamo and J. Joh, “GaN HEMT reliability,” *Microelectronics Reliability*, vol. 49, no. 9–11, pp. 1200–1206, Sep. 2009.

BIOGRAPHICAL SKETCH

Anderson earned his Bachelor of Science in electrical engineering from the Florida A&M University -Florida State University (FAMU-FSU) College of Engineering (2003), and a Master of Science in electrical engineering from the University of Central Florida (2005), where his specialization was electromagnetics. He also has a Master of Science in materials science and engineering from the University of Florida (2009). His research specialization area while finishing a PhD in Materials Science and Engineering at UF is electronic materials.